REVIEWS

Environmental remediation by photocatalysis

R. Vinu AND Giridhar Madras

Abstract | Photocatalysis refers to the oxidation and reduction reactions on semiconductor surfaces, mediated by the valence band holes and conduction band electrons, which are generated by the absorption of ultraviolet or visible light radiation. Photocatalysis is widely being practiced for the degradation and mineralization of hazardous organic compounds to CO_2 and H_2O, reduction of toxic metal ions to their non-toxic states, deactivation and destruction of water borne microorganisms, decomposition of air pollutants like volatile organic compounds, NO_x, CO and NH_3, degradation of waste plastics and green synthesis of industrially important chemicals. This review attempts to showcase the well established mechanism of photocatalysis, the use of photocatalysts for water and air pollution control, visible light responsive modified-TiO_2 and non-TiO_2 based materials for environmental and energy applications, and the importance of developing reaction kinetics for a comprehensive understanding and design of the processes.

1. Introduction

Environmental pollution is a serious day-to-day problem faced by the developing and the developed nations in the world. Air, water and solid waste (plastics) pollution due to the anthropogenic sources contribute a major share to the overall imbalance of the ecosystem. The common pollutants include toxic organic compounds like chlorinated and non-chlorinated aliphatic and aromatic compounds, dyes, detergents and surfactants, agro wastes like insecticides, pesticides and herbicides, disinfection byproducts, volatile organic compounds, plastics, inorganic compounds like heavy metals, noxious gases like NO_x, SO_x, CO and NH_3, and pathogens like bacteria, fungi and viruses. Hence, strict environmental legislations on the use of these recalcitrant pollutants and their safe disposal drives the research community to develop clean and green processes to degrade the pollutants before they are admitted into the atmosphere and water bodies.

Photocatalysis refers to the acceleration of the rate of chemical reactions (oxidation/reduction) brought about by the activation of a catalyst, usually a semiconductor oxide, by ultraviolet (UV) or visible radiation. History dates backs to 1972, when Fujishima and Honda[1] discovered that water can be split, i.e., simultaneously oxidized to oxygen and reduced to hydrogen, when a bias potential is applied to an "illuminated" TiO_2 single crystal electrode. This remarkable discovery marked the onset of photo induced redox reactions on semiconductor surfaces. It was soon realized that such redox processes could be utilized for environmental cleanup applications, when Frank and Bard,[2] in 1977, showed the photocatalytic oxidation of CN^- and SO_3^- using different semiconductor materials like TiO_2, ZnO, CdS, Fe_2O_3 and WO_3. This was followed by the demonstration of the TiO_2 catalyzed photodegradation of chlorinated organic compounds by Ollis,[3,4] and the Pt-loaded-TiO_2 catalyzed photochemical sterilization of

Department of Chemical Engineering, Indian Institute of Science, Bangalore – 560012, India
giridharmadras@gmail.com, giridhar@chemeng.iisc.ernet.in

Figure 1: Evolution of international journal publications in the field of photocatalysis since 1990. (Source: *ISI Web of Science*)
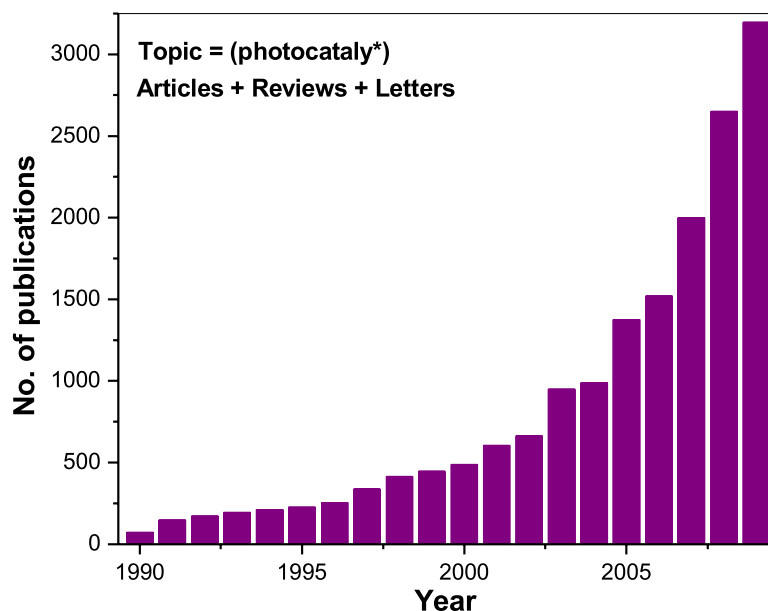
microorganisms by Matsunaga et al.[5] in the early 1980s. Later, O'Regan and Grätzel,[6] in 1991, showed the first high-efficiency solar cell based on dye-sensitized colloidal TiO_2 films for photovoltaic power generation. Thus, a brilliant start in TiO_2 photocatalysis was followed by some notable developments including, metal ion doped TiO_2 (1994), superhydrophilic TiO_2 films (1997), anion doped TiO_2 (2001), and visible light responsive TiO_2 thin films for large scale water splitting (2006).[7] Photocatalysis is widely employed in water and air purification, self-cleaning surfaces, self-sterilizing surfaces, antifogging surfaces, anticorrosive surface treatments, lithography, photochromic materials, microchemical systems, selective and green synthesis of organic compounds, and the generation of hydrogen.

Photocatalysis, as a research area, has witnessed a sea change over the past two decades with significant advancements being made in the synthesis of novel materials and nano-structures, and the design of efficient processes for the degradation of pollutants and the generation of energy. This is evident from the evolution of the number of international journal publications since 1990 to the current date, as depicted in Figure 1. This shows that there is an exponential growth in the publications and hence the knowledge in photocatalysis. Several classic review articles are dedicated to the principles

and mechanism of photocatalysis,[8–23] with special emphasis on the electron transfer processes, lattice and electronic structure of TiO_2, surface chemistry of semiconductor oxides, generation of reactive radicals, chemisorption of small and large molecules, surface modification by doping, photooxidation of organic and inorganic substrates, green synthesis of organic compounds, and the generation of hydrogen. Hence, photocatalysis can be regarded a well understood field; yet, immense challenges and opportunities exist in realizing this technology for large scale practical applications in the decontamination of the environment, and the generation of clean energy.

Photocatalysis has become an integral part of the advanced oxidation processes (AOPs), i.e., processes which employ oxidizing agents like hydrogen peroxide (H_2O_2), ozone (O_3) and Fenton's reagent ($H_2O_2 + Fe^{2+}$) for the effective detoxification of the pollutants. Invariably, the above oxidants are used in conjunction with UV radiation and/or photocatalysis in order to accelerate the rate of degradation of the pollutants. Recently, ultrasound (US), microwave radiation and electrolysis are being coupled to the above AOPs in order to further enhance the decomposition of the pollutants. A common feature that all the above AOPs share is the generation of reactive hydroxyl radicals ($OH^\bullet$), which are the precursors of degradation of any organic or inorganic compound. These hydroxyl species possess a higher oxidation potential (2.80 V) compared to the other common oxidants like atomic oxygen (2.42 V), O_3 (2.07 V), H_2O_2 (1.78 V), hydroperoxy radicals (1.70 V) and chlorine dioxide (1.57 V).[15] Thus the hybrid AOPs, which involve a combination of two or more techniques, aim to synergistically produce more hydroxyl radicals to effectively degrade the pollutants. The mechanism by which the hydroxyl radicals are generated in each of the above processes are discussed in the following sections.

In this review, we will first describe the mechanism of UV photocatalysis, and the synthesis of nano-TiO_2 by various techniques. We then exclusively discuss the photocatalytic degradation of a variety of water, air and solid contaminants like aliphatic and aromatic compounds, dyes, pesticides, pharmaceutical compounds, microorganisms, volatile organic compounds, NO_x, and polymers and plastic wastes, in terms of their pathway of degradation. The different methods of inducing the visible light response of TiO_2 are discussed. The potential of novel non-semiconductor based materials as photocatalysts is also examined. Finally, the future prospects in realizing this technology for a safer environment are discussed.
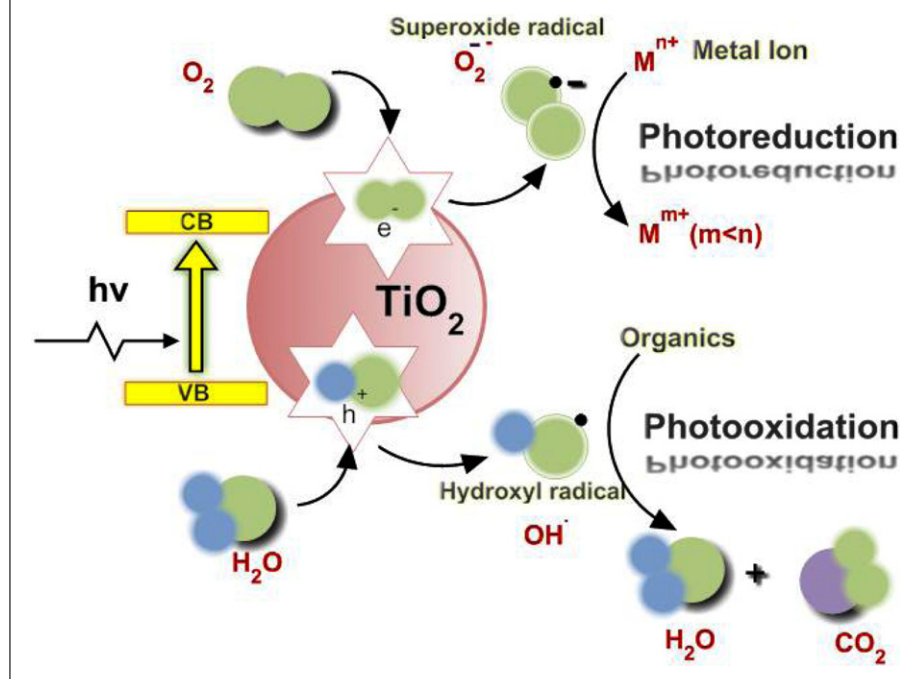
2. Mechanism of UV photocatalysis

The mechanism of UV photocatalysis involves the generation of valence band (VB) holes (h_{VB}^+) and conduction band (CB) electrons (e_{CB}^-), when a semiconductor photocatalyst absorbs light photon of energy greater than or equal to its band gap ($hv \geq E_{BG}$). The holes mediate the oxidation of organic compounds by the formation of hydroxyl radicals, and the electrons mediate reduction and oxidation reactions by the formation of superoxide radicals. A pictorial representation of the mechanism of TiO_2 photocatalysis is shown in Figure 2. The following steps provide a detailed mechanism of photocatalytic degradation of organic compounds, which is well documented.[8,10,17,18] While TiO_2 has been used as the semiconductor photocatalyst for the sake of representation, most of the following reactions are applicable for other semiconductor photocatalysts as well.

Charge carrier generation:

$$TiO_2 + hv \xrightarrow{hv > E_{BG}} h_{VB}^+ + e_{CB}^- \quad (1)$$

Charge carrier trapping:

$$Ti^{IV} - OH^- + h_{VB}^+ \longrightarrow Ti^{IV} - OH^\bullet \quad (2)$$

Surface trap:

$$Ti^{IV} - OH^- + e_{CB}^- \longleftrightarrow Ti^{III} - OH^- \quad (3)$$

Deep trap: $Ti^{IV} + e_{CB}^- \xrightarrow{\rightarrow} T_i^{III} \quad (4)$
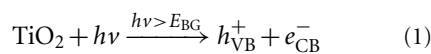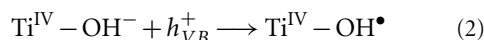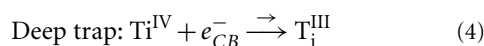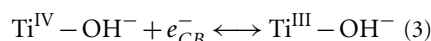
Electron–hole recombination:

Free electron with a trapped hole:

$$Ti^{IV} - OH^\bullet + e_{CB}^- \longrightarrow Ti^{IV}OH^- \quad (5)$$
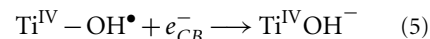
Free hole with a trapped electron:

$$Ti^{III} + h_{VB}^+ \longrightarrow Ti^{IV} \quad (6)$$

Free hole with a free electron:

$$h_{VB}^+ + e_{CB}^- \longrightarrow \text{heat.} \quad (7)$$

Generation of hydroxyl radicals in the aqueous medium:

Hole pathway:

$$Ti^{IV} - H_2O + h_{VB}^+ \longrightarrow Ti^{IV} - OH^\bullet + H^+. \quad (8)$$

Electron pathway:

$$Ti^{III} + O_2 \longleftrightarrow Ti^{III} - O_2^- \bullet \quad (9)$$

$$Ti^{IV} - O_2^{-\bullet} + 2H^+ + e_{CB}^- \longleftrightarrow Ti^{IV} - H_2O_2 \quad (10)$$

$$Ti^{IV} - O_2^{-\bullet} + H^+ \longleftrightarrow Ti^{IV} - HO_2^\bullet \quad (11)$$

$$Ti^{IV} - 2HO_2^\bullet \longrightarrow Ti^{IV} - H_2O_2 + O_2 \quad (12)$$

$$Ti^{IV} - H_2O_2 + e_{CB}^- \longrightarrow Ti^{IV} - OH^\bullet + OH^- \quad (13)$$

$$Ti^{IV} - H_2O_2 + O_2^{-\bullet} \longrightarrow$$
$$Ti^{IV} - OH^\bullet + OH^- + O_2. \quad (14)$$
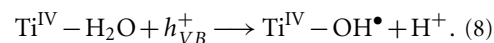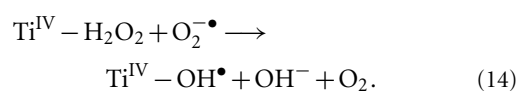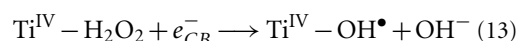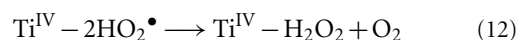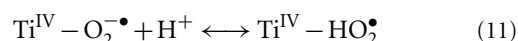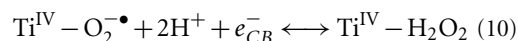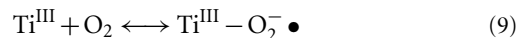
Adsorption–Desorption of a reductant (any organic substrate S):

$$\text{Ti}^{IV} + S \longleftrightarrow \text{Ti}^{IV} - S \qquad (15)$$

$$\text{Ti}^{IV} - OH^\bullet + S \longleftrightarrow \text{Ti}^{IV} - OH^\bullet - S. \qquad (16)$$
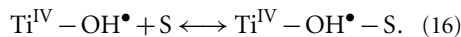
Adsorption–Desorption of an oxidant (eg. metal ion):

$$\text{Ti}^{IV} + M^{n+} \longleftrightarrow \text{Ti}^{IV} - M^{n+}. \qquad (17)$$
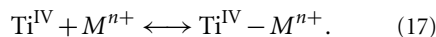
Photooxidation of a reductant:
Direct hole attack:

$$\text{Ti}^{IV} - S + \text{Ti}^{IV}(h_{VB}^+) \longrightarrow$$
$$\text{Ti}^{IV} + \text{Ti}^{IV} - I \longrightarrow CO_2 + H_2O. \qquad (18)$$

Hydroxyl radical attack:

$$\text{Ti}^{IV} - S + \text{Ti}^{IV} - OH^\bullet \longrightarrow \text{Ti}^{IV} +$$
$$\text{Ti}^{IV} - I \longrightarrow CO_2 + H_2O \qquad (19)$$

$$\text{Ti}^{IV} - S + OH^\bullet \longrightarrow \text{Ti}^{IV} - I \longrightarrow$$
$$CO_2 + H_2O \qquad (20)$$

$$\text{Ti}^{IV} - OH^\bullet - S \longrightarrow$$
$$\text{Ti}^{IV} - I \longrightarrow CO_2 + H_2O. \qquad (21)$$
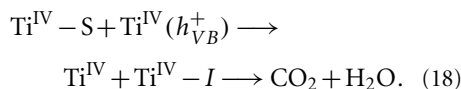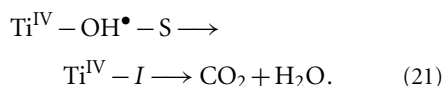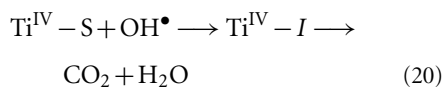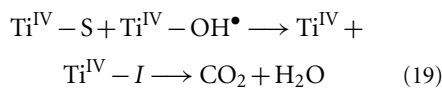
Adsorption–Desorption of the organic intermediate:

$$\text{Ti}^{IV} + I \longleftrightarrow \text{Ti}^{IV} - I. \qquad (22)$$
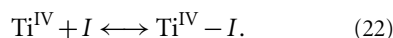
Photoreduction of a metal ion:

$$\text{Ti}^{IV} - M^{n+} + me^- \longrightarrow \text{Ti}^{IV} - M^{(n-m)+}. \qquad (23)$$
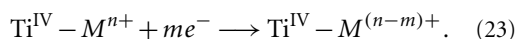
In all the above reactions, Ti^{IV} denotes the four coordinated surface functionality of TiO_2 or the "active site". Hoffmann et al.[8] have found by laser flash photolysis studies that the characteristic time scale for the generation of charge carriers is of the order of femto seconds (fs). The charge carriers thus generated gets trapped to the TiO_2 surface, which occurs over a time scale of tens of nano seconds (ns). Reaction (2) represents the trapping of the holes by the surface hydroxyl groups present in TiO_2, and reactions (3) and (4) represent the reversible trapping of the electrons in the surface of TiO_2 (shallow traps), and the irreversible trapping or relaxation of the electrons to the bottom of the CB (deep traps), respectively. Reactions (5)–(7) represent the electron–hole recombination reaction, which occurs at surface states of the TiO_2, or in the bulk medium due to the delocalization of the electrons and holes. This is one of the detrimental reactions in photocatalysis as this affects

the interfacial charge transfer processes and hence the quantum efficiency of the photoprocess.

Reaction (8) represents the generation of hydroxyl radicals ($OH^\bullet$) by the reaction of surface adsorbed water molecules with the holes, and reactions (9)–(14) shows the formation of superoxide ($O_2^{\bullet-}$), hydroperoxy ($HOO^\bullet$) and hydroxyl species through the electron pathway. All the above radical species are referred to as the "active species". When the reactions are carried out in non-aqueous (organic) medium, the surface bound hydroxyl species present in the semiconductor plays a major role (reaction (2)), and the contribution of reactions (8)–(14) for the overall oxidation of the substrate is negligible.

Once the active species are generated, the reactants are adsorbed onto the surface of the photocatalyst (reactions (15)–(17)). This is followed by the oxidation of the reductant and the concomitant reduction of the oxidant by the attack of the hydroxyl radicals and CB electrons, respectively (reactions (18)–(21)). The above two processes occur at characteristic time scales of 100 ns and milliseconds, respectively.[8,13] This means that, the oxidizing power of the VB hole or the hydroxyl radicals is always higher than that of the reducing power of the CB electrons. Moreover, these interfacial electron transfer steps compete with the electron-hole recombination reaction (10 ns) and hence, the practical efficiency or quantum yield is always lesser than that of the theoretical yield. The organic compounds degrade through the formation of intermediates (I), which transform finally to CO_2 and H_2O. Reaction (22) shows that the products desorb from the surface thereby freeing the TiO_2 active site. Similarly, when metal ions are present in the system, they are reduced to their thermodynamically stable oxidations states by the CB electrons (reaction (23)). Therefore, the overall photocatalysis reaction can be depicted as follows, wherein, the oxidants are reduced and the reductants are oxidized by the action of UV radiation on the semiconductor photocatalyst

$$(Ox_1)_{ads} + (Red_2)_{ads} \xrightarrow{h\nu/TiO_2} Red_1 + Ox_2 \qquad (24)$$
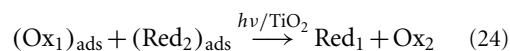
3. Semiconductor photocatalytic materials

Several metal oxides (TiO_2, ZnO, MoO_3, ZrO_2, WO_3, α-Fe_2O_3, SnO_2, $SrTiO_3$) and metal chalcogenides (ZnS, CdS, $CdSe$, WS_2, MoS_2) can be used as photocatalysts.[10,12,17,18,22−24] However, according to the thermodynamic requirement, the VB and CB of the semiconductor photocatalyst should be positioned in such a way that, the oxidation potential of the hydroxyl radicals (E^0(H_2O/$OH^\bullet$) = 2.8 V vs NHE) and

Figure 3: Band gap energy and band edge positions of different semiconductor oxides and chalcogenides, along with selected redox potentials. (Redrawn from ref. 10,12,17,18,22–24).
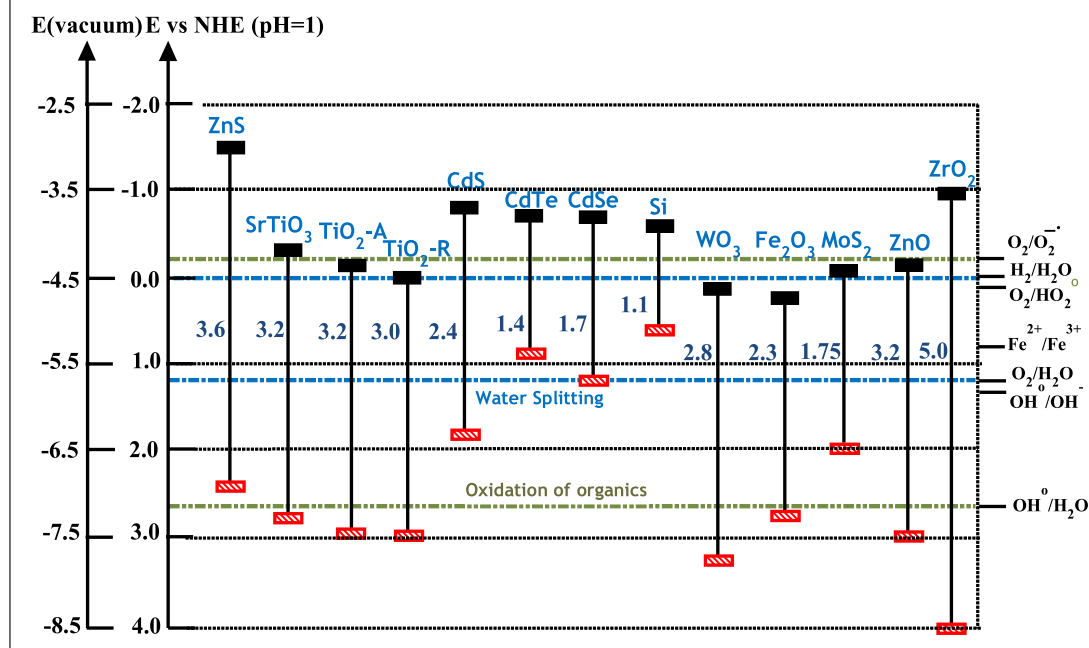
the reduction potential of superoxide radicals $(E^0(O_2/O_2^{\bullet-}) = -0.28$ V vs NHE), lie well within the band gap. In other words, the redox potential of the VB hole must be sufficiently positive to generate hydroxyl radicals and that of the CB electron must be sufficiently negative to generate superoxide radicals. Figure 3 depicts the band structure diagram of different materials, along with the potentials of the redox couples. It is clear that, TiO_2, ZnO, $SrTiO_3$ and ZrO_2 exhibit favorable band-gap positions compared to the other materials. The material selection is also based on the stability of the material towards photocorrosion. For eg. ZnO and CdS have only one stable oxidation state ($+2$), and hence are prone to decomposition by VB holes, according to the following reactions[22]

$$ZnO + 2h^+ \longrightarrow Zn^{2+} + 1/2 O_2 \qquad (25)$$

$$CdS + 2h^+ \longrightarrow Cd^{2+} + S. \qquad (26)$$
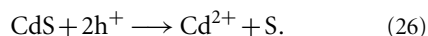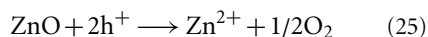
Furthermore, ZnO undergoes incongruous dissolution, yielding $Zn(OH)_2$ on the surface, thereby leading to the deactivation of the material over a period of time.[18,22] However, Ti in TiO_2 is capable of reversibly changing its oxidation state from $+4$ and $+3$, and hence TiO_2 is more favored compared to the other materials. Although TiO_2 exists in two forms, viz., anatase and rutile, anatase phase TiO_2 ($E_{BG} = 3.2$ eV) is more active for photocatalysis applications, even though rutile

phase TiO_2 ($E_{BG} = 3.0$ eV) possesses a smaller band gap, indicating the possibility of absorption of long wavelength radiation. This is because, the CB position of anatase TiO_2 is more negative compared to rutile, which results in the higher reducing power of anatase. In addition to the above advantages, other factors like the non-toxic nature (environmentally benign), low cost and the ease of synthesis makes TiO_2 the "photocatalyst of choice" for photocatalytic degradation reactions.

4. Synthesis and properties of TiO_2

For photocatalytic applications, "nano-sized" TiO_2 is preferred compared to bigger sized TiO_2 particles. The two most important properties of a nano material, which makes it superior to other microscopic or macroscopic particles for applications in catalysis, are (i) the high surface to volume ratio, and (ii) the quantum confinement at the nano scale. The first property results in catalysts with high surface area and high porosity, which ensures enhanced reaction rates due to the high level of interaction of the reactants with the active sites. The second property governs the transport of electrons and holes from the bulk to the surface of the material, whose length scale is also of the order of a few nanometers (called as electron Bohr radius). Moreover, for photo-applications, the catalyst should absorb, and not block or scatter, incident radiation, and generate charge carriers

Table 1: Physicochemical properties of nano-TiO$_2$ by various synthesis techniques.

Sl. No.	Synthesis method	Highlights/Properties of TiO$_2$	Reference
1	Thermal decomposition of ammonium titanyl sulfate	Properties of TiO$_2$ tuned by varying the gas atmosphere and reaction temperature; mesoporous texture with mean pore dia. = 15 nm; particle size = 20–30 nm; surface area c.a. 64 m^2 g^{-1}	[25]
2	Precipitation of a mixture of titanium (IV)isopropoxide, calculated amount of stearic acid and 1-propanol, followed by calcination at different temperatures	Pore size tuned by adjusting the molar composition of stearic acid; pore dia. = 5–15 nm; surface area = 92–130 m^2 g^{-1}	[26]
3	Four different synthesis routes involving the hydrolysis of titanium (IV) isopropoxide or TiCl$_4$ followed by calcination at different temperatures	Samples made from TiCl$_4$ exhibited the highest photoactivity; 100% anatase phase TiO$_2$ was obtained with crystallite size = 7–30 nm; surface area = 100 m^2 g^{-1}; pore size = 7–14 nm	[27]
4	Combustion of aqueous titanyl nitrate with stoichiometric amounts of glycine at 350 °C; Precursor - titanium (IV) isopropoxide	100% anatase phase TiO$_2$ was obtained; particle size = 8±2 nm; band gap = 2.21 and 2.85 eV; surface area = 246 m^2 g^{-1}; TGA wt. loss = 15.5%; high surface acidity	[28]
5	Hydrothermal synthesis using TiCl$_4$ using cationic surfactants like CTAB and CPB	Crystallite size = 10–18 nm; morphology change – nano-spheres to cotton fibrils; surface area = 240–418 m^2 g^{-1}; pore size = 2–4 nm; mixture of anatase and rutile phase was obtained	[29]
6	Sol-gel synthesis using titanium (IV) isopropoxide	Effect of hydrolyzing agent, reactant molar ratio, aging temperature, aging time and calcinations temperature were studied; max. surface area = 125 m^2 g^{-1}; min. crystallite size = 6 nm; band gap = 3.2±0.1 eV; mixture of anatase and rutile phase was obtained	[30]
7	One-pot hydrothermal synthesis using tetramethylammonium hydroxide (TMAOH)	Anatase phase TiO$_2$ nano-pillar arrays were grown on Ti substrate; c.a. 250 nm in width and c.a. 700 nm in length with a tetrahedral bipyramidal tip; optimum conditions – 1M TMAOH, 200 °C, 8 h	[31]
8	Combustion of aqueous titanyl nitrate with stoichiometric amounts of glycine at 350 °C; precursor – tetrabutyl titanate	100% anatase phase TiO$_2$ was obtained; crystallite size = 4–6 nm; surface area = 257 m^2 g^{-1}; band gap = 2.92 eV	[32]

CTAB – cetyltrimethylammonium bromide; CPB – cetylpyridinium bromide

by band gap excitation. This is possible only with nano-sized semiconductor materials with suitable band gap energy. Therefore, owing to the enhanced molecular transport properties at the surface, it is evident that nano-sized materials are beneficial as photocatalysts.

Nano-TiO$_2$ photocatalysts have been synthesized in different shapes and morphologies, which include, nanoparticles, nanorods, nanotubes, nanopillars and nanowire arrays, nanobowls, nanowhiskers, aerogels, nanosheets, opal and inversed opals.[12,14] The synthesis routes can be broadly classified as solution phase and gas phase techniques. Solution phase synthesis is the most preferred technique for the preparation of TiO$_2$ in the form of powders and thin films. Some of the solution phase techniques are precipitation method, hydrothermal synthesis, solvothermal synthesis, sol-gel method, sol method (nonhydrolytic sol-gel), micelle and inverse micelle method, combustion synthesis, electrochemical synthesis, sonochemical synthesis and microwave synthesis methodologies. Gas phase technique is widely employed for the synthesis of thin film samples. Some of the gas phase techniques include chemical vapor deposition (CVD), physical vapor deposition and spray pyrolysis deposition. Each of the above synthesis methods possesses a unique advantage over the other techniques and the characteristics of the final product vary from one method to another. Chen and Mao[14] have discussed the above synthesis techniques in detail, with particular emphasis on the morphology, size,

shape and properties of the final TiO$_2$ product obtained in each method. Table 1[25–32] presents a representative list of the different solution phase techniques adopted for the synthesis of TiO$_2$. A careful evaluation of the results presented in the table shows that the final properties of the TiO$_2$ nanoparticles like the phase composition (anatase:rutile), particle size, porosity, surface area, band gap and surface hydroxyl content can be tailored by varying the reaction conditions like: the precursor compound (TiCl$_4$, titanium(IV) isopropoxide, etc.), hydrolyzing agent (in the case of sol-gel synthesis), fuel (in the case of solution combustion synthesis), molar composition of the reactants, reaction temperature, reaction time (ageing time), calcination temperature and presence of gas atmosphere (air, Ar, NH$_3$).

We have synthesized nano-TiO$_2$ by the solution combustion methodology[28] (henceforth denoted as combustion synthesized TiO$_2$–CS TiO$_2$). This technique involves the combustion of a stoichiomeric mixture of titanyl nitrate with the fuel, glycine at 350 °C in a muffle furnace. Titanyl nitrate is synthesized by the hydrolysis and subsequent nitration of the precursor compound, titanium tetra-isopropoxide. The stoichiometric reaction can be represented as

$$9\text{TiO(NO}_3)_{2(aq)} + 10\text{C}_2\text{H}_5\text{O}_2\text{N}_{(aq)} \xrightarrow{350\,^\circ\text{C}} 9\text{TiO}_{2(s)}$$

Titanyl nitrate   Glycine

$$+\ 14\text{N}_{2(g)} \uparrow +\ 20\text{CO}_{2(g)} \uparrow +\ 25\text{H}_2\text{O}_{(g)} \uparrow .$$
(27)
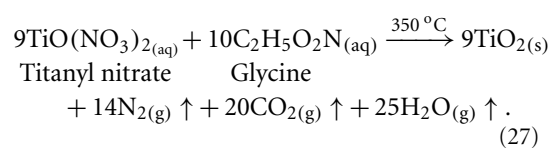
Figure 4: UV/visible diffuse reflectance spectra of combustion synthesized TiO_2 samples using different fuels. (O) – Oxalyl dihydrazide, (H) – Hydrazine hydrate, (G) – Glycine. [Inset: TGA weight loss profiles of above catalysts]. It is clear that TiO_2 synthesized using glycine exhibits the highest weight loss, and hence the highest surface hydroxyl content. (Redrawn from ref. 28).
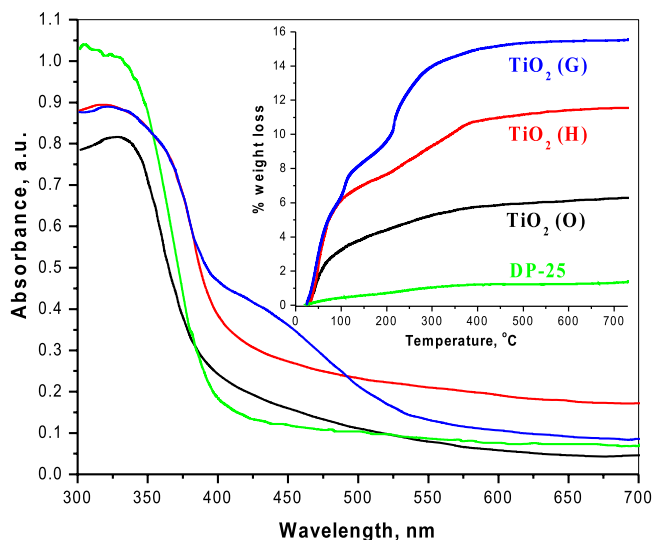
The combustion mixture initially undergoes dehydration and froths. Flame was not observed and hence the combustion is of smoldering type. The above reaction indicates that 9 moles of titanyl nitrate reacts with 10 moles of glycine to yield 9 moles of TiO_2 and nearly 60 moles of gaseous products. The evolution of such high amounts of gases results in high porosity and hence, high surface area of TiO_2. Moreover, low overall temperature results in the formation of anatase phase TiO_2.

Nagaveni et al.[28] have carried out a thorough study of the effect of different fuels on the properties of CS TiO_2. Three different fuels were employed, viz., glycine (G), hexamethylene tetramine (H) and oxalyl dihydrazide (O). Different characterization of the TiO_2 samples like crystal structure and crystallite size determination using powder X-ray diffraction (XRD), phase confirmation using Raman spectroscopy, particle size measurement by transmission electron microscopy (TEM), ionic state determination by X-ray photoelectron spectroscopy

(XPS), band gap using diffuse reflectance UV/visible spectroscopy, surface hydroxyl species by Fourier transform-infra red (FT-IR) spectroscopy and thermo-gravimetric analysis (TGA), surface acidity by thermal desorption, and BET surface area by porosimetry were carried out. Solution combustion synthesis yields TiO_2, which is 100% anatase without any rutile impurity. The crystal structure of anatase phase TiO_2 is body centered tetragonal in the space group, $I4_1/amd$. Table 2 presents a comparison of the different physicochemical properties of TiO_2 synthesized using the above three fuels. It is clear that CS TiO_2 (G) possesses low particle size, high surface area, low band gap and high surface hydroxyl content compared to the other TiO_2 samples. CS TiO_2 (G) exhibits two absorption edges at 560 nm and 435 nm, corresponding to two band gap energies of 2.21 and 2.85 eV, respectively. This is depicted in Figure 4, where a broad absorption band in the visible range 400–550 nm is observed for CS TiO_2 (G), which is not observed for the other TiO_2 samples. This is attributed to carbide ion substitution for oxide ion, of the form $TiO_{2-2x}C_xV_x$, where 'V' denotes the oxide ion vacancy. This is one of the primary reasons for the photocatalytic activity exhibited by CS TiO_2 in the visible region. Previously, Khan et al.[33] have shown that C-doped TiO_2, like the one above, exhibits enhanced visible light activity for the photoelectrochemical splitting of water to H_2 and O_2.

Figure 5 shows the TEM images of CS TiO_2 (G),[28] and the most widely used commercial TiO_2, Degussa P-25 TiO_2 (DP-25), produced by Degussa Corporation. It is clear that DP-25, with 80% anatase and 20% rutile phase, is composed of 37 nm anatase and 90 nm rutile grains,[34] with a surface area of 50 m^2 g^{-1}, much lesser compared to CS TiO_2. Furthermore, the amount of surface bound hydroxyl species is many times lesser in DP-25 (Figure 4). Table 3[28,34–38] compares the characteristics of CS TiO_2 with many other commercially available TiO_2 samples. It is evident that CS TiO_2 exhibits unique properties in terms of small particle size, high surface acidity and high surface hydroxyl contant compared to all other TiO_2 samples. Ryu and Choi[35] have investigated the photocatalytic degradation of 19 test substrates using 8 commercial TiO_2 samples, and concluded that each TiO_2 sample exhibited high photoactivity for specific substrates. Thus the activity of the photocatalyst cannot be standardized based on any single property, but by striking a balance between the different physicochemical properties. In a series of publications we have shown that under similar reaction conditions, photoactivity of CS

Table 2: Comparison of the properties of combustion synthesized TiO_2 using different fuels.

Property	TiO_2(G)	TiO_2(H)	TiO_2(O)
Particle size from TEM, nm	6–8	7–9	11–13
BET surface area, m^2 g^{-1}	246	164	143
Band gap, eV	2.21, 2.85	2.85	2.98
Surface hydroxyl content (% wt. loss from TGA)	15.5	11.5	6.3

G – Glycine, H – Hexamethylene tetramine, O – Oxalyl dihydrazide

Figure 5: TEM micrographs of (a) CS TiO$_2$(G) and (b) DP-25 TiO$_2$. Reprinted with permission from ref. 28,34. Copyright 1998 and 2004 American Chemical Society.

(a)

(b)

Figure 6: Schematic of the immersion type photocatalytic reactor set up for the degradation of organic compounds. HPML – High pressure mercury vapor lamp.
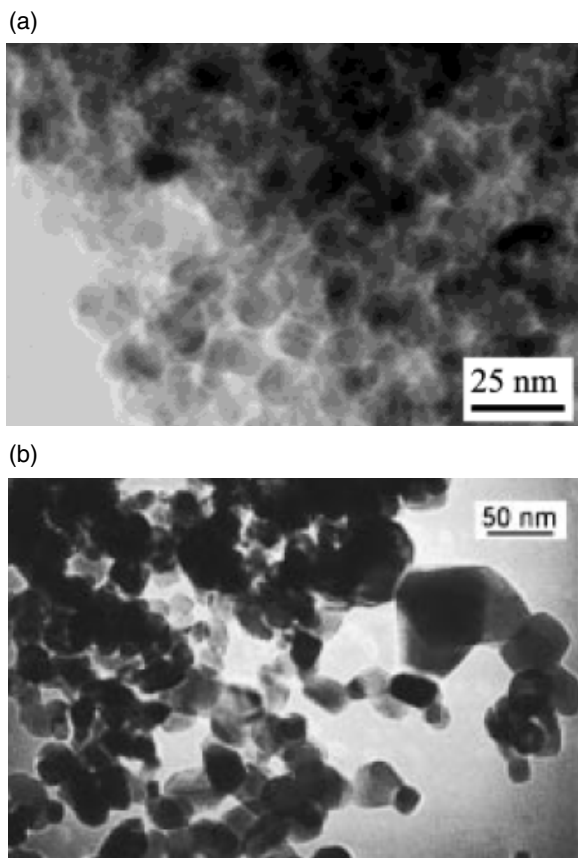
TiO$_2$ towards the photooxidation of different class of dyes,[39–41] phenolic compounds like chlorophenols, nitrophenols and multiple substituted phenols,[42,43] substituted nitrobenzenes,[44] water soluble polymers and plastics,[45,46] and the reduction of metal ions,[47] is much higher compared to that of DP-25. Detailed discussions on the degradation of organic compounds and polymers using CS TiO$_2$ are available in later sections.

5. Photocatalytic reactor

Photocatalytic reactors of volume ranging from 0.1–10 L are widely used to evaluate the photocatalytic activity of the newly synthesized materials for the degradation of organic compounds. Different reactor configurations have been found to be suitable for photocatalytic degradation reactions,[48] which include, thin film reactor, flat plate reactor, fluidized bed reactor, packed bed reactor, rotating disc reactor, fountain type slurry reactor, tubular reactor, membrane reactor, fiber reactor, monolithic reactor, bubble column reactor, air-lift loop reactor, Taylor-vortex flow reactor, and

concentrating and non-concentrating solar reactors. Among the different configurations, immersion type photoreactor with the catalyst particles in suspension has been found to yield higher rates of degradation of the organic compounds. We have used a home made immersion photocatalytic reactor for most our degradation studies.[39–41] The reactor, depicted in Figure 6, consists of a jacketed quartz tube, which houses the radiation source. The source is usually a high pressure mercury vapor lamp for UV radiation, and a tungsten filament lamp or fluorescent lamp for visible radiation. The mixture of pollutant and catalyst is taken in the outer, jacketed cylindrical borosilicate reactor. Cold water was circulated in the annulus of both the inner and the outer reactor to maintain the solution temperature at 35 °C. The inner quartz tube was immersed into the solution at different levels based on the degradation rates observed for different organic compounds. The intensity and photon flux of the light source were determined by actinometric techniques.[41] Further details about the geometry of the reactor are available elsewhere. Although such a reactor cannot be used in industrial settings owing to the separation of the fine catalyst particles from the reaction solution, it is the preferred one

Table 3: Comparison of the physicochemical properties of combustion synthesized TiO_2 (CS TiO_2) with commercially available TiO_2 samples.

TiO_2	BET surface area, $m^2\ g^{-1}$	Crystallite size, nm	pH_{zpc}	Surface hydroxyl concentration	Reference
CS TiO_2	246	8±2 nm	2.4	15.6% total wt. loss (from TGA analysis)	[28]
DP-25 (80% A: 20% R)	50	A – 37; R – 90	6.3	1.4% (TGA) 163 (FTIR)	[28,34]
Hombicat UV 100 (Sachtleben chemie)	290	5	6.0	843 (FT-IR)	[35,36]
Junsei	9.7	34	4.4	52 (FT-IR)	[35]
Aldrich Anatase	9.2	37	4.2	54 (FT-IR)	[35]
Aldrich Rutile	1.9	40	4.8	19 (FT-IR)	[35]
Millenium PC 10	11	75	-	-	[37]
Millenium PC 50	50	25	-	-	[37]
Millenium PC 100	89.6	21	5.9	505 (FT-IR)	[35,37]
Millenium PC 500	287	5–10	6.2	-	[37]
Tronox A-K-1	90	20	-	-	[38]
Ishihara ST-01	340	11	5.8	719 (FT-IR)	[34]
Rutile P-25	29.2	34	6.1	56 (FT-IR)	[34]

A – Anatase; R – Rutile; Aldrich Rutile and Rutile P-25 are 100% R; All the other TiO_2 samples are 100% A

to study the mechanism, kinetics and pathway of degradation of a wide variety of organic compounds and microorganisms.

A solution to the problem of post-catalyst separation in suspension type photocatalytic reactors is to immobilize the catalyst on a suitable support material. Many different supports have been found to be suitable for the immobilization of TiO_2, viz., glass beads,[49] flexible fibre glass cloth,[50] glass tubes,[51] cotton,[52] PTFE mesh sheets,[53] polystyrene beads,[54] perlite,[55] and porous lavas (pumice stone).[56] The various design considerations for a support material and the catalyst coating procedures are described elsewhere.[51]

6. UV photocatalytic degradation of organic compounds

Organochlorine compounds like dichloromethane (CH_2Cl_2), chloroform ($CHCl_3$), carbon tetrachloride (CCl_4) and trichloroethylene (TCE, C_2HCl_3) were, in fact, the first organic pollutants to be degraded using photocatalysis.[3,4] These toxic organic compounds are widely used as solvents, pesticides, refrigerants, and in plasticizers and plastics. Ollis and coworkers[3,4] have demonstrated a complete mineralization of the above compounds in aqueous phase to HCl and CO_2, using TiO_2 as the photocatalyst. The degradation of TCE involved the formation of trichloroacetaldehyde as the intermediate. They have found that chloride ions generated during the degradation inhibits the conversion of the above compounds. The order of degradation exhibited by the chloromethanes follow:

$CHCl_3 > CH_2Cl_2 > CCl_4$. A general stoichiometric reaction for the photocatalytic degradation of the organochlorine compounds can be written as:[8]

$$C_xH_yCl_z + \left(x + \frac{y-z}{4}\right)O_2 \xrightarrow{hv,\ TiO_2}$$

$$xCO_2 + zHCl + \left(\frac{y-z}{2}\right)H_2O. \quad (28)$$
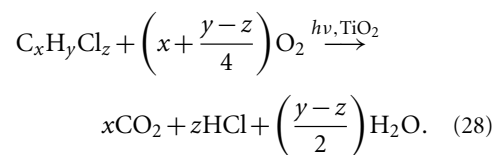
Further studies on the photocatalytic degradation of chlorinated aliphatic compounds indicated that the relative ease of degradability follows: chloroolefins > chloroparaffins > chloroacetic acids.[57] Interestingly, brominated compounds like tribromo methane ($CHBr_3$) and dibromomethane (CH_2Br_2) exhibit higher degradation rates compared to the corresponding chloromethanes. Turchi and Ollis[58] have proposed a detailed mechanism of photocatalytic degradation based on the primary events of photocatalysis, and showed that the degradation of organic compounds follow the classical Langmuir–Hinshelwood kinetic model. Further details about the model are discussed in the following subsection.

Many studies have been devoted to the photocatalytic degradation of chlorinated aromatic compounds like chlorophenols and chlorobenzenes, chlorinated pesticides like DDT,[59] hexachlorobenzene, atrazine and parathion, surfactants like sodium dodecyl benzene sulfonate[59] and trimethyl phosphate, aliphatic and olefinic compounds, dyes, nitrogeneous compounds like nitrophenols and nitrobenzenes, carboxylic acids, alcohols and heteroatom compounds. A compendium of the different studies on the

photocatalytic degradation of different classes of organic compounds is available in the review articles by Hoffmann et al.,[8] Mills and Hunte,[10] Legrini et al.,[15] Bhatkhande et al.[17] and Blake.[60] In the following subsections, we will discuss the photocatalytic degradation of common water pollutants like dyes, phenolic compounds, pesticides, pharmaceutical compounds, and the destruction of microorganisms, by stressing the importance of reaction mechanism, pathway and kinetics.

6.1. *Dyes*

Dyes find numerous applications in our daily life in clothing, food, paper, leather, cosmetics, plastics, drugs, electronics and printing. Nearly 80% of the synthetic dyes produced in the world are consumed by the textile industry. One of the major bottlenecks in the textile industry is the dye fixation, i.e., spent dye baths, residual dye liquors and water from washing operations contain dye in the hydrolyzed and unfixed form. Nearly 10% of the dyes are discharged into the effluent as a result of this process. Conventional treatment of waste water like neutralization of acidic and alkaline liquors, flocculation and chemical oxidation result in 70–80% of decolorization, while still maintaining the organic carbon load in the effluent. Biodegradation methods are effective in reducing the biological oxygen demand of the effluent, but reducing the chemical oxygen demand and toxicity to permissible levels is a challenging task. Hence, the role of AOPs in the degradation of dye waste waters is very critical. Many reviews exclusively discuss the degradation of different class of dyes under UV and visible light exposure,[61,62,63] various parameters that affect the degradation of dyes,[64] and modified TiO_2 for the degradation of dyes.[65]

Based on the functional group that constitutes the dyes, dyes are classified as azoic, anthraquinonic, heteropolyaromatic, aryl methane, xanthene, indigo, acridine, nitro, nitroso, cyanine and stilbene. The photodegradation of azo dyes has been investigated extensively,[63] as these dyes contribute 50% of the commercial dyes. Dyes are the most widely used organic substrates to test the photocatalytic activity of nano-sized catalysts. This is because of the simplicity in the analysis of the dyes. The degradation of a dye can be characterized in two ways: percent decolorization and percent mineralization. Decolorization refers to the reduction in concentration of the parent dye molecule under consideration at its characteristic wavelength, but does not refer to the complete removal of the organic carbon content. This is due to the formation of colored dye intermediates, which absorb at different wavelengths. Hence,

complete degradation or mineralization occurs when all the organic carbon is converted to CO_2. Therefore, analyzing the mineralization of the dyes in terms of the total organic carbon (TOC) content assumes importance. The mechanism of CO_2 evolution follows the photo-Kolbe decarboxylation mechanism,[66] which is given by

$$\Phi - COO^- + h_{VB}^+ \longrightarrow \Phi^\bullet + CO_2 \qquad (29)$$
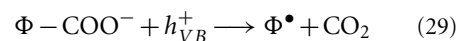
where, Φ denotes the organic component of the dye or the dye intermediate. The radical Φ° formed as a result of this reaction can undergo further transformation to yield other intermediates with smaller size.

Epling and Lin[67] have studied the degradation of 15 dyes belonging to different class by functionality in presence of visible light. The order of degradation among the different dyes followed the order: indigo ≈ phenanthrene > triphenyl methane > azo ≈ quinoline > xanthenes ≈ thiazine > anthraquinone. The order of degradation of the dyes in the presence of different light sources followed: natural sunlight ≫ 90 W halogen flood light > 150 W spotlight. The presence of electron withdrawing groups was found to retard the degradation rate of the dye. They have attributed the degradation of the dye to both photosensitized oxidation and reduction mechanisms.

We have recently[41] reported the degradation of 5 anionic, 8 cationic and 3 solvent dyes, each belonging to a different class by molecular structure, with CS TiO_2 and DP-25 in presence of UV irradiation. The anionic dyes exhibited higher decolorization rates compared to the cationic dyes, and the solvent dyes exhibited adsorption dependent degradation. No simple correlation was observed between the degradation rates of the dyes and the dye structure. In fact, the order of degradation of the dyes with CS TiO_2 and DP-25 was different, and this was correlated with the surface charge of the catalysts. By monitoring the shifts in characteristic wavelength of the dyes during degradation, it was concluded that the highly acidic surface of CS TiO_2 resulted in the faster consumption of the intermediates, while the intermediates were long-lived in presence of DP-25.

Silva et al.[68] have studied the degradation of mono-, di- and tri-azo dyes and found that the decolorization followed the order: Solophenyl Green BLE (tri-azo) > Erionyl Red B (di-azo) > Chromotrop 2R (mono-azo). However, the mineralization of the dyes followed the opposite trend. All the above studies suggest that a consensus could not be reached between the degradation rate of the dye with the dye structure

or the functional groups that characterize the dye. Therefore, a thorough understanding of the pathway of degradation of the dyes is essential in order to assess the stability of the different intermediates.

Table 4[66,69–76] lists the intermediates that are observed during the degradation of some common classes of dyes. The possible sites of cleavage of the dye and hydroxyl radical attack are depicted

Table 4: Intermediates detected during the photocatalytic degradation of dyes with nano-TiO$_2$. (The broken lines represent the possible sites of bond cleavage).

Dye/Dye class	Intermediates detected
Acid Orange 7 (Mono azo)[69]	• 22 intermediates detected • Coumarin • 2-Naphthol • Naphthoquinone derivatives • Phthalic acid • Phthalimide • Benzoic acid derivatives • Succinic, malonic and maleic acid
Metanil Yellow (Mono azo)[70]	• Benzene sulfonic acid • Hydroxylated diphenyl amine • Diphenyl amine • Benzene • Phenol • Aniline • Hydroquinone
Remazol Brilliant Blue R (Anthraquinonic)[71]	• Amino substituted anthraquinone • Hydroxy substituted anthraquinone • Amino substituted phthalic acid • Phthalic acid
Indigo Carmine (Indigo)[72]	• 2-Nitrobenzaldehyde • 2,3-Dihydroxy indoline • Anthranilic acid • Amino fumaric acid • Pyruvic, malonic, malic, glycolic, oxalic, acrylic, acetic acids
Methylene Blue (Heteropolyaromatic)[66]	• (3-Dimethyl amino) aniline • Benzene sulfonic acid • Phenol • Hydroxylated products of amino and sulfoxide groups
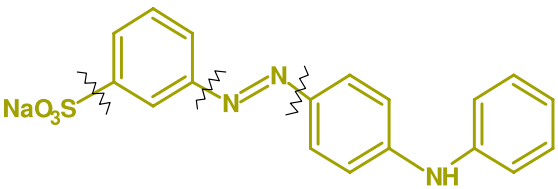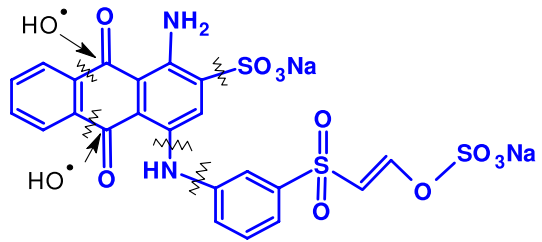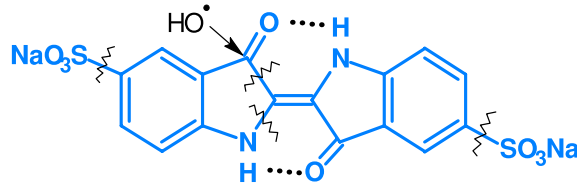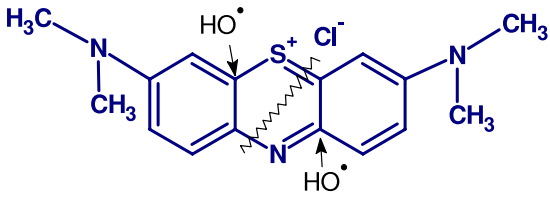
Continued.

Table 4: Continued.

Procion Red MX-3B (Triazine + azo)[73]

- 12 intermediates detected
- p-Hydroxy-phenyl-3-hydroxy propanedioic acid
- 2-Hydroxy benzoic acid,
- p-Hydroxy cinnamic acid
- Phthalic acid
- Malic acid
- Oxalic acid
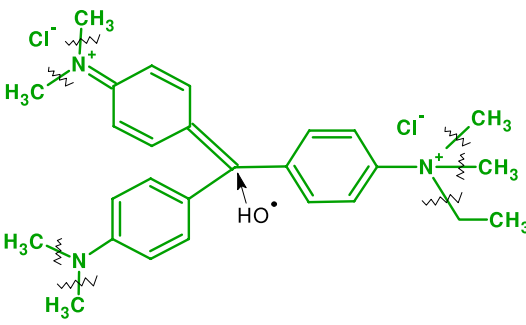
Methyl Green (Triphenyl methane)[74]

- 33 intermediates detected
- Colorless Carbinol Base and Crystal violet dye
- Degradation proceeds by N-de-methylation and N-de-alkylation pathway
- N-de-methylated and N-de-alkylatated derivatives of aminophenol and benzophenone
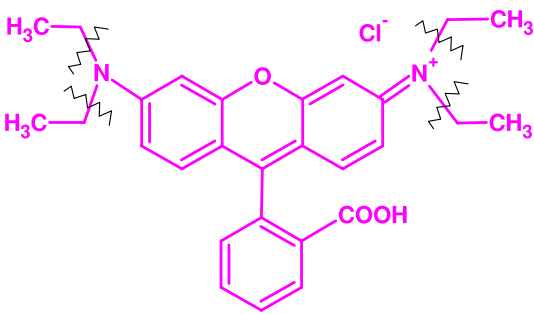
Rhodamine B (Xanthene fluorene)[75,76]

- Rhodamine 110 dye
- Degradation proceeds by N-de-ethylation pathway
- Mono-, di-, tri- and tetra-N-de-ethylated rhodamine species

along with the structure of the dyes. An extensive list of the studies on the degradation pathway of azo and non-azo dyes is provided by Rajeshwar et al.[61] A general conclusion from the various studies on the mechanism of degradation of the dyes can be summarized as follows:

(i) Degradation of azo dyes involves cleavage in the vicinity of the azo bond and results in the formation of naphthol intermediates, which further gets transformed to benzoic acid intermediates.[69,70]

(ii) Degradation of anthraquinonic dyes result in the formation of phthalic acid intermediates.[71]

(iii) The presence of hydrogen bonds in indigo carmine results in the faster degradation compared to all the other dye classes.[72]

(iv) Triphenyl methane or rhodamine dyes,[74–76] which contain alkyl (methyl or ethyl) groups substituted in the amino nitrogen, degrade by the N-de-alkylation mechanism, which involves the abstraction of the alkyl groups by the hydroxyl radicals resulting in the formation of the corresponding aldehyde as a side product. Once complete dealkylation occurs, fragmentation of the molecule occurs, which results in the formation of different substituted benzene compounds.

(v) N-de-alkylation results in the formation of stable dye intermediates, which usually exhibit a blue shift in the characteristic wavelength.

(vi) At long exposure periods, cleavage of the benzene ring occurs in all the dye intermediates, which result in the formation of low molecular weight organic acids.

The dye molecules also contain other hetero atoms like N, S, Br and Cl in their structure, and hence an assessment of the fate of these elements during mineralization is also critical. It is well established that sulfonate groups ($-SO_3^-$) in anionic dyes are transformed to innocuous sulfate ions (SO_4^{2-}), primary ($-NH_2$) and secondary ($-NH-$) amino groups are converted into ammonium ions (NH_4^+), azo nitrogen ($-N=N-$) is converted to N_2, and halogen atoms are released into the solution as their respective anions. The following reactions describe the mechanism by which the above transformations take place.[66]

Formation of ammonium ion:

$$\Phi-NH-\Phi'+H^{\bullet} \rightarrow \Phi^{\bullet}+\Phi'-NH_2 \quad (30)$$

$$\Phi'-NH_2+H^{\bullet} \rightarrow \Phi'^{\bullet}+NH_3 \quad (31)$$

$$NH_3+H^+ \rightarrow NH_4^+. \quad (32)$$

Formation of N_2:

$$\Phi-N=N-\Phi'+H^{\bullet} \rightarrow$$
$$\Phi-N=N^{\bullet}+\Phi'-H \quad (33)$$

$$\Phi-N=N^{\bullet} \rightarrow \Phi^{\bullet}+N\equiv N. \quad (34)$$
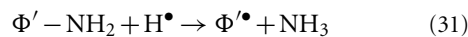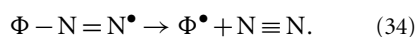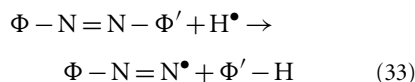
Formation of sulfate ions:

$$\Phi-SO_3^-+OH^{\bullet} \rightarrow \Phi-OH+SO_3^{\bullet-} \quad (35)$$

$$SO_3^{\bullet-}+OH^- \rightarrow H^{\bullet}+SO_4^{2-}. \quad (36)$$
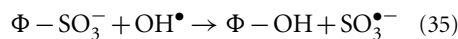
Formation of chloride/bromide ions:

$$\Phi-Cl/Br+OH^{\bullet} \rightarrow \Phi-OH+Cl^-/Br^-. \quad (37)$$
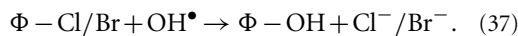
The rate of photocatalytic degradation of the dyes or any organic compound follows the classical Langmuir–Hinshelwood (L–H) kinetics.[59] A mechanistic rate equation for the photocatalytic degradation of dyes was derived by Sivalingam et al.[39] by accounting the fundamental reactions described in Section 2. The rate equation, which resembles the L–H equation is given by

$$-r_A = \frac{K_0((k_{0h}/K_0)+k_0)C_A}{1+K_0C_A} \quad (38)$$

where, r_A denotes the rate of consumption of the organic compound, C_A is the concentration of the organic compound, K_0 is the equilibrium adsorption rate coefficient, which includes the adsorption of the organic substrate and the hydroxyl radicals. The rate coefficients k_{0h} and k_0 signify the oxidation of the organic compound by direct hole attack and by the hydroxyl radicals, respectively. Hence, the compound coefficient $k_r = (k_{0h}/K_0)+k_0$ denotes the oxidation of the organic compound. The rate coefficients K_0 and k_r can be determined by the initial rate method. By this method, the equation is inverted and rearranged so that a plot of $1/C_{A0}$ versus $1/r_{A0}$ yields the slope and intercept, from which K_0 (in L mg^{-1}) and k_r (in mg L^{-1} min^{-1}) can be evaluated. The rearranged equation is given by

$$-\frac{1}{r_{A0}} = \frac{1}{k_r K_0}\frac{1}{C_{A0}}+\frac{1}{k_r}. \quad (39)$$

It is important to note that the equilibrium adsorption coefficient, K_0 determined from the L–H equation is different from that of the adsorption coefficient that is determined by the Langmuir adsorption isotherm. This is because, the equilibrium adsorption coefficient determined by the Langmuir isotherm denotes the adsorption–desorption of the organic compound in the dark, while K_0 signifies the adsorption of the organic compounds onto the catalyst surface and desorption of the products from the surface during the photoreaction. Hence, it is imperative to note that K_0 is dependent on other reaction parameters like the intensity of UV irradiation, concentration of oxygen and the catalyst concentration.

However, most of the organic compounds are present at trace levels in the atmosphere or effluent stream, and hence the term K_0C_A can be neglected in equation (38) compared to unity. Hence, the rate equation gets simplified to a first-order equation, with 'k' ($=K_0k_r$) as the first order rate constant as[42]

$$-r_A = -\frac{dC_A}{dt} = kC_A. \quad (40)$$

The solution of the above equation is given by $C_A = C_{A0}\exp(-kt)$. The rate coefficient, k can be determined by a linear plot of $\ln(C_{A0}/C_A)$ versus t. The rate coefficient, k, is dependent on the type of the catalyst (anatase/rutile TiO_2), intensity of the UV radiation, catalyst loading, and other reaction parameters like pH and the presence of other ions.

Wu and Chern[77] have adopted a cyclic network reduction technique to derive a rate expression for the degradation of methylene blue. The decomposition rate was found to depend on the

Figure 7: Detailed pathway of degradation of phenol and 4-chlorophenol adapted from different studies. Some of the primary and secondary intermediates are identified as Ph – phenol, 4CP – 4-chlorophenol, Cat – catechol, HQ – hydroquinone, 4cCat – 4-chlorocatechol, PY – pyrogallol, MU – muconic acid and HHQ – hydroxyl hydroquinone. (Redrawn from ref. 42,43,78.)
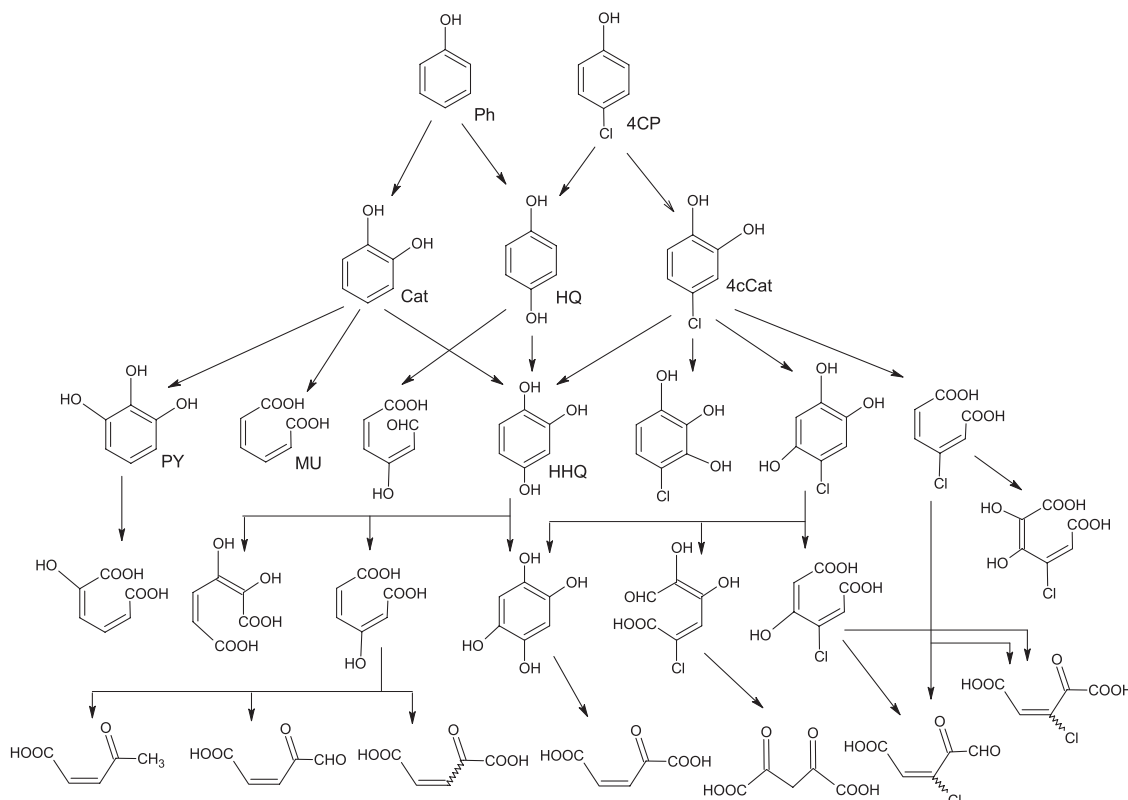
initial concentration of the dye, light intensity, TiO_2 loading and dissolved oxygen concentration. Their rate expression was given by

$$-r_A = \frac{k'_a C_A}{1 + k'_b C_A} \qquad (41)$$

where, $k'_a = \frac{k_4[hv][TiO_2]}{1+k_1[hv]}$ and $k'_b = \frac{k_2+k_3[hv]}{1+k_1[hv]}$. The concentration profiles were simulated by integrating the equation in the limits $C_A|_{t=0} = C_{A0}$ and $C_A|_{t=t'} = C_{At}$. The rate coefficients were determined by non-linear curve fitting of the following expression with the experimental data

$$\ln\left(\frac{C_{At}}{C_{A0}}\right) + k'_b(C_{At} - C_{A0}) = -k'_a t. \qquad (42)$$

6.2. Phenolic compounds

Phenolic compounds like phenol, chlorophenols, nitrophenols, aminophenols, and other substituted phenols are widely used as intermediates for the synthesis of fine chemicals, pesticides, herbicides, and drugs in the chemical industry. Early works on the photocatalytic degradation of organic compounds have thoroughly investigated the mechanism and pathway of mineralization of a number of phenolic compounds. The degradation of phenolic compounds proceeds primarily by the attack of the hydroxyl radicals, which results in the hydroxylation of the parent compound at the ortho- or para-position, due to the ortho- or para-directing nature of the phenolic –OH group.[42,43] These are the primary intermediates, which on further exposure results in the formation of a fully hydroxylated secondary intermediate species. Further oxidation results in the fragmentation of the benzene ring to form C-6 and C-5 aliphatic carboxylic acids and aldehydes. In the case of chloro- or nitro-substituted phenols, the hydroxyl group replaces the substituent group before the ring fragmentation. The longer (C-6, C-5, C-4) chain organic acids and aldehydes on longer exposure periods yield C-3, C-2 and C-1 organic acids. Finally, these shorter chain compounds mineralize to form CO_2 and H_2O. Li et al.[78] have elucidated the mechanism of formation of the intermediates during the photocatalytic degradation of 4-chlorophenol and 4-chlorocatechol. Figure 7 shows the degradation

pathway of phenol and 4-chlorophenol, adapted from different studies.[42,43,78] The photocatalytic degradation of phenol and 4-chlorophenol yield catechol, hydroquinone and chlorocatechol as the primary hydroxylated intermediates. The secondary hydroxylation step results in the formation of pyrogallol, hydroxy hydroquinone, and 4-chloro dihydroxy phenols. This step is followed by the fragmentation of the dihydroxy phenols to form chloro- and hydroxyl- substituted muconic acid and muconic aldehydes. Muconic acid further degrades to small organic acids like oxalic acid, maleic acid, succinic acid, fumaric acid, acrylic acid, etc. Finally, these acids mineralize to CO_2 and H_2O at long exposure periods.

Sivalingam et al.[42] have studied the effect of different substituents like chloro-, nitro- and methyl group on the kinetics of photocatalytic degradation of phenol using CS TiO_2 and DP-25. The order of degradation follows: pentachlorophenol > trichlorophenol > dichlorophenol > 4-chlorophenol $\approx$ 2-chlorophenol > 2-methyl phenol $\approx$ 3-methyl phenol > phenol. Similarly, Priya and Madras[43] have conducted a thorough study on the effect of multiple substitutions of the above groups on the degradation of phenol. Their results show that chloro-methylphenols (cresols) degrade much faster compared to chloro-nitrophenols, which can be attributed to the ring deactivating nature of the nitro group for the hydroxyl radicals to react with the phenolic compound. Moreover, it was found that the degradation is independent of the position of the substituents, but depends on the nature of the substituent group. In another study,[44] nitro-substitution was found to retard the degradation rate of nitrobenzene, while chloro- and hydroxy-substitution resulted in an enhancement in the degradation rate.

We have investigated the photocatalytic degradation of mixtures of 4-chlorophenol and 4-nitrophenol to simulate the industrial effluent, which is usually composed of a mixture of many organic compounds.[79] It was found that the degradation of chlorophenol was unaffected by the presence of nitrophenol, while the degradation of nitrophenol was significantly affected by the presence of the chlorophenol. The rate of degradation of chlorophenol (cp) and nitrophenol (np) was modeled using the following rate equations with individual L–H rate parameters (k_{cc}, K_{cp}, k_{nn} and K_{np}) and interaction parameters (k_{cn} and k_{nc}).

$$-r_{cp} = \frac{(k_{cc} - k_{cn}C_{np})C_{cp}}{1 + K_{cp}C_{cp} + K_{np}C_{np}} \quad (43)$$

$$-r_{np} = \frac{(k_{nn} - k_{nc}C_{cp})C_{np}}{1 + K_{cp}C_{cp} + K_{np}C_{np}}. \quad (44)$$

The above model accounts for the inhibition of the rate of degradation of cp by np, and np by cp through the competition of cp and np for the active site of TiO_2. The rate coefficients were determined by linearizing the above expressions.

As described before, phenolic compounds or any organic compound mineralize to CO_2 and H_2O through the formation of intermediates during the degradation. The formation and consumption rate of these intermediates provide useful insights on the relative importance of the different reaction steps that lead to the mineralization of the organic compound. Previous studies on the degradation of phenolic compounds, dyes, and pesticides have monitored the concentration of the various intermediates during degradation. The predominant intermediates that were observed during the degradation of phenol include, catechol, hydroquinone, hydroxyl hydroquionone, benzoquinone, and oxalic acid. A simple series reaction mechanism with first order reactions can be used to model the formation and consumption rate of the intermediates. This is represented as[42,43]

$$A \xrightarrow{k_f} \text{Intermediate} \xrightarrow{k_c} \text{Product} \quad (45)$$
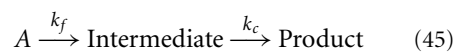
where, k_f and k_c are the formation and consumption rate coefficients of the intermediates. By writing rate equations for A, intermediate and the product, an expression for the concentration of the intermediate can be derived as[80]

$$\frac{C_{int}}{C_{A0}} = \frac{k_f}{k_c - k_f}\left(\exp(-k_f t) - \exp(-k_c t)\right). \quad (46)$$

The above expression suggests that the concentration profiles of the primary hydroxylated species show an initial increase and then decrease with time due to the subsequent formation of secondary hydroxylated species. Hence, there is a time (t_{max}) at which the concentration of the intermediate is maximum (C_{max}). Therefore, by differentiating the above equation with respect to t and C_{int}, expressions for t_{max} and $C_{int,max}$ can be derived as[80]

$$t_{max} = \frac{\ln(k_f/k_c)}{k_c(k_f/k_c - 1)} \quad (47)$$

$$\frac{C_{int,max}}{C_{A0}} = \left(\frac{k_f}{k_c}\right)^{1/(1-k_f/k_c)}. \quad (48)$$

Thus by solving the above two equations with t_{max} and $C_{int,max}$ data from the experiments, k_c and k_f can be determined. More importantly, the ratio k_c/k_f, which signifies the relative rate at which the intermediate is consumed, can be used as a quantifying factor to assess the stability of the different intermediates during the mineralization of the parent compound.

Figure 8: Pathway of degradation of the pesticide methyl parathion (MP) in presence of DP-25 TiO_2 under UV illumination. Some of the intermediates are identified as MPO – methyl paraoxon, 4-NP – 4-nitrophenol, HQ – hydroquinone, HHQ – 2-hydroxy hydroquinone, AA – aliphatic acid, FA – formic acid. (Redrawn from ref. 83.)
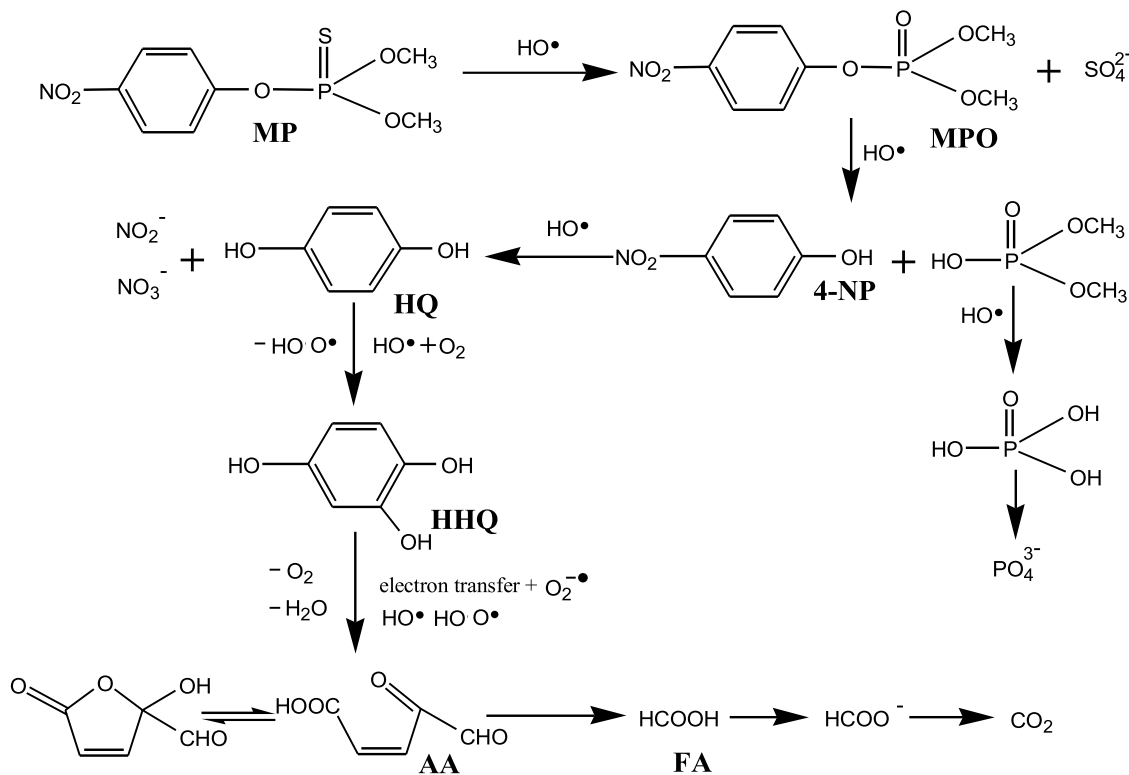
6.3. Pesticides

Pesticides are widely used for protecting agricultural crops from insects, pathogens, weeds, moths, microbes, etc. However, the continuous usage of pesticides results in poor soil quality, reduced nitrogen fixation for plants and poisoned food sources for animals. More importantly, pesticide contamination in drinking water results in serious health hazards for human beings and animals. Based on the chemical structure, pesticides are classified as organochlorine compounds, organo phosphorous compounds and carbamate compounds, which contain nitrogen, phosphorous, sulfur, chlorine and heterocyclic nitrogen atoms in their molecule. Therefore, the mineralization of the pesticides should result in the conversion of these hazardous compounds to innocuous products of N, S and P, along with CO_2 and H_2O. Many studies have elucidated the pathway of degradation of commonly used pesticides like atrazine,[81] pyridaben,[82] methyl parathion,[83] methamidophos,[84] triazophos,[85] dicofol,[86] etc. using TiO_2, by monitoring the formation of intermediates by HPLC/MS/MS and GC/MS techniques. It was found that, during mineralization,

phosphorous is converted to orthophosphoric acid (H_3PO_4), nitrogen to NO_3^- and NH_4^+ ions, and sulphur to SO_4^{2-} ions. Figure 8 depicts the pathway of degradation of methyl parathion, an organophosphorous insecticide.[83]

6.4. Pharmaceutical compounds

Recently, photocatalytic degradation of pharmaceutical compounds and drugs are widely studied, as these compounds are admitted into waste water and aquatic bodies by the manufacturing operations, spillage, human and animal excretion, and hospital wastes, in μg L^{-1} to ng L^{-1} levels. Besides leading to serious hazards like genotoxicity, endocrine disruption and aquatic toxicity, these xenobiotic substances increase the resistance of the pathogenic bacteria in waste water. As these compounds are resistant towards biological degradation and other common oxidation techniques, they build up their concentration in the ecosystem. In fact, clofibric acid, which is used as a regulator of lipids in the blood is still detected in lakes and rivers, even after 21 years of persistence in the environment.[87]

A wide class of pharmaceutical compounds has been photocatalytically degraded using TiO_2. Some

Table 5: Photocatalytic disinfection of microorganisms using different catalysts and different reaction conditions.

Sl. No.	Microorganism	Catalyst material	Reaction conditions	Reference
	Disinfection in presence of UV radiation			
1	*Legionella pneumophila*	TiO_2	I = 108 μW cm^{-2}; [C] = 1 g L^{-1}; [M] = 10^7 cfu mL^{-1}	[95]
2	*Bacillus anthracis*	TiO_2	I = 0.42-2.43 mW cm^{-2}; [C] = 10–100 mg; [M] = 700–1900 cfu mL^{-1}	[96]
3	*E. coli, Lactobacillus helveticus*	TiO_2 and ZnO	I = 20 W m^{-2}; [C] = 1,2 g L^{-1}; [M] = 10^8 cfu mL^{-1}	[97]
4	*E. coli, Bacillus megaterium*	TiO_2, V doped TiO_2, Au capped TiO_2 composites	Different [C]; [M] = 10^8–10^9 cfu mL^{-1}	[98]
5	*E. coli*	Ag impregnated TiO_2	I = 0.5 W m^{-2}; [C] = 2 g L^{-1}; [M] = 10^9 cfu mL^{-1}	[99]
	Disinfection in presence of visible radiation			
6	*E. coli, Staphylococcus aureus*	AgI/TiO_2	I = 2.8 mW cm^{-2}; [C] = 0.2 g L^{-1}; [M] = 5×10^7 cfu mL^{-1}	[100]
7	*E. coli*	Montmorillonite supported Ag/TiO_2	[C] = 0.4 g L^{-1}; [M] = 1–4×10^8 cfu mL^{-1}	[101]
8	*E. coli, Pseudomonas aeruginosa, Staphylococcus aureus*	PdO and N doped TiO_2	I = 0.4–1.6 mW cm^{-2}; [C] = 1 g L^{-1}; [M] = 10^7 cfu mL^{-1}	[102]
9	*E. coli*	Graphene oxide-TiO_2 thin films	Sunlight; [M] = 10^6 cfu mL^{-1}	[103]
10	*Microcystin-LR*	N-F-codoped TiO_2	I = 78 μW cm^{-2}; [M] = 1 mg L^{-1}	[104]

I – Light intensity; [C] – catalyst concentration; [M] – concentration of microorganism

of them include (i) antibiotics (chloramphenicol,[88] ciprofloxacin,[89] sulfamethoxazole[90]), (ii) analgesics and antipyretics (paracetamol,[91] phenazone[87]), (iii) non-steroidal anti inflammatory drugs (diclofenac, naproxen, ibuprofen)[92], (iv) beta blocker (atenolol)[93] and (v) anticholestric (clofibric acid).[87] Generally, it is observed that the time taken for the complete mineralization is longer compared to the removal of the parent compound, indicating that the degradation intermediates are quite stable. Moreover, toxicity tests prove that the intermediates formed during the degradation are more toxic compared to the parent pharmaceutical compound. Calza et al.[94] have studied the photocatalytic degradation and ecotoxicity of amiloride, a diuretic agent, and conclude that although amiloride is non-toxic, the degradation intermediates are toxic compounds. Thus, it is more important to mineralize the pharmaceutical compounds rather than just investigating the disappearance of the parent compound.

6.5. *Inactivation of microorganisms*
Microorganisms like pathogenic bacteria, fungi, viruses and protozoa in drinking water and air are hazardous to human and animal life, as they lead to infectious diseases like cholera, gastroenteritis, malaria, yellow fever, tuberculosis, anthrax, etc. Conventional low cost disinfectants include chlorine, chlorine dioxide (ClO_2), hypochlorite (OCl^-) and ozone, which are used in a wide range of pH. However, the application of the above disinfectants result in the formation of halomethanes and halo acetic acids, which are carcinogenic even at low concentrations. Hence, photolytic (UV-C radiation at 254 nm) and photocatalytic disinfection (UV-A at 365 nm or visible radiation) using TiO_2 as the photocatalyst has been researched extensively over the past two decades. Table 5 shows the different studies[95–104] devoted to the deactivation of various kinds of microorganisms using different catalysts. *Escherichia coli* (*E. coli*), a Gram negative rod shaped bacterium is the most common microorganism that is found in waste waters, due to its presence in the intestine of humans, animals and birds. Hence, it is used a biological indicator to test the environmental samples for faecal contamination. Unlike the organic compounds, the concentration of microorganisms is usually expressed in terms of the number of colony forming units per mL of the solution (cfu mL^{-1}). CFU refers to the number of viable microbial colonies, which are measured by counting the cell aggregates on an agar plate.

The mechanism of photocatalytic disinfection of microorganisms is quite complex compared to the degradation and mineralization of organic compounds, due to the large size and complex structure of bacteria and other living microorganisms compared to organic molecules. This results in several pathways of cell rupture and regeneration. Cho et al.[105] have shown that the inactivation time (for 2-log reduction) of *E. coli* under different reaction conditions is directly proportional to the hydroxyl radical concentration in the system. In fact, hydroxyl radicals are more important than the reactive oxygen species, and it is many times as effective as common oxidants like chlorine, chlorine dioxide or ozone.

Matsunaga et al.[106] have proposed that the cell wall damage of the microorganism during

photocatalytic degradation is due to a decrease in Coenzyme A (CoA) content of the cell, which is a mediator of electron transport between the cell and TiO_2. Saito et al.[107] have observed a "rapid" leakage of potassium ions and a "slow" release of protein and RNA during the lysis of *Streptococcus sobrinus*, in presence of UV/TiO_2. Thus they concluded that the loss of permeability of the cell wall of the bacteria leads to inactivation. Maness et al.[108] have suggested that the attack of active species like hydroxyl, hydroperoxy and superoxide radicals on the polyunsaturated phospholipids of *E. coli* result in lipid peroxidation, and hence result in the loss of respiratory activity of the cell. Thus it is certain that the cell wall damage induced by the active species in presence of UV/TiO_2 is the primary cause for the death of the microorganisms. However, complete disinfection (99.999%), even after the removal of TiO_2 and radiation, has to be ensured, because, the presence of active bacteria might result in their reproduction, as the organic compounds like aldehydes, ketones and carboxylic acids, which are usually the products of cell lysis, serve as nutrients for further growth. Moreover, the inactivation rate of microorganisms in pure deionized water is higher compared to that in the presence of tap water or water contaminated with ionic species or humic substances.[109] This is due to the osmotic stress in deionized water, which results in the easy leakage of potassium, calcium and magnesium ions through the cell membrane, thereby leading to the loss of permeability. Moreover, humic substances compete for the reactive radicals, which results in the inhibition of the disinfection rate.

From Table 5, it is clear that TiO_2 and its modified forms exhibit superior UV and visible light photocatalytic activity for the disinfection of a wide class of Gram-positive and Gram-negative bacteria and other microorganisms, in a broad range of initial concentrations (10^5–10^9 cfu mL^{-1}). It is also observed in most of the studies that, the optimum catalyst concentration required for the degradation of microorganisms is lesser than that required for the degradation of organic compounds. Many studies have also shown that the presence of Ag in TiO_2 results in higher disinfection rates compared to bare TiO_2.[99,100,101] Ag promotes the biocidal activity of TiO_2 in three different ways: (i) due to the inherent antimicrobial activity, Ag^+ complements the disinfection ability of TiO_2, (ii) Ag, when impregnated on the surface of TiO_2, acts as electron trapping sites, which retards the unwanted charge-carrier recombination, (iii) due to the surface-plasmon excitation, nano-sized Ag promotes the formation of more electrons in presence of

visible radiation, which results in the formation of hydroxyl radicals through the superoxide radical pathway. The synthesis of Ag nanoparticles and their incorporation onto different substrates by different techniques, and the anti-microbial activity are discussed elsewhere.[110]

Microorganisms exhibit quite different photodegradation kinetics compared to organic compounds, as the inactivation profiles are characterized by three distinct regimes,[111] viz., (i) a "shoulder" or slow deactivation of the microorganisms due to the self-defence and autorepair mechanism of the bacterial cell membrane against the hydroxyl radicals, (ii) a log-linear reduction in concentration due to the perforation of the bacterial membrane, and (iii) a slow reduction in concentration or tailing of the concentration profile due to the competition between the organic compounds released into the medium and the microorganisms. Several empirical models have been proposed to account for the different regimes of deactivation of microorganisms.[112] These include delayed Chick-Watson equation, modified Chick-Watson equation, Hom, and modified Hom equations. The modified Hom equation, which best fits the bacterial concentration profile is expressed as

$$\log \frac{C_0}{C} = k_1[1 - \exp(-k_2 t)]^{k_3} \qquad (49)$$

where, C_0 and C are the initial concentration and concentration at time 't' of the microorganism in the system, and k_1, k_2 and k_3 are the fitting parameters, which bear no physical significance.

Marugán et al.[112] have recently proposed a mechanism for the deactivation of *E. coli*, which is represented as

$$C_{\text{undamaged}} \xrightarrow{k_1} C_{\text{damaged}}$$

$$\xrightarrow{k_2} C_{\text{inactivated}} \xrightarrow{k_3} C_{\text{product}} \qquad (50)$$
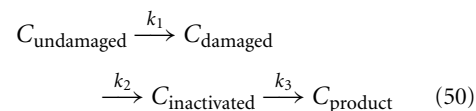
where, $C_{\text{undamaged}}$ denotes the undamaged population of the microorganism, C_{damaged} denotes the lumped population at all intermediate levels of damage, $C_{\text{inactivated}}$ denotes the microorganisms in the inactive state, and C_{product} denotes the products of microbial cell lysis that are released into the reaction medium. The L–H-like model for the above mechanism is given by[112]

$$\frac{dC_{\text{undamaged}}}{dt} =$$

$$-k \frac{K C_{\text{undamaged}}^n}{1 + K C_{\text{undamaged}}^n + K C_{\text{damaged}}^n} \qquad (51)$$

$$\frac{dC_{\text{damaged}}}{dt} =$$

$$k\frac{KC^n_{\text{undamaged}} - KC^n_{\text{damaged}}}{1 + KC^n_{\text{undamaged}} + KC^n_{\text{damaged}}} \quad (52)$$

where, the rate coefficients k, K and n correspond to the interaction of the hydroxyl species with the microorganism, microorganism with TiO_2 and the products of bacterial lysis with the hydroxyl species, respectively. The rate coefficients K, k and n signifying the pseudo-adsorption, inactivation and inhibition, represent the initial lag, log-linear decrease and final lag phases of the bacterial disinfection profiles, respectively. The above model has been validated for the deactivation of *E. coli* with different catalysts of varying catalyst concentrations, and in presence of anions like chloride, bicarbonate and phosphate, and humic acids.[113]

6.6. *Presence of anions and oxidizing agents*
Industrial effluents are composed of a large number of organic compounds, humic substances and inorganic substances like anions and metal ions. Hence, an evaluation of the degradability of the organic compound under the influence of such externally added ions assumes importance. Generally, anions like carbonate, bicarbonate, chloride and sulfate ions retard the degradation of organic compounds by scavenging the hydroxyl radicals to form the respective anion radicals, according to the following reactions[61−64]

$$CO_3^{2-} + OH^\bullet \longrightarrow CO_3^{\bullet-} + OH^{\bullet-} \quad (53)$$

$$HCO_3^- + OH^\bullet \longrightarrow CO_3^{\bullet} + H_2O \quad (54)$$

$$Cl^- + OH^\bullet \longrightarrow Cl^\bullet + OH^- \quad (55)$$

$$SO_4^{2-} + OH^\bullet \longrightarrow SO_4^{\bullet-} + OH^-. \quad (56)$$
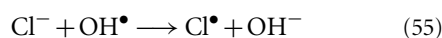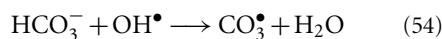
Azevedo et al.[114] have evaluated the effect of saline media on the photocatalytic degradation of phenol, and concluded that at low concentrations of NaCl (2 g L^{-1}), the rate was unaffected, while at high concentrations of NaCl (50 g L^{-1}), there was a drastic reduction in the rate of degradation of phenol. Devi et al.[115] have evaluated the effect of anions on the degradation of anionic and cationic dyes, and found that the presence of sulfate anion results in the highest reduction in the degradation rate of the dyes, while the presence of oxalate anion shows the lowest reduction in rate. Thus the reduction in rate due to the presence of different anions for the degradation of Rhodamine B follows the order: $SO_4^{2-} > Cl^- > HCO_3^- > NO_3^- > CO_3^{2-} > C_2O_4^{2-}$. Similar retardation effect was also observed for the inactivation of *E. coli*.[109]

The order of inactivation follows: $Cl^- > NO_3^- > SO_4^{2-} \gg HCO_3^- > HPO_4^{2-}$, where the chloride and phosphate ions exhibit the minimum and maximum inhibiting effect, respectively.

The presence of oxidizing agents like persulfate and H_2O_2 has a positive effect on the degradation rate of the organic compound, and it is attributed to the generation of more hydroxyl radicals by these oxidizing agents, according to the following reactions[61−64]

$$S_2O_8^{2-} + e_{CB}^- \longrightarrow SO_4^{2-} + SO_4^{\bullet-} \quad (57)$$

$$SO_4^{\bullet-} + H_2O \longrightarrow SO_4^{2-} + OH^\bullet + H^+ \quad (58)$$

$$H_2O_2 + O_2^{\bullet-} \longrightarrow OH^\bullet + OH^- + O_2. \quad (59)$$
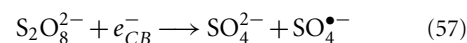
It was observed that, when the concentration of H_2O_2 is above an optimum concentration, the following reactions occur, which result in the quenching of the hydroxyl radicals, thereby resulting in a reduction in the degradation rate

$$H_2O_2 + OH^\bullet \longrightarrow H_2O + HOO^\bullet \quad (60)$$

$$HOO^\bullet + OH^\bullet \longrightarrow H_2O + O_2 \quad (61)$$
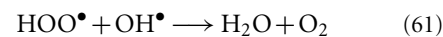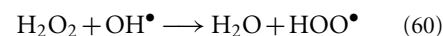
Therefore, a careful optimization of the concentration of the oxidants is necessary to achieve the maximum photocatalytic degradation rates.

6.7. *Presence of metal ions*
Metal ions are discharged into the water bodies as a result of an array of manufacturing and processing operations involved in chemical, metallurgical, electroplating, and photographic industries. Many metal ions like Ag^+, Hg^{2+}, Cu^{2+}, Pb^{2+}, Cd^{2+}, Ni^{2+} and Cr^{6+} are toxic and have infinite lifetimes. Their accumulation in the environment leads to biomagnification. Many studies have evaluated the photocatalytic reduction of metal ions from their toxic to non-toxic states.[47,116] Chen and Ray[116] have studied the photocatalytic reduction of most of the above mentioned metal ions using Hombicat UV 100 TiO_2 and DP-25 TiO_2. They have observed that DP-25 was very effective compared to Hombicat TiO_2 in the reduction of metal ions like Ag^+, Hg^{2+}, Fe^{3+} and Cr^{6+}. It was also observed that the presence of ferrous ion enhanced the reduction rate of mercury. It is imperative to note that metal ion reduction occurs primarily through the formation of conduction band electrons, and hence, the presence of electron scavengers like dissolved O_2 in the system results in retardation of the reduction rate.

A number of studies have also evaluated the simultaneous oxidation of organic compounds and reduction of metal ions using TiO_2. Prairie et al.[117] have studied the effect of different organic

Figure 9: Concentration profiles of phenol, Cu^{2+} ions, and the intermediates, catechol and hydroquinone during the simultaneous photocatalytic degradation of phenol and reduction of Cu^{2+} to Cu^+. It is clear that the presence of phenol increases the rate of reduction of Cu^{2+}. The lines for hydroquinone and catechol are model fits based on equation (47) and (48). (Redrawn from ref. 122.)

Cu^{2+} and F^- ions using DP-25 TiO_2. The first order degradation rate coefficient of phenol in presence of different ions exhibited the following trend: $k(Cu^{2+}+F^-) > k(F^-) > k(Cu^{2+}) > k(without Cu^{2+} or F^-)$. They have attributed the above effect to the enhanced charge-carrier separation induced by the presence of both Cu^{2+} and F^-.

Solution pH is one of the key factors that influences the reduction of metal ions. Many studies have carried out the degradation-reduction reactions in the acidic pH regime (pH = 3 to 5). The reduction of Cr^{6+} to Cr^{3+} occurs in the presence of protons, according to the following reaction[122]

$$2Cr_2O_7^{2-} + 16H^+ \rightarrow 4Cr^{3+} + 8H_2O + 3O_2. \quad (62)$$
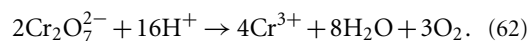
It is clear that an acidic medium can provide excess protons for the reduction of Cr^{6+} compared to the neutral or basic medium. Moreover, metal ions like Cr^{6+} and Cu^{2+} precipitate as hydroxides in the basic pH regime, which prevents them from getting adsorbed onto the TiO_2 surface.

Vinu and Madras[122] have recently observed that the presence of phenol accelerated the reduction of Cu^{2+} to Cu^+, while this was not possible in the absence of phenol (Figure 9). The presence of Cu^{2+} ions did not significantly affect the degradation rate of phenol, while the presence of Cr^{6+} enhanced the degradation of phenol. Moreover, the presence of metal ions resulted in the formation of stable intermediates, viz., catechol and hydroquinone, which were not observed during the degradation of phenol in the absence of metal ions. Therefore, it can be summarized that the simultaneous degradation-reduction of such two-component systems containing an organic compound and a metal ion is dependent on the pH of the solution, concentration of the metal ion and the organic compound, adsorption of the metal ion and the electronic state of the metal ion.

The kinetic modeling of such multicomponent systems shed useful insights on the interaction among the different species in the system, competition of the reactants and products for the active TiO_2 site, and the mechanism of degradation. The retardation of the rate of degradation of dyes in presence of metal ions was modeled by Aarthi et al.,[40] and their kinetic model relating the rate of degradation of the dye (r_D) with the concentration of the dye $[D]$ and the metal ion $[M^{n+}]$ is given by

$$-\frac{1}{r_D} = \left(\frac{1}{[D]} + K_2\right)\frac{(1 + K_6[M^{n+}])}{(k_0 + K_6 k_7[M^{n+}])}. \quad (63)$$

The lumped rate coefficients in the above model, viz., K_2, K_6, k_0 and k_7 were determined by non-linear

compounds on the reduction of different metal ions, and vice versa, and have shown that the highest degradation rate of salicylic acid is observed in the presence of Au^{3+}, and highest reduction rate of Cr^{6+} to Cr^{3+} is observed in the presence of Na_2-EDTA, salicylic acid and citric acid. They have also observed that the rate of the reduction of Cr^{6+} to Cr^{3+} is strongly dependent on the concentration of salicylic acid, and the rate constant exhibits a sudden drop at salicylic acid concentrations higher than the optimum value. An important outcome of their study indicated that only those metal ions whose half-reaction standard reduction potential is greater than 0.3 V (vs NHE) can be treated by photocatalysis.

A careful evaluation of the works of Chen et al.,[118] Aarthi and Madras,[40] and Kyung et al.[119] shows that the rate of degradation of Rhodamine B decreases in the presence of Cu^{2+}, Fe^{3+}, Zn^{2+} and Al^{3+}, while an enhancement in the rate is observed in the presence of Cr^{6+} and Ag^+ ions. In another study, it was found that, among the different metal ions like Cu^{2+}, Fe^{3+}, Mn^{4+}, Ce^{4+} and V^{5+}, only Cr^{6+} enhanced the degradation rate of 4-chlorophenol.[120] Similarly, the presence of 4-chlorophenol also increased the reduction rate of Cr^{6+}. The above studies collectively suggest that the electronic state of the metal ions plays a major role in deciding the degradability of the organic compound. Wang et al.[121] have studied the photocatalytic degradation of phenol in presence of

Figure 10: Dual cycle network mechanism depicting the simultaneous photocatalytic oxidation of phenol and the reduction of Cu^{2+}. (Redrawn from ref. 122.)
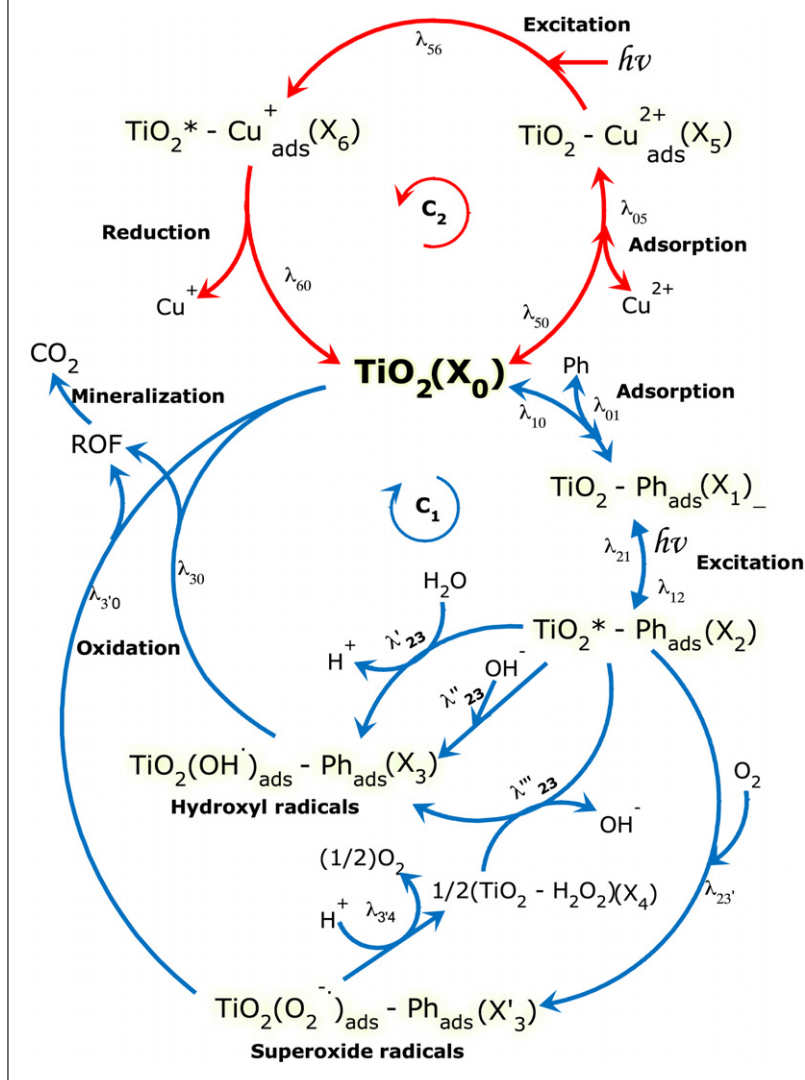
regression, and the model was successfully validated for the degradation of different dyes like Rhodamine B,[40] Rhodamine 6G,[40] Sulforhodamine B[40] and Azure B,[123] in presence of Cu^{2+}. However, the above model does not account for the rate of reduction of metal ions during the degradation of the organic compound. Hence, we have recently modeled the simultaneous and synergistic degradation of phenolic compounds (phenol and 4-nitrophenol), and the reduction of metal ions (Cu^{2+} and Cr^{6+}), by assuming competitive adsorption of the metal ions and the phenolic compound onto the TiO_2 surface.[122] Figure 10 shows the proposed dual-cycle network mechanism. The steady state rates through the individual phenol degradation pathway (C_1) and metal ion reduction pathway (C_2) were derived

using the network reduction technique, and are given by

$$\left(-\frac{1}{r_{Ph,0}} - K_2\right) = \frac{1}{[Ph]_0}\left(\frac{1}{K_1} + \frac{[M^{n+}]}{K_3}\right) \quad (64)$$

$$\left(-\frac{1}{r_{M^{n+},0}} - K_5\right) = \frac{1}{[M^{n+}]_0}\left(\frac{1}{K_4} + \frac{[Ph]}{K_6}\right) \quad (65)$$

where, $r_{Ph,0}$ and $r_{Mn+,0}$ denote the initial rate of degradation of the phenolic compound and the reduction of metal ions, respectively. This model accounts for the contribution of the metal ions on the rate of degradation of the phenolic compound and vice-versa. Using this model, the rate coefficients were uniquely determined by simple linear regression.

Figure 11: Normalized concentration profiles of 4-nitrophenol, when degraded photocatalytically in presence of different metal substituted TiO₂. The low degradation rates obtained with all the metal substituted TiO₂ compared to the unsubstituted TiO₂ are evident from the figure. (Redrawn from ref. 128.)
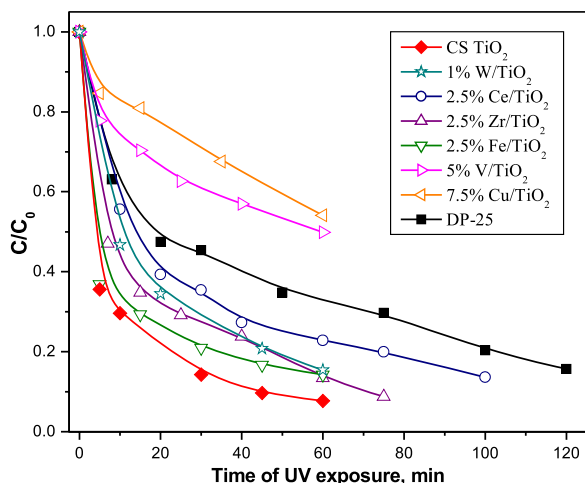
7. Visible light degradation of organic compounds

7.1. Second generation TiO₂ photocatalysts

Undoubtedly, the first generation TiO₂ or pristine TiO₂ is an efficient photocatalyst in the UV region. However, the wide band-gap (3.2 eV) of anatase TiO₂, corresponding to an absorption threshold of 390 nm, restrains its use in the visible range (400–800 nm) for practical applications using solar radiation as the light source. Hence, the second generation TiO₂ photocatalysts encompass a wide variety of the cationic and anionic substituents (or dopants) in TiO₂. The cationic dopants like lower valent (+1, +2, +3), iso valent (+4) and higher valent (+5, +6) metal ions, belonging to the class of noble metals, transition metals, lanthanide metals and alkaline metals are substituted for 'Ti', and anionic dopants like C, N and S are substituted for 'O' in the TiO₂ crystal lattice. Table 6[124–131] presents a sample of the various studies conducted on the photocatalytic activity of metal ion doped TiO₂. Although there is a general consensus that metal ion doping extends the absorption spectrum of TiO₂ to the visible region, the photocatalytic activity of the metal ion doped TiO₂ compared to the undoped TiO₂ varies across different studies. From the table, it is evident that doping of some metal ions enhances the photoactivity, while others result in a reduction in photoactivity.

Figure 11 presents the photocatalytic degradation profiles of 4-nitrophenol in presence of different metal ion substituted TiO₂ samples,

synthesized by solution combustion technique. It is evident from the figure that CS TiO₂ exhibits the fastest and DP-25 exhibits the slowest degradation rate, while all the metal ion doped TiO₂ samples exhibit intermediate degradation rates. To elucidate this behavior, Nagaveni et al.[128] have conducted a thorough photoluminescence study of the different metal ion doped TiO₂ ($M_x Ti_{1-x} O_{2\pm\delta}$) samples, and concluded that the decrease in photocatalytic activity is due to a reduction in the emission intensity of the metal ion doped samples. The metal ions form inter-band energy levels above the valence band or below the conduction band, which result in the lower band gap of the doped TiO₂ materials. The efficiency of a metal ion doped TiO₂ photocatalyst depends on whether the metal ion energy levels aid in the interfacial charge transfer or act as recombination centers. Choi et al.,[124] by studying the transient absorption decay of the trapped electrons, have shown that the dopant energy levels serve as trap sites for the electrons and holes, apart from the surface trap sites. Therefore, the low activity exhibited by metal ion doped TiO₂ is due to the fact that these states act as recombination centers according to the following reactions.[124]

$$e_{CB}^- \rightarrow e_{tr}^- \text{ (as Ti}^{3+} \text{ or } M^{(n-1)+}) \ \tau \approx 30 \text{ ps} \quad (66)$$

$$h_{VB}^+ \rightarrow h_{tr}^+ \text{ (as } > OH^\bullet \text{ or } M^{(n+1)+}) \ \tau \approx 250 \text{ ns} \quad (67)$$

$$e_{tr}^- + h_{VB}^+ \rightarrow TiO_2 \ \tau \approx 30 \text{ ns} \quad (68)$$

$$e_{tr}^- + h_{tr}^+ \rightarrow TiO_2 \text{ slow.} \quad (69)$$
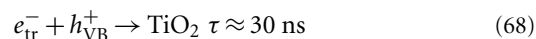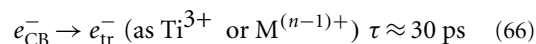
Based on the time scales, it can be said that the recombination of the trapped electron with the valence band hole (reaction (68)) is more feasible compared to reaction (69). Hence, it can be concluded that the photoactivity of metal ion doped TiO₂ strongly depends on the dopant concentration, energy level of the dopant within the TiO₂ lattice, d-electronic configuration, distribution of dopant, interfacial charge transfer and light intensity. Serpone and coworkers[125] have shown that doping of Cr^{3+}, Fe^{3+} and V^{5+} in the lattice of TiO₂ results in a lower photoactivity for the oxidation of oxalic acid, whereas the doped TiO₂ catalysts show an enhanced activity for the photoreduction of water to H₂. We have recently found that Pd^{2+} ion substitution in CS TiO₂ to be beneficial for gas phase NO reduction by CO, and NO decomposition,[129] while it exhibited a negative effect for liquid phase degradation of organic compounds.[132] In another study, we observed a high selectivity for the formation of cyclohexanone from cyclohexane using 1% Ag^+ substituted TiO₂, while the same catalyst exhibited lower rates for the degradation of dyes.[130] The above discussion shows that a generalization

of the activity of metal doped TiO_2 compared to the undoped TiO_2 is not possible for a wide class of reactions.

Metal ions can also be incorporated in TiO_2 by impregnation on the surface. Paola et al.[133] have investigated the effect of different transition metal impregnated TiO_2 for the photocatalytic degradation of aliphatic and aromatic compounds, and have found that the highest mineralization efficiency was obtained with bare TiO_2. In addition to the above result, Vinu and Madras[129,130] have shown that Pd and Ag impregnated TiO_2 exhibit higher photoactivity compared to the substituted TiO_2. The higher activity exhibited by the metal ion impregnated TiO_2 compared to the doped one can be attributed to the formation of Schottky barrier, which results in the scavenging of electrons and holes, thereby preventing the unfavorable recombination reaction.

Anion substituted TiO_2 is represented as $TiO_{2-x}D_x$, where D is usually N, C or S. The first study on anion substituted TiO_2, $TiO_{2-x}N_x$, was carried out by Asahi et al.[134] for the photocatalytic degradation of methylene blue and gaseous acetaldehyde in presence of visible radiation. Based on X-ray photoelectron spectroscopic analysis, they have observed an optimum concentration of N to be 0.25 at.% . Khan et al.[33,135] have synthesized $TiO_{2-x}C_x$, with a band gap of 2.32 eV by flame pyrolysis, and demonstrated the high activity for photosplitting of water (photoconversion efficiency = 8.35%). Unlike the cation doped TiO_2, anion doped TiO_2 exhibit high photoactivity in the visible region compared to the undoped and the commercial DP-25, by the narrowing of the band gap. This is because, anion doping results in the creation of a new valence band by the mixing of the anion dopant and O 2p orbitals. For example, the mixing of N 2p and O 2p orbitals contribute to the narrowing of the band gap of N doped TiO_2. The rules of thumb for any non-metal to be doped for oxygen in TiO_2 to elevate the valence band, are as follows:[136] (i) the electronegativity of the non-metal dopant should be lesser than that of oxygen, and (ii) the radius of the dopant should be comparable to that of oxygen for a more uniform distribution. However, Serpone[137] has demonstrated that the visible light activity of the anion doped TiO_2 is not due to the narrowing of the band-gap, but due to the defects associated with the oxide ion vacancy, which gives rise to the formation of color centers. The color centers are essentially a single or a pair of electrons associated with an oxygen vacancy. For MgO, it has been shown that the ground state of the color centers lie above the O 2p valence band. Table 7 (entries 1 to 7)[138–144] shows the different studies on the anion doped TiO_2 for the visible light degradation of organic compounds.

7.2. Heterostructuring of TiO_2
Heterostructuring refers to the modification of the surface of pristine TiO_2 by employing (i) narrow band gap semiconductor dopants (like CdS, PbS, CdSe, Bi_2S_3), (ii) dyes as sensitizers, and (iii) co-catalysts.[136] Different schemes of charge carrier transfer have been proposed for heterostructured TiO_2 materials, viz., traditional charge-carrier transfer, sensitization, indirect Z-scheme, direct Z-scheme, vectorial electron transfer and co-catalyst coupling. The main idea of the

Table 6: Effect of different metal ion substitutions in TiO_2 for the photocatalytic degradation of organic compounds.

Sl. No.	Organic compound	Substituted metal ion in TiO_2	Results	Reference
1	CCl_4 and $CHCl_3$	Fe^{3+}, Mo^{5+}, Ru^{3+}, Os^{3+}, Re^{5+}, V^{4+}, Rh^{3+}, Co^{3+}, Al^{3+}	Co^{3+} and Al^{3+} doping reduces the photoactivity, while all other metal ions in the concentration range of 0.1 to 0.5 at.% enhance the photoactivity	[124]
2	Oxalic acid	Cr^{3+}, Fe^{3+}, V^{5+}	The photoactivity of all the samples was lower compared to naked TiO_2	[125]
3	2-Chlorophenol	Nd^{3+}, Pd^{2+}, Pt^{4+}, Fe^{3+}	Order of photoactivity: Nd^{3+} > Pd^{2+} > Pt^{4+} ≈ undoped > Fe^{3+}	[126]
4	5,5-Dimethyl-1-pyrroline N-oxide (DMPO spin trap)	Cr^{3+}, Mn^{2+}, Co^{2+}	Absorption spectra of the doped samples shifted to the visible region; all the metal ion doped samples exhibit a lower photocatalytic activity for the generation of DMPO-OH and DMPO-O_2^- compared to undoped DP-25	[127]
5	4-Nitrophenol	Cu^{2+}, Fe^{3+}, Ce^{4+}, Zr^{4+}, V^{5+}, W^{6+}	Order of photoactivity: undoped CS TiO_2 > Fe/TiO_2 > W/TiO_2 > Ce/TiO_2 > Zr/TiO_2 > V/TiO_2 ≈ Cu/TiO_2	[128]
6	Various dyes and phenolic compounds	Pd^{2+}, Ag^+	Both the substitutions showed a lesser activity compared to undoped CS TiO_2; Pd^{2+} and Ag^+ impregnated TiO_2 showed a better activity compared to the doped TiO_2	[129,130]
7	Orange II	La^{3+}, Ce^{4+}, Pr^{3+}, Nd^{3+}, Sm^{3+}, Eu^{3+}, Dy^{3+}, Gd^{3+}	All the rare earth doped TiO_2 samples exhibit high visible light photoactivity compared to undoped TiO_2 in the concentration range of 0.5 to 1 wt.%	[131]

Table 7: A non-exhaustive survey of the different studies on the photocatalytic degradation of organic pollutants in presence of visible light using (a) anion-doped TiO_2, (b) sensitized TiO_2, (c) other semiconductor oxides and metal chalcogenides, and (d) VOCs.

Sl. No.	Organic compound	Photocatalyst / loading	Light source	Initial conc	% deg.	Time taken	Ref.
	Anion doped TiO_2						
1	Orange G	CS TiO_2; 1 g L^{-1}	Sunlight; 753 W m^{-2}	25 ppm	100	2 h	[138]
	RBBR			100 ppm	80	1.5 h	
	MB			100 ppm	90	4 h	
2	MB	C-doped TiO_2; 1 g L^{-1}	Sunlight; 21.28 W m^{-2}	10 ppm	100	1 h	[139]
3	MB	$Ti_{1-x}Ce_xO_{1-y}N_y$; x =0.007; 1 g L^{-1}	30 W FL	15 ppm	100	4 h	[140]
4	Phenol	S-doped TiO_2; 1 g L^{-1}	380 W Xe	100 ppm	100	100 min	[141]
5	4-Cp	CS TiO_2; 1 g L^{-1}	250 W Xe; 30 mW cm^{-2}			4 h	[142]
6	2,4-Dcp	C deposited TiO_2; 1 g L^{-1}	1000 W HL	50 ppm	60	5 h	[143]
	AO7			20 ppm	100	4 h	
7	Reactive Brilliant Red X-3B	C, N, S – tri doped mesoporous TiO_2; 1.5 g L^{-1}	250 W HL	100 ppm	70	2 h	[144]
	Sensitized TiO_2						
8	MB	3% Poly(aniline)/TiO_2	500 W Xe		80	5 h	[145]
	RhB				80	100 min	
9	MB	Nafion coated TiO_2, 45 mg nafion/g TiO_2; 0.5 g L^{-1} TiO_2	450 W Xe	13 ppm		11 h	[76]
	RhB			17.5 ppm		2 h	
	AO7			19 ppm		4 h	
10	MB, Malachite Green, R6G, RhB	Fluorinated TiO_2; 1 g L^{-1}	500 W HL	20 μM		30-120 min	[146]
11	MB	Mesoporous iron oxide-layered titanate nanohybrids	400 W Xe	10 μM	100	2 h	[147]
	Dichloroacetic acid			100 μM	60	5 h	
12	MB	DP-25 TiO_2/ graphene nano composite; 0.75 g L^{-1}	500 W Xe; 2mW cm^{-2}	10 ppm	65	1 h	[148]
13	MB	CdS quantum dot sensitized mesoporous TiO_2; 1.3 g L^{-1}	300 W WHL	10 ppm	95	3 h	[149]
	4-Cp			100 μM	70	4h	
14	MO	MoS_2 and WS_2 coupled TiO_2; 0.35 g L^{-1} for MB; 1 g L^{-1} for 4-CP	300 W WHL	8 ppm	60	4 h	[150]
	4-Cp			220 μM	70	6 h	
15	MO	Poly(3-hexyl thiophene) modified TiO_2; 1 g L^{-1}	300 W IWL	10 ppm	90	10 h	[151]
16	MO	1% Ag/$InVO_4$-TiO_2 composite thin film	15 W energy saving lamp; 30 mW cm^{-2}	10 ppm	45	15 h	[152]
17	Crystal Violet	3D-TiO_2 with core/shell – polymer/sensitizing dye	500 W Xe	400 ppm	75	30 min	[153]
18	Phenol	Pt deposited on I_2 doped TiO_2; 1 g L^{-1}	400 W dysprosium lamp	23.5 ppm	80	4 h	[154]
19	Phenol	TiO_2 and TiO_2/Pt sensitized by metallophthalocyanines; 1 g L^{-1}	100 W HL with 1M $K_2Cr_2O_7$ liquid filter	100 ppm	90	1 h	[155]
20	Phenol	TiO_2 deposited on multi walled carbon nanotubes; 1 g L^{-1}	500 W HPML	50 ppm	90	7 h	[156]
21	4-Cp	2% Pt(dcbpy)Cl_2-TiO_2; 1 g L^{-1}	300 W Xe	250 μM	80	3 h	[157]
22	4-Cp	Al tertacarboxy phthalocyanine adsorbed TiO_2; 1 g L^{-1}	500 W HL	230 μM	90	8 h	[158]
23	2,4-Dcp	Xanthene dyes sensitized DP-25 TiO_2; 0.4 g L^{-1}	500 W HL	16 ppm		5 h	[159]
24	Formic acid	V, Cr, Fe substituted, TiO_2 loaded MCM-41; 1 g L^{-1}	200 W MPML	460 ppm	25	3 h	[160]
	4-Cp			128 ppm	20	3 h	
	2,4,6-Tcp			197 ppm	50	3 h	
25	Acetaldehyde	Pt modified TiO_2	White FL; 5700 lux	150 ppm	90	1 h	[161]
26	Atrazine	Tetra(4-carboxy phenyl) porphyrin adsorbed TiO_2	Xe	20 ppm	80	1 h	[162]
27	Terbutyl azine	Rose Bengal (10 ppm)/ DP-25 TiO_2; 1 g L^{-1} TiO_2	500 W Xe	5 ppm	50	2h	[163]
28	Trichloroacetate and CCl_4	Pt/TiO_2 and Pt/TiO_2/$Ru^{II}L_3$ (10 μM); TiO_2 =0.5 g L^{-1}	450 W Xe	1 mM		2 h – 3 h	[164]

Table 7: Continued.

Sl. No.	Organic compound	Photocatalyst / loading	Light source	Initial conc	% deg.	Time taken	Ref.
	Other semiconductor oxides and metal chalcogenides						
29	Five organic compounds	Tin porphyrin immobilized on SiO_2	450 W Xe; 100 mW cm^{-2}	100 μM		2 h	[170]
30	R6G	Ag-ZnO; 3 mol.% Ag-ZnO; 1.2 g L^{-1}	Simulated sunlight; 0.68 W cm^{-2}	5 μM	100	4 min	[171]
31	Phenol, RhB, MO	Poly(fluorene-co-thiophene) modified ZnO; 1 g L^{-1}	Three 1 W LEDs	10 ppm phenol	40	2 h	[172]
32	Acid Red 66	Chitosan capped CdS composite nanoparticles; 0.7 g L^{-1}	300 W Xe; 2 W cm^{-2}	20 ppm	95	80 min	[173]
33	AO7	N and C co-doped ZnS (500 ^{o}C); 1.25 g L^{-1}	500 W Xe	2.5 ppm	100	10 h	[174]
	Volatile Organic Compounds (VOCs)						
34	Toluene	$TiO_{2-x}N_x$; 3 mg	500 W Xe; 4.3 mW cm^{-2}	100 ppm	100	720 min	[196]
35	Acetaldehyde TCE	N-F-co-doped TiO_2; 0.6 g	Blue LEDs; 4 mW cm^{-2}	930 ppm 943 ppm	55* 35*	350 min	[197]
36	Ethylene	$TiO_{2-x}N_x$ and $ZrO_2/TiO_{2-x}N_x$; 0.28 g	450 W HPML	227 ppm	50	50 min	[198]
37	Acetaldehyde	Bi_2WO_6 flake balls; 50 mg	300 W Xe	2200 ppm	100	12 h	[199]
38	Benzene	$Pt/TiO_{2-x}N_x$, $TiO_{2-x}N_x$; 1.2 g; H_2/O_2 =0.02	500 W Xe	825 ppm$_v$	80% mineralization		[200]

HPML – High pressure mercury lamp; MPML – medium pressure mercury lamp; deg. – degradation; MB – Methylene Blue; Rhodamine B – RhB; RBBR – Remazol Brilliant Blue R; AO7 – Acid Orange 7; R6G – Rhodamine 6G; MO – Methyl Orange; cp – chlorophenol; dcp – dichlorophenol; tcp – trichlorophenol; FL – Fluorescent lamp; Xe – Xenon arc lamp; HL – Halogen lamp; WHL – Tungsten halogen lamp; IWL – Iodine tungsten lamp; * - values represent the CO_2 yield.

above heterostructuring procedures is to isolate the oxidation reaction due to the holes, and the reduction reaction due to the electrons at two different sites, in order to prevent the charge-carrier recombination. Moreover, the incorporation of small band gap semiconductors, dyes and co-catalysts, increases the probability of absorption of radiation in the visible range. Liu et al.[136] have reviewed the above schemes in terms of their mechanism, materials and the key issues involved in their implementation. Some of the important design considerations of such heterostructured systems for the effective interfacial charge transfer are as follows:

(i) The wide band gap semiconductor (S1, usually TiO_2) and the narrow band gap semiconductor (S2) should have suitable electronic structure, i.e., S2 should have a higher conduction band minimum and valence band maximum compared to S1, for the smooth injection of electrons downhill from the conduction band of S2, and the transfer of holes uphill to the valence band of S2.

(ii) The above condition is also applicable for sensitizers, although there is no transfer of holes to the HOMO. Moreover, high surface area of TiO_2 is necessary for the enhanced adsorption of the sensitizer.

Table 8: Listing of the studies on the liquid phase and solid state degradation of polymers.

Sl. No.	Polymer	Reference
1	UV degradation of poly(acrylic acid), poly(methacrylic acid) and poly(vinyl pyrrolidone) in presence of H_2O_2	[176]
	Liquid phase degradation using TiO_2	
2	Poly(ethylene oxide), poly(acrylamide)	[45]
3	Poly(acrylamide-co-acrylic acid)	[177]
4	Poly(bispenol-A-carbonate)	[46]
5	Poly(methyl acrylate), poly(ethyl acrylate) and poly(butyl acrylate)	[178]
6	Poly(methyl methacrylate-co-alkyl acrylate) copolymers	[179]
	Solid phase degradation in the form of nano-composites	
7	Polystyrene-TiO_2	[180]
8	Low density polyethylene (LDPE)-TiO_2	[181]
9	Isotactic polypropylene-ZnO	[182]
10	Polyaniline-TiO_2	[183]
11	Poly(butylene succinate)-TiO_2	[184]
12	Poly(vinyl butyral)-TiO_2	[185]

Figure 12: Traditional charge transfer between two semiconductors with a narrow and wide band gap, depicting the isolation of reaction sites for oxidation and reduction.
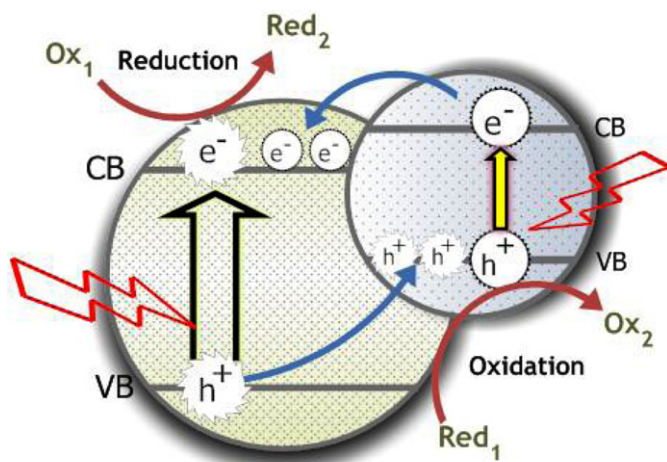
(iii) Intimate contact between the two different phases (PN junction in case of traditional transfer or Ohm/Schottky contact in case of co-catalysts) is necessary.

(iv) Suitable redox mediators (like Fe^{2+}/Fe^{3+}, I^-/IO^{3-}, Br^-/BrO^{3-}) are essential for the indirect Z-scheme and some sensitizer based systems.

Most of the above reaction schemes like the dye sensitized systems, indirect Z-scheme and co-catalyst coupling are widely employed for the water splitting reaction, although a number of studies have also reported the degradation of organic compounds (Table 7 (entries 8–28)[76,145−164]). Figure 12 depicts the traditional charge carrier transport mechanism for S1-S2 kind of heterojunction materials. In a series of reports, Bessekhouad and co-workers[165−167] have developed CdS/TiO_2, Bi_2S_3/TiO_2, Cu_2O/TiO_2, Bi_2O_3/TiO_2, $ZnMn_2O_4/TiO_2$ and PbS/TiO_2 heterojunctions, by the precipitation of the sensitizer with TiO_2. All the above materials exhibit enhanced absorption in the visible region 400–650 nm, and exhibit high visible light activity for the degradation of organic compounds like Orange II, 4-hydroxy benzoic acid, benzamide and eosin, compared to bare TiO_2. By optimizing the concentration of the sensitizers, it was found that the energy losses involved in the electron transfer can be minimized if the conduction band position of the dopant and the TiO_2 were matched. By comparing the band gap and emf of the heterojunctions, it was proposed that, for efficient photocatalytic degradation, the narrow band gap semiconductor should be the major absorber of light in the visible region, and the emf of the heterojunction should be low enough to obtain fast electron transfer kinetics.

7.3. *Mechanism of dye sensitized degradation*

This section describes the mechanism of electron transport in sensitized catalysts, for the degradation of organic compounds. Some of the common sensitizers include organic dyes, conjugated polymers and metal complexes. The sensitizers can either themselves be the organic pollutants to be degraded (as in the case of dyes), or they might induce electron transfer to the TiO_2 to induce the degradation of another organic compound in the system. Figure 13 depicts the network mechanism for the dye sensitized degradation of phenolic compounds. The various reaction pathways involved in the mechanism are numbered sequentially in the figure. The description of the reaction pathways are as follows.

(1) The first step is characterized by the adsorption of the dye (D) on the surface of TiO_2. The binding of the dye is dependent on (i) the functional groups that constitute the dye molecule (like hydroxyl, carboxyl and phosphoric acid end groups), and (ii) the surface charge of TiO_2.

(2) The adsorbed dye absorbs visible light photon ($\lambda > 400$ nm), and gets excited from HOMO (highest occupied molecular orbital) to the LUMO (lowest unoccupied molecular orbital).

(3) Photoexcitation of the dye is followed by the transfer of electron from the LUMO to the conduction band of TiO_2.[168] The driving force for this reaction is the energy difference between the LUMO and the conduction band of TiO_2. For Eosin Y, this driving force is 0.6 V (vs NHE at pH=3). The electron injection is accompanied by the concomitant formation of the dye radical cation ($D^{\bullet+}$) from the excited triplet state of the sensitizer.

(4) Generally, 50% of these radical cations escape into the bulk solution, while the rest undergoes the recombination reaction with the injected electron to form the ground state dye.[168] A pictorial representation of the electron injection process and the generation of hydroxyl radicals is given in Figure 14.

(5) This step denotes the degradation of the dye radical cation in the bulk solution.

(6) The trapped electrons in the conduction band are scavenged by the dissolved oxygen in the solution to form superoxide radicals. This undergoes a series of reactions, as shown in pathway -6-, and forms the hydroxyl species along with the regeneration of the ground state dye.

(7) Pathway -7- represents the generation of hydroxyl radicals from the excited state dye, through the formation of the semi-reduced form of the dye (DH•).[169]

(8) Surface adsorbed hydroxyl radicals are also formed via the adsorption of the dye onto the surface hydroxyl groups of TiO_2.

(9) Phenol (or any organic compound in the system) adsorbs onto the dye-TiO_2-OH· surface.

(10) Phenol undergoes oxidation due to the attack of hydroxyl radicals, and results in the formation of hydroxyl substituted intermediates. These undergo ring fragmentation on long exposure periods to form organic acids, which finally mineralize to CO_2 and H_2O.

Thus, the entire cycle is completed, when the products are desorbed from the surface of dye adsorbed TiO_2. The above mechanism accounts for the degradation of the dye along with the degradation of the organic compound, which is observed in dye sensitized systems.

The mechanistic differences observed with direct UV and dye sensitized systems are shown in Figure 14. Although the generation of hydroxyl radicals through the electron pathway is the same in both the mechanisms, the generation of electrons in the conduction band is through electron injection from the excited state of the dye in dye sensitized system, while it is through direct band gap excitation in UV photocatalysis. Therefore, it is imperative to note that valence band holes, which are strong oxidizing agents, are not involved in dye sensitized systems, and so the degradation efficiency is expected to be lower compared to the UV photocatalysis. Some of the recent examples of dye sensitized systems with TiO_2 for the degradation of organic compounds can be found in Table 7 (entries 8–28). Apart from TiO_2, other photocatalysts like ZnO, CdS and SiO_2 have also been used for this purpose (Table 7, entries 29–33)[170−174]. Some general observations from the various studies in Table 7 are worth noting. Although the catalyst concentration in the different studies varies from 0.4 to 5 g L^{-1}, 1 g L^{-1} was found to be the optimal loading in different studies. Xenon arc lamp and halogen lamp of different intensities, with cut-off filters were used as visible light sources in most of the studies. Hence, the time taken for the nearly complete degradation of organic compounds varies from 30 min to 10 h, which depends on the catalyst loading and the intensity of visible light radiation. Therefore, in order to have a proper comparison of the efficiency of the different catalyst systems for the degradation of organic compounds, the kinetic treatment of the experimental data assumes importance.

8. Photocatalytic degradation of polymers and plastics

Polymeric materials and plastics have become an indispensable part of the day-to-day life. However, the discarded plastics pose a potential threat to the environment, as they take a very long time to degrade under natural conditions. Plastic wastes contribute to about 9% of the total 1.20 lakh tons per day of the municipal solid waste generated in India.[175] Besides affecting the aesthetics of the environment, the ingestion of waste plastics, usually the packaging materials, results in the death of aquatic organisms, animals and birds. Many plastics are also non-biodegradable, and hence contribute to white-pollution. Historic waste disposal technique by landfilling is ineffective, as plastic bags at landfill sites take several decades to photodegrade. Hence, stringent regulations on the plastic waste disposal have led to the development of novel techniques for the degradation of the polymers. One of the conventional methods is by the incineration of the plastic waste. This method involves high temperatures and results in the generation of toxic gases before the polymer is fully mineralized. Therefore, polymer photodegradation has emerged as a non-conventional mode of degrading and recycling the waste polymers and plastics.

Photodegradation is an important mode of polymer degradation wherein the incident light radiation itself induces the scission of the macromolecule by the initiation of polymer radicals, or results in the generation of hydroxyl (·OH) radicals in presence of oxidizing agents and/or catalysts, which then attack the polymer backbone to initiate the radicals. Photodegradation of the polymers can be carried out either in the solid or liquid phase. In the solid state, the polymeric materials are exposed to UV radiation or sunlight in the form of thin films or sheets, while in the liquid phase, the polymers are dissolved in aqueous or organic solvents. Although the degradation of polymers in the solid state is more realistic from a practical viewpoint, liquid phase degradation is faster, owing to the homogeneous medium which offers enhanced mass transfer of the reactants and products. Moreover, liquid phase degradation is useful in studying the kinetics of chain scission of the polymers, by following the time evolution of the polymer molecular weight by gel permeation chromatography (GPC). Solid state degradation is monitored by different techniques, viz., reduction in weight of the sample with time, monitoring the changes in the surface morphology using scanning electron microscopy (SEM) and by monitoring the transmittance of the films by UV/vis or FT-IR spectroscopy.

Figure 13: Network mechanism for the dye sensitized degradation of phenolic compounds in presence of nano-TiO_2.
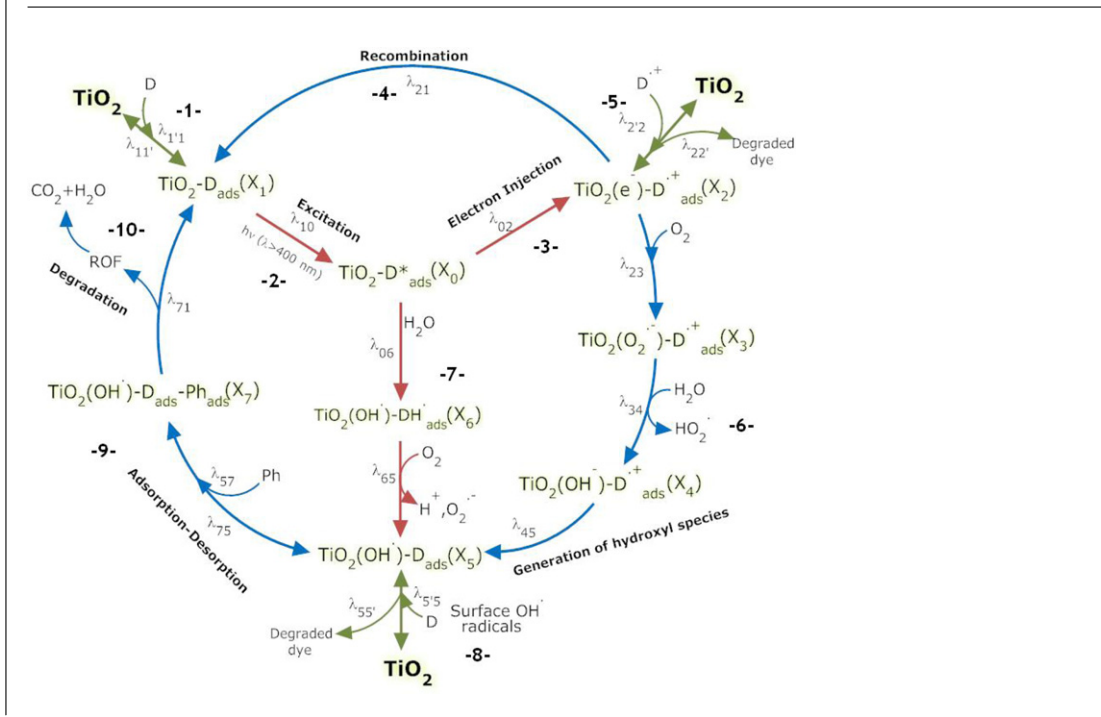
Figure 14: Mechanism of generation of hydroxyl radicals by the excitation of TiO_2 using UV radiation (left half), and the excitation of the adsorbed dye (Eosin Y) using visible radiation (right half). The mechanism of electron injection and the formation of dye radical cations are also shown.
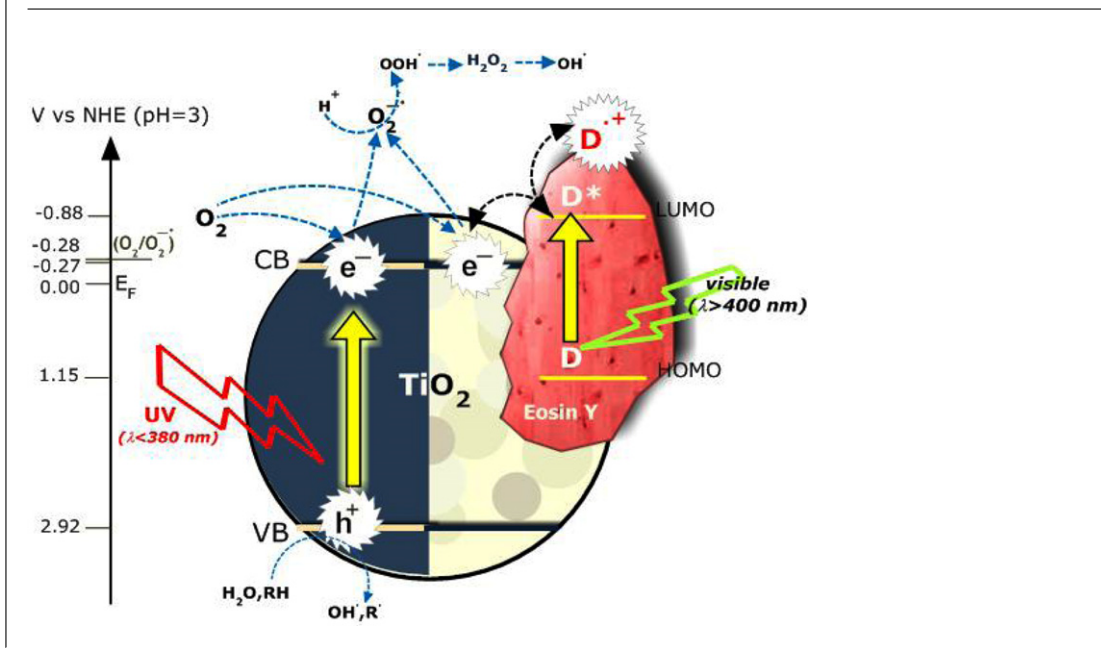
Recent focus is laid on the photocatalytic degradation of the polymers, where a semiconductor photocatalyst like TiO_2 is used to enhance the degradation. In the solid state degradation, a composite of the polymer and TiO_2 is used, while in the liquid state, the TiO_2 particles are suspended in the polymer solution. However, the mechanism of photodegradation is unaffected by the state in

Figure 15: Reduction of normalized molecular weight, during the photocatalytic degradation of PAM, P(AM-co-AA) and PAA in presence of CS TiO$_2$. The inset shows the magnified portion of the degradation curve till 60 min. The values in the inset figure indicate the percentage of AA in the copolymer. It is evident that the copolymer degrades at a higher rate with the inclusion of more AA units. (Redrawn from ref. 177.)
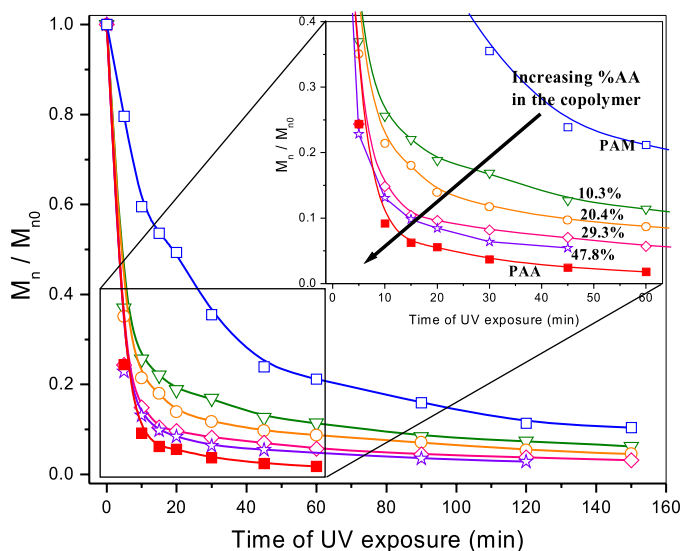
which the polymer is degraded. Table 8[45,46,176–185] presents a listing of the different polymers that were photocatalytically degraded in both solid and in solution. It is clear that a wide variety of polymers based on acrylates, methacrylates, styrene, poly(olefins), poly(carbonate), and a few biodegradable polymers have been degraded, mostly in presence of TiO$_2$.

The first step in the photocatalytic degradation of the polymers is the formation of the hydroxyl radicals ($\cdot$OH) from the TiO$_2$ surface. In the presence of organic solvents or in the absence of moisture, surface hydroxyl groups present in TiO$_2$ serve as the key source of hydroxyl radicals. The UV photon and/or the $\cdot$OH radicals generated according to reactions (1)–(14) (section 2) attacks the polymer, resulting in the generation of polymer α-radical [P$\cdot$]. These α-radicals are the precursors of chain breakage. The next step is the reaction of [P$\cdot$] with atmospheric oxygen to form polymer peroxy radicals [POO$\cdot$]. These combine bimolecularly with one another and form [POO-OOP] species. Thus, with the exclusion of oxygen, polymer oxy radicals are formed [PO$\cdot$]. Finally, the scission of the polymer oxy radical produces a radical and a non-radical fragment. A detailed discussion on the various aspects of the mechanism of chain scission

of the different class of polymers is provided by Rabek.[169]

Sivalingam and Madras[46] have studied the photocatalytic degradation of poly(bisphenol-A-carbonate) and have shown that bond cleavage occurs by Photo-Fries rearrangement of the aromatic carbonate unit, resulting in the formation of phenyl salicylate and dihydroxybenzophenone. The time evolution of molecular weight of this polymer indicated the presence of weak and strong links, which degraded at faster and slower rates, respectively. Recently, we have shown that acrylic acid units in poly(acrylamide-co-acrylic acid) (p(AM-co-AA)) form weak linkages and acrylamide units form strong linkages, which degrade at faster and slower rates, respectively.[177] Figure 15 shows the reduction in molecular weight of p(AM-co-AA) of different comonomer composition, when degraded in aqueous medium. It is clear that the inclusion of acrylic acid units reduce the photostability of the copolymer. It was shown that the scission rate coefficients corresponding to the weak and strong links exhibit linearity with respect to the acrylic acid content in the copolymer.[177] Figure 16 shows the possible mechanism of scission of the acrylic acid units in the p(AM-co-AA) copolymer based on the above discussion. It is evident that the scission product includes the formation of carbonyl moiety (aldehyde or ketonic groups), which was verified by UV/vis spectroscopy. Chiantore et al.[186] and Kaczmarek et al.[187] have proposed alternate pathways for the formation of carbonyl groups, carboxylic acid groups and lactones during the photodegradation of alkyl acrylate and alkyl methacrylate polymers.

Zan et al.[180] have observed the formation of cavities and cracks in the polystyrene-TiO$_2$ nanocomposite films, when exposed to UV radiation and sunlight illumination. At long exposure periods, whitening of the composite films was observed, which was confirmed by the reduction in transmittance of the films. After 400 h of exposure in air atmosphere, nearly 30% weight loss was observed for the composite films with 2% TiO$_2$ under UV irradiation, and 20% weight loss under sunlight illumination. Similar morphological changes were also observed for the degradation of low density polyethylene (LDPE)-TiO$_2$ composites.[181] The weight loss of the LDPE-2% TiO$_2$ films was 60% and the number average molecular weight reduction was nearly 94% after 400 h of irradiation. Similar studies on the degradation of other polymer composite films have unequivocally shown that the composite films show a higher reduction in weight loss and significant morphological changes compared to the pure polymer films without TiO$_2$.

Figure 16: Mechanism of main chain scission of the copolymer P(AM-co-AA) in presence of UV radiation. The by-products involve the formation of aldehydes. (Redrawn from ref. 177.)
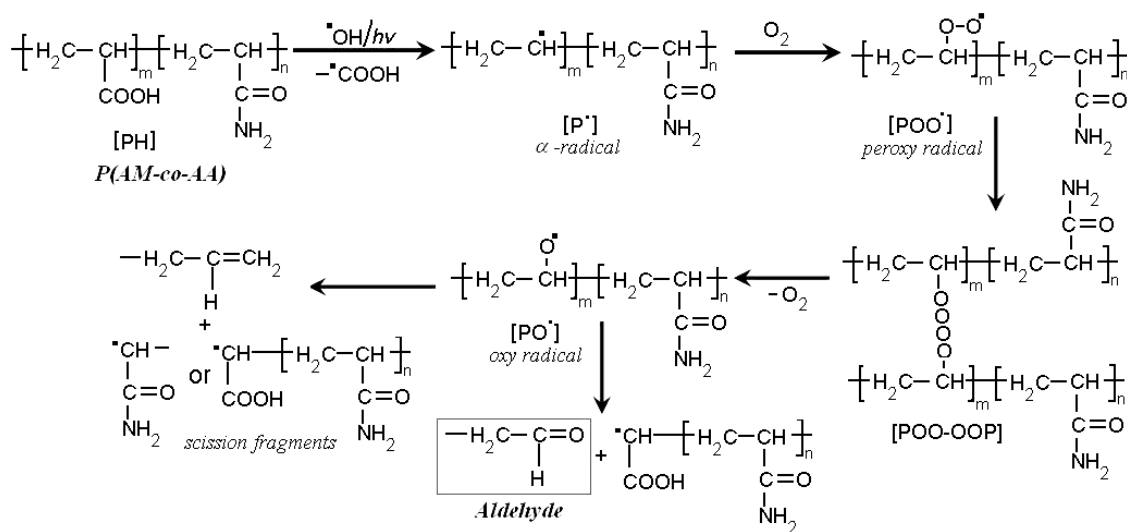
9. Photocatalytic degradation of gaseous contaminants

9.1. Volatile organic compounds (VOCs)

VOCs refer to those organic compounds which possess a high vapor pressure at ambient conditions. VOCs are common indoor air pollutants, which when inhaled can cause irritation, headache, nausea and other health hazards. Common solvents, refrigerants, perfumes, pesticides, paints, markers and fuels are some of the common classes of VOCs. Benzene, a common organic solvent and VOC, is toxic and carcinogenic even at very low concentrations. The usual concentration of the VOCs in the atmosphere ranges from 100 ppb (parts per billion) to a few ppm (parts per million). Common solvents like acetone,[188] 2-propanol,[188] methanol,[189] trichloroethylene (TCE),[190,191] benzene,[192] toluene[192,193] and ethyl benzene,[192] pesticides (dichlorvos),[194] and foul gas (methyl mercaptan)[195] have been shown to photodegrade in the gas phase in presence of TiO_2 under UV illumination. All the above studies have evaluated the degradation of the VOCs in terms of the time evolution of CO_2. TCE is a classic example of a VOC that has been subjected to extensive research in terms of the elucidation of the mechanism and pathway of degradation.[190,191,193] It is well established that hydroxyl radical attacks the CCl_2 side of TCE, and results in the formation of monochloroacettic acid and 2,2'-dichloroethanol.

One of the important parameters that determine the rate of degradation of an organic compound in the gas phase is the relative humidity (RH) or moisture content in the feed stream. Besides providing sufficient hydroxyl species to promote the oxidation of the VOCs and preventing the recombination of the charge carriers at low concentrations, water vapor competes with the VOCs and the reaction intermediates for the active adsorption sites on the catalyst at moderate to high concentrations. Hence, there is always an optimum humidity at which the reactions are carried out. This value was observed to be 43% for the degradation of methyl mercaptan.[195] Sleiman et al.[194] have observed a change in the reaction pathway of degradation of the pesticide, dichlorvos, under dry (RH = 0%) and humid conditions (RH = 40%). Under dry conditions, chlorinated products like trichloroacetaldehyde, $CHCl_3$ and CCl_4 were observed, while at humid conditions, these were not observed and there was drop in the mineralization efficiency.

Recent studies focus on the visible light degradation of VOCs in presence of anion substituted TiO_2 (Table 7 (entries 34–38)[196−200]). Nitrogen substituted TiO_2, N-F-codoped TiO_2 and ZrO_2 modified $TiO_{2−x}N_x$ have been found to be beneficial for this purpose. Li et al.[197] have shown, by photoluminescence studies, that the high activity of N-F-codoped TiO_2 for the mineralization of acetaldehyde and TCE is due to the creation of surface O_2 vacancies, increase in surface acidity and Ti^{3+} ions, along with the absorption in the visible range. In another study, Amano et al.[199] have shown that the adsorption of acetaldehyde on the exposed Bi_2WO_6 (0 1 0) surface is the primary reason for the

high mineralization rates observed with Bi_2WO_6 flake-balls. The rate of CO_2 liberation exhibits a linear increase with the surface area of Bi_2WO_6 and the surface coverage of acetaldehyde. Table 7 shows some of the recent studies conducted on the visible light degradation of VOCs using the above materials. Overall, it can be said that TiO_2 and its modified forms are still the preferred catalysts for the degradation of VOCs, although some materials like β-Ga_2O_3[192] and Bi_2WO_6[199] have shown better activities compared to TiO_2 in the UV and visible range, respectively.

9.2. NO_x abatement

NO_x refers to the two oxides of nitrogen, viz., nitric oxide (NO) and nitrogen dioxide (NO_2). Based on the origin, NO_x can be classified as thermal NO_x, fuel NO_x and prompt NO_x.[201] Thermal NO_x refers to NO produced by the oxidation of N_2 in air at high temperatures (>1300 K). The Zeldovich mechanism involving the reaction of N_2 with oxygen radicals, and O_2 and OH species with nitrogen radicals describes the formation of thermal NO_x. The oxidation of N_2 present in coal and fuel oils contribute to fuel NO_x. Prompt NO_x or Fenimore NO_x is formed as a result of the reaction between atmospheric N_2 and the hydrocarbon radicals in the flame zone of hydrocarbon flames. This type of NO_x is accompanied by the formation of CN radicals and HCN. NO_x poses several adverse effects on the environment. Vehicle traffic and transportation contributes to nearly 50% of NO_x emitted into the atmosphere, while the rest comes from the domestic and industrial combustion processes.[201] The potential of NO_x to react with ozone results in the depletion of the ozone layer in the lower portion of the stratosphere. Other harmful effects of NO_x include the formation of acid rain and photochemical smog, when NO_x reacts with water and VOCs in the atmosphere, respectively.

NO_x abatement refers to the conversion of NO_x to N_2, O_2 and nitrates (NO_3^-). This is achieved in four different ways, viz. (i) the complete decomposition of NO to N_2 and O_2, (ii) reduction of NO to N_2 in presence of CO, H_2 or NH_3, (iii) selective catalytic reduction (SCR) of NO by NH_3 or hydrocarbons in presence of O_2, and (iv) oxidation of NO_x to nitrates. The reviews by Roy et al.,[201] and Roy and Baiker[202] discuss in detail about the mechanism of catalytic deNO$_x$, and NO_x storage-reduction catalysis, respectively. This section aims to address the photocatalytic approach towards the abatement of NO_x by some of the above mentioned techniques. One of the main advantages of using UV or visible radiation lies in the ambient conditions at which high conversions can be achieved for the above reactions, as opposed to high temperatures involved in the conventional thermal deNO$_x$ techniques.

9.2.1. NO decomposition and reduction

The general reaction for the decomposition of NO can be written as[201]

$$NO \longrightarrow 1/2N_2 + 1/2O_2; \quad \Delta H = -86.6 \text{ kJ mol}^{-1}.$$
(70)
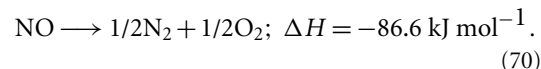
The above reaction is energetically feasible without the presence of any reducing agents. It has been identified that adsorption of NO on the catalyst surface is the first step in the NO decomposition reaction. The adsorption of NO on a metal surface can either be molecular or dissociative. Early synchrotron radiation studies have shown that NO chemisorption is molecular on noble metal surfaces like Pt(1 0 0) and Pd(1 1 0), while it is dissociative on the surface of base metals.[203] However, based on vibrational spectroscopy studies, it was later found that the the geometry of NO plays a key role in the adsorption and dissociation on metal surfaces. NO assumes a "bent" geometry on the metal surface during adsorption, while it changes the configuration to "side on" during dissociation to N and O.[204] NO dissociation is highly dependent on the coverage on the surface, with high coverages hampering the dissociation. This shows that the presence of vacant sites helps in the reorientation of the adsorbed NO from the bent to side on configuration, so that O atom comes in contact with the metal surface, before dissociation can occur.

Many studies have evaluated the photocatalytic decomposition of NO on the surface of TiO_2. Lim et al.[205] have studied the decomposition of NO in a fluidized bed photocatalytic reactor. The decomposition of NO was found to increase with low initial concentration of NO and longer gas residence time. A power law dependence of the NO decomposition rate with the UV intensity was observed. Upto 70% NO decomposition was achieved. In another study,[206] anatase TiO_2 with high surface area and surface hydroxyl content was found to exhibit high efficiency for NO decomposition to N_2, O_2 and N_2O, in a flow reactor. Furthermore, the presence of O_2 along with NO in the feed stream resulted in the adsorption of NO onto TiO_2, and its oxidation to NO_2 in the dark condition. Bowering et al.[207] have found that high pretreatment temperatures reduce the activity of DP-25 TiO_2 for NO decomposition. Anpo and coworkers have demonstrated NO decomposition over Ag^+/ZSM-5 zeolite,[208] and TiO_2 with Y-zeolites[209] as support, prepared by ion-exchange method. The selectivity for the formation of N_2 was found to decrease with an increase in the Si/Al ratio of the zeolite. Unsupported DP-25 TiO_2 exhibited the least selectivity for N_2 (N_2:N_2O=27:73). We have recently shown that 1% Pd^{2+} ion substituted

Figure 17: Photocatalytic reduction of NO by CO over different Pd substituted and impregnated nano-catalysts. 1% Pd substituted TiO_2 exhibits the highest conversion of NO. (Redrawn from ref. 132.)
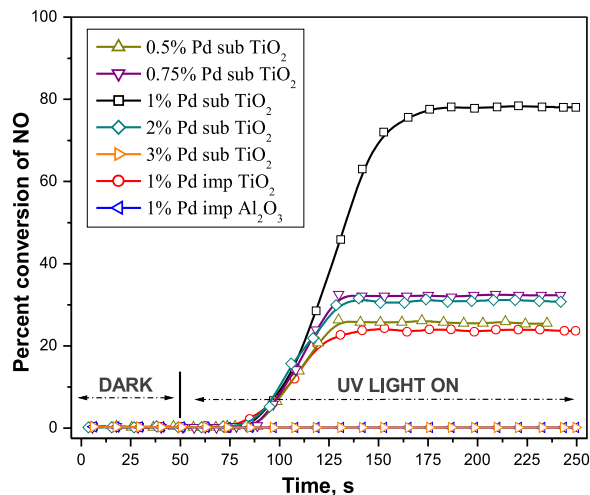
TiO_2 ($Pd_{0.01}Ti_{0.99}O_{2-\delta}$) exhibits 45% conversion of NO, with N_2 and N_2O in the ratio 2:1.[132] However, repeated runs of NO decomposition reaction with intermittent switching on/off the UV lamp indicated that %NO decomposition decreased to less than 5% after 5 cycles. This is a clear indication of the adsorption of O_2 on the surface of the catalyst. The formation of O_2 occurs by the following surface reactions[207]

$$2O_{ads} \longrightarrow O_{2ads} \qquad (71)$$

$$2NO_{ads} \longrightarrow N_{2(g)} + O_{2ads}. \qquad (72)$$
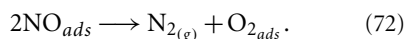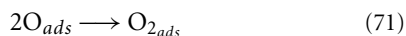
Usually, in catalytic converters, a three-way catalyst is employed, which is used to simultaneously convert CO to CO_2, along with NO decomposition. This can also be viewed as the reduction of NO by CO to form N_2 and CO_2. It is represented by the following reaction[201]

$$NO + CO \rightarrow 1/2N_2 + CO_2;$$

$$\Delta H = -328 \text{ kJ mol}^{-1}. \qquad (73)$$
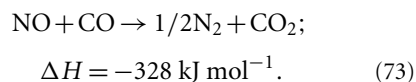
Bowering et al.[207] have also observed an increase in selectivity of N_2 formation when CO was used as the reductant in the ratio of 4:1 (NO/CO). In a recent investigation of the photocatalytic reduction of NO by CO using Pd/TiO_2, synthesized by solution combustion technique, Roy et al.[132] have found that 1% substitution of Pd in the lattice of TiO_2 yields an overall NO conversion of 80%, while

lower concentrations of Pd result in two fold lesser conversions (Figure 17). Compared to the ionic dispersion of Pd, impregnation of Pd on the surface of TiO_2 shows the lowest conversion of 24%. Repeated cycles of NO reduction by CO showed that the overall NO conversion remained the same after 5 cycles. This is suggestive of the fact that the adsorbed oxygen species is utilized in the oxidation of CO to form CO_2.

Cho[210] has investigated the mechanistic importance of the reaction between N_2O and CO in the kinetics of NO reduction by CO, and shown that the rate of N_2O + CO reaction is much faster compared to the NO + CO reaction on Rh/Al_2O_3 catalyst. The reactions are

$$2NO + CO \longrightarrow N_2O + CO_2 \qquad (74)$$

$$N_2O + CO \longrightarrow N_2 + CO_2. \qquad (75)$$
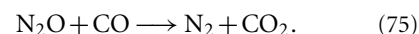
We have proposed a detailed mechanism based on the surface processes for the reduction of NO by CO over Pd/TiO_2 catalyst.[211] Following are the set of reactions involved

$$CO + S_{Pd} \longleftrightarrow CO_{Pd} \qquad (76)$$

$$NO + S_{Pd} \longleftrightarrow NO_{Pd} \qquad (77)$$

$$NO + "V" \longrightarrow N - "O" \qquad (78)$$

$$N - "O" + e_{CB}^- \longrightarrow N - "O"^{\bullet-} \qquad (79)$$

$$N - "O"^{\bullet-} + h_{VB}^+ + "V" \longrightarrow "N" + "O" \qquad (80)$$

$$N - "O" + "N" \longrightarrow N_2O + 2"V" \qquad (81)$$

$$NO_{Pd} + "N" \longrightarrow N_2O + "V" + S_{Pd} \qquad (82)$$

$$"O" + CO_{Pd} \longrightarrow CO_2 + S_{Pd} + "V" \qquad (83)$$

$$"N" + "N" \longrightarrow N_2 + 2"V" \qquad (84)$$

$$"O" + N - "O" \longrightarrow "NO_2" + "V";$$

$$\text{"V" - oxide ion vacancy.} \qquad (85)$$
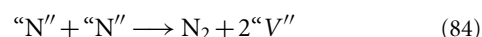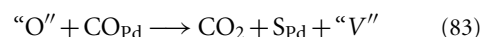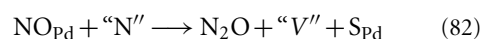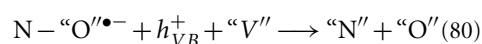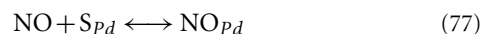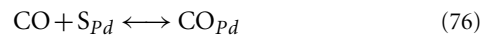
The above mechanism involves the following steps, (i) competitive, reversible adsorption–desorption of CO and NO on Pd^{2+} site, (ii) photo induced dissociation of NO in the oxide ion vacancy, (iii) formation of N_2O, (iv) oxidation of CO by the reaction with trapped "O" in the vacancy, (v) formation of N_2 and NO_2 in the oxide ion vacancy. By writing balance equation for each of the species involved in the above mechanism, and applying pseudo steady state approximation for all the adsorbed species on the vacancy, a non-linear model was derived relating the conversion of NO with the ratio of weight of the catalyst (W) to the flow rate of NO (F). Figure 18 shows the model fit with the experimental data. It is clear that the conversion of

Figure 18: Validation of the kinetic model proposed by Sounak et al. for the reduction of NO by CO using 1% Pd substituted TiO_2. W/F denotes the ratio of weight of the catalyst to the flow rate of the gas. (Redrawn from ref. 132.)
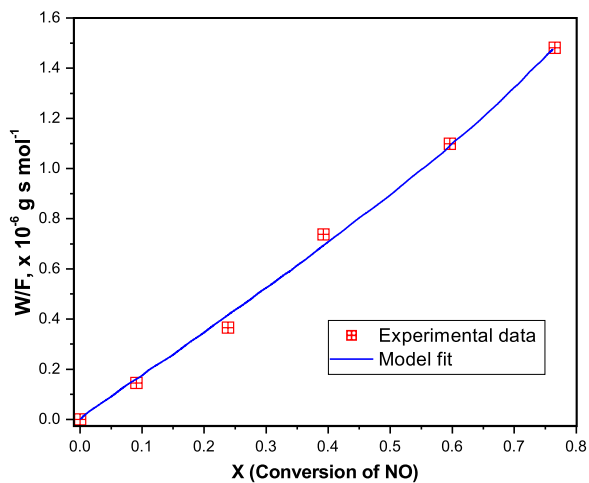
NO can be increased by either increasing the mass loading of the catalyst, which improves the active sites, or by reducing the flow rate of NO, which enhances the contact time with the catalyst.

Teramura et al.[212] have studied the reduction of NO in presence of NH_3 in the presence and absence of O_2. The mechanism proposed based on FT-IR analysis shows that (i) NH_3 is adsorbed preferentially compared to NO on Ti^{4+} Lewis acid sites as $Ti-NH_2$ and $Ti-OH$, (ii) NO from the gas phase reacts with $-NH_2$ to from the nitrosamide species, (iii) nitrosamide is decomposed to N_2 and H_2O in presence of O_2, (iv) NO adsorption onto TiO_2 produces nitrate species in presence of O_2. In the absence of O_2, N_2O is formed from NO. The overall reactions in the presence and absence of O_2 can be written as[212]

$$4NO + 4NH_3 + O_2 \longrightarrow 4N_2 + 6H_2O \quad (86)$$

$$4NO + 2NH_3 \longrightarrow 2N_2 + N_2O + 3H_2O. \quad (87)$$
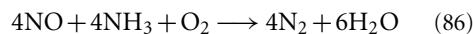
9.2.2. NO oxidation

NO oxidation refers to the conversion of NO to NO_2 and nitrate species (NO_3^-). This occurs primarily due to the attack of hydroxyl and superoxide radicals on NO, and the following mechanism is widely accepted[213–215]

$$NO + OH_{ads}^{\bullet} \longrightarrow HNO_2 \quad (88)$$

$$HNO_2 + OH_{ads}^{\bullet} \longrightarrow NO_2 + H_2O \quad (89)$$

$$NO_2 + OH_{ads}^{\bullet} \longrightarrow HNO_3 \quad (90)$$

$$NO + O_{2ads}^{\bullet -} \longrightarrow NO_3^- \quad (91)$$

$$3NO_2 + 2OH_{ads}^- \longrightarrow 2NO_3 + NO + H_2O. \quad (92)$$
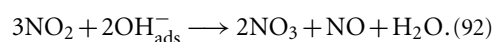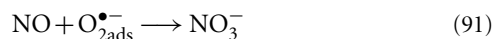
Wu and Cheng[214] have conducted an extensive FT-IR study, and found that NO adsorbs onto the surface of TiO_2 in the form of bidentate nitrite. This reacts with the superoxo species ($TiOO^{\cdot}$), and forms nitrate in either bidentate or monodentate form. In the presence of metal (like Cu, Cr, V) on TiO_2, nitrosyls ($NO^{(\delta+)}$) were also formed, which were preferentially oxidized by the superoxo species to nitrates. Many catalysts[215] like Pd impregnated TiO_2,[216] NH_3 pretreated TiO_2[217] and TiO_2-MCM-41[218] have been developed, which exhibit superior activity compared to DP-25 for the oxidation of NO to NO_2 and HNO_3. It has to be emphasized that NO_2 is still hazardous and the concentration of NO_2 at the outlet has to be maintained at a minimum level during the oxidation of NO. In this regard NH_3-TiO_2 has been found to be effective.[218] Recently, Ohko et al.[219] have studied the deactivation of the surface of TiO_2 thin films by HNO_3, formed by the oxidation of NO_2. It was found that HNO_3 diffuses into the TiO_2 film at a rate of c.a. 1.5 $\mu m\ h^{-1}$ and gets distributed homogeneously at the bottom of the film, with a density of c.a. 2 molecules nm^{-2}. In another novel study, Brouwers and coworkers[220] have simulated the oxidation of NO_x on concrete pavement coated with TiO_2. Detailed kinetic models were developed based on the L–H rate equation and the effect of operating conditions like inlet NO concentration, NO flow rate and reactor height were studied. Recent studies focus on the visible light induced oxidation of NO_x using modified TiO_2 materials like C-doped TiO_2,[221] CdS quantum dots embedded mesoporous TiO_2,[222] ZrO_2/TiO_2[223] and PtO_x-modified TiO_2.[224] Therefore, it can be concluded that TiO_2 and its modified forms are promising as photocatalytic deNO_x catalysts. However, the nearly complete conversion of NO_x to innocuous N_2 is still a challenge, and further research on the materials and processes is indispensable for the commercialization of this technology.

10. Photocatalysis using non-TiO_2 based materials

TiO_2 has served as a "benchmark photocatalyst" for the degradation of a wide class of organic compounds and microorganisms in the UV range. Many modifications of TiO_2 through anion doping and heterostructuring have shown that TiO_2 can also be used in the visible region. However, there are also other interesting materials, which exhibit photocatalytic activity in the UV and visible region. Research efforts on the development of such new materials are essential not only to find alternative photocatalysts to TiO_2 in terms of photoactivity and economics, but also to know if such catalysts

Table 9: Non-TiO$_2$ based materials used as potential photocatalysts for the degradation of different organic compounds and destruction of microorganisms.

Sl. No.	Catalyst material	Structure/space group	E$_{BG}$ eV	Surface area, m^2 g^{-1}	Organic compound/s	UV/Vis	Ref.
Metal Organic Frameworks (MOFs)							
1	[Co$_2$(C$_{10}$H$_8$N$_2$)][OBA]$_2$ [Ni$_2$(C$_{10}$H$_8$N$_2$)][OBA]$_2$.2H$_2$O [Zn$_2$(C$_{10}$H$_8$N$_2$)][OBA]$_2$	Monoclinic $C2/c$ Triclinic $P\bar{1}$ Triclinic $P\bar{1}$	3.11 3.89 4.02	-	OG, MB, RBBR, RhB	UVA	[226]
2	Mixed-metal pyridine dicarboxylates [M(H$_2$O)$_3$Co{C$_5$N$_1$H$_3$(COO)$_2$}$_3$})$_\infty$] M=Gd, Dy, Y	Trigonal $P3$	c.a. 3.7	-	RBBR, OG	UVA	[227]
3	Cadmium thosulfate MOFs [Cd(C$_{10}$H$_8$N$_2$)(H$_2$O)$_2$S$_2$O$_3$].2H$_2$O Cd$_2$(C$_{10}$H$_8$N$_2$)$_3$(S$_2$O$_3$)$_2$ Cd$_2$(C$_{10}$H$_8$N$_2$)$_{2.5}$(S$_2$O$_3$)$_2$	Monoclinic $P2_1/n$ $C2/c$ $P2_1/c$	2.91 2.75 2.75	c.a. 3.0	12 dyes belonging to triarylmethane, azo, xanthene and anthraquinone classes	UVA and solar	[228]
Polyoxometalates (POM)							
4	Silica immobilized POMs: Na$_6$W$_7$O$_{24}$, H$_4$W$_{10}$O$_{32}$, H$_3$PW$_{12}$O$_{40}$, H$_6$P$_2$W$_{18}$O$_{62}$	Amorphous	3.55, 3.23, 3.42, 3.38	407, 381, 326, 275	4-Chlorophenol	UVA	[229]
5	H$_3$PW$_{12}$O$_{40}$ on Millenium PC-500 TiO$_2$	Amorphous	3.16±0.2	158–235	4-np and 2-propanol (gas phase)	UV	[230]
Bismuth Molybdates							
6	BaBi$_2$Mo$_{4-x}$W$_x$O$_{16}$ (x=0.25–1.0)	Fluorite Monoclinic $C2/c$	3.23	Negligible	Phenol, 2-np, 4-np, 4-cp, 4-methylphenol, 2,4-dnp, 4-c-2-np, 4-n-2-cp, acetic acid, chloroacetic acid	UVA	[231,232]
7	Ba$_2$Bi$_{24}$Mo$_{10}$O$_{69}$, La$_2$Bi$_{24}$Mo$_{10}$O$_{69}$, Bi$_{26}$Mo$_{10}$O$_{69}$	Fluorite Monoclinic $P2/c$	2.74, 2.9, 3.22				
Orthovanadates							
8	Lanthanide orthovanadates: LnVO$_4$ (Ce, Pr and Nd) by SS	Tetragonal zircon $I4_1/amd$	2.74, 2.86, 2.99	< 1.0	MB	UVA	[233]
9	Li$_{0.1}$Ce$_{0.9}$VO$_{4+\delta}$, Ca$_{0.25}$Ce$_{0.75}$VO$_{4+\delta}$, Fe$_{0.05}$Ce$_{0.95}$VO$_{4+\delta}$ by SS	Tetragonal zircon $I4_1/amd$	2.8, 2.6, 2.9	1.0 – 2.0	MB, OG, RhB, RBBR, RBL, MO, phenol, chloro- and nitro-substituted phenols	UVA	[234]
10	Fe$_x$Ce$_{1-x}$VO$_4$ (x=0.01–0.1) by CS	Tetragonal zircon $I4_1/amd$	2.12 – 2.02	22 – 10	OG, RBBR, ACG, R6G, MV, MG	UVA	[235]
11	**Molybdovanadates** Ln$_{0.95}$Mo$_{0.15}$V$_{0.85}$O$_4$ (Ln=Ce, Pr, Nd) by SS	Tetragonal zircon $I4_1/amd$	2.33, 2.21, 2.14	< 1.0	MB, OG, ARS, RBL, RhB, RBBR, chloro- and nitro-phenols	UVA and solar	[236]
Perovskites							
12	GdCoO$_3$ nanoparticles (3, 12 and 200 nm)	-	-	28, 9, 5	RhB, RBL, OG, RBBR, phenol, 4-cp, 4-np and 4-mp	UVA	[237]
13	BaBiO$_3$	Monoclinic $I12/m1$	2.05	1.2	Acetaldehyde and MB	Vis	[238]
14	LnVO$_3$ and Ln$_{1-x}$Ti$_x$VO$_3$ (Ln=Ce, Pr, Nd)	Orthorhombic $Pnma$	2.8	< 1.0	MB, RBBR, OG, RhB, ARS, RBL, MG, phenol, cp, np and chloro-nitrophenols	UVA	[239]

Table 9: Continued.

Sl. No.	Catalyst material	Structure/space group	E_{BG} eV	Surface area, $m^2\ g^{-1}$	Organic compound/s	UV/Vis	Ref.
	Conjugated polymers						
15	Poly(3-hexyl thiophene) and MEH-PPV	-	2.0, 2.33	-	OG, ARS, ACG, RBBR, phenol, effect of Cu^{2+}	UVA	[240]
	Mesoporous materials						
16	Co doped mesoporous SBA-15 zeolite	Enhanced absorption in the 400–700 nm compared to undoped SBA-15		690	MV, methyl thionine chloride	Solar	[241]
	Other materials						
17	$LiBi_4M_3O_{14}$ (M = Nb, Ta)	Aurivillus phase Monoclinic C2/c	3.0(Nb), 3.5(Ta)	c.a. 0.3	OG, ARS, ACG, MV, Coomassie Brilliant Blue, phenol, 4-np	UVA	[242]
18	$Co_3O_4(1)/BiVO_4(2)$ – p-n heterojunction semiconductor	Scheelite Monoclinic	2.07(1), 2.28(2)	1.38	Phenol	Vis	[243]
19	Bi_2WO_6 nanoplates	Russellite Orthorhombic	2.50	51.5	RhB, *E. coli*	Vis	[244,245]
20	BiOBr	Matlockite Tetragonal	2.54	24.45	MO	Vis	[246]
21	CeO_2	Cubic Fluorite	Wide	42	Acid Orange 7	Vis	[247]

OBA – 4,4'-oxybis(benzoate), OG – Orange G, MO – Methyl Orange, RBBR – Remazol Brilliant Blue R, ARS – Alizarin Red S, ACG – Alizarin Cyanine Green, MB – Methylene Blue, MV – Methyl Violet, RhB – Rhodamine B, RBL – Rhodamine Blue, R6G – Rhodamine 6G, MG – Malachite Green, cp – chlorophenol, np – nitrophenol, mp – methyl phenol, SS – solid state synthesis, CS – combustion synthesis, UVC – reaction was carried out in presence of ultraviolet C radiation (λ centered at c.a. 254 nm), UVA –ultraviolet A radiation (λ centered at c.a. 365 nm), Vis –visible radiation ($\lambda > 420$ nm), Solar – direct sunlight irradiation.

can significantly change the degradation pathway of organic compounds and exhibit substrate specific activity.

These materials include conjugated polymers, metal organic framework (MOF) compounds, mesoporous materials (aluminosilicates), polyoxometalates (POM), mixed metal oxides (perovskites), bismuth molybdates, Bi(oxy)halides, layered oxides and pyrochlore compounds. In a classic review on the alternative photocatalysts to TiO2, Hernández-Alonso et al.[225] have discussed the recent developments in catalysis with novel materials, for a variety of applications like generation of hydrogen by water splitting, detoxification of water and air, green synthesis of aldehydes and ketones by the selective oxidation of organic compounds, and the fixation of CO_2 by the reduction of CO_2 to methanol or hydrocarbons. Table 9 presents a sample of the different studies[226−247], which describe the synthesis, characterization and photocatalytic activity of different materials, for the degradation of a wide variety of organic compounds in the UV and visible range. All the compounds have shown either comparable or mostly higher degradation rates for the organic compounds with respect to the "yardstick TiO2 catalyst", DP-25. Most of the works cited in the table have been conducted in our lab at the Indian Institute of Science.

One of the interesting classes of materials which exhibit higher photocatalytic activity for the degradation of organic compounds is the metal-organic frameworks (MOFs). MOFs belong to the family of two dimensional or three dimensional coordination polymers, which are constituted by metal ions or metal ion clusters, and organic ligands.[248] MOFs are characterized by extremely high porosity, surface area (eg. 5640 $m^2\ g^{-1}$ for MOF-177), poresize, zero dead volume, regularity of the pores, and a wide range of chemical inorganic-organic composition. MOFs are known to catalyze a wide variety of organic transformations.[249] The photocatalytic activity exhibited by the MOF compounds is due to its semiconductor-like behavior. Mahata et al.[226] have studied the charge transfer mechanism in oxybis(benzoate) based framework compounds using photoluminescence spectroscopy, and concluded that the activation of O_2 by the M^{2+} ions through the ligand-to-metal charge transfer (LMCT) is responsible for the activation of charge carriers. Recently, Alvaro et al.[250] have found by laser flash photolysis that MOF-5 undergoes charge separation upon excitation, which decays in microseconds. The band gap of this material was found to be 3.4 eV, with conduction band energy of 0.2 V (vs NHE). The photoinduced charge separation and charge transfer in MOF-5 in

presence of an aqueous solution of methyl viologen dichloride (V^{2+}) can be represented as[250]

$$MOF-5 + V^{2+} \xrightarrow[\text{charge separation}]{h\nu} +$$

$$[MOF-5]^{\bullet} + V^{2+} \longrightarrow MOF-5^{\bullet+} + V^{\bullet+}$$
$$(93)$$
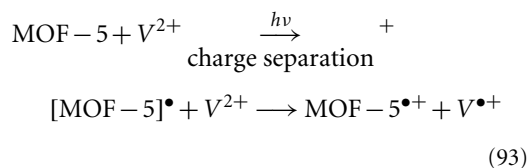
Recently, we have investigated the photocatalytic activity of MOFs based on cadmium thiosulfate chains and 4,4'-bipyridine as building units.[228] These materials exhibit superior adsorption in the aqueous medium and desorption in alcoholic medium for the anionic dyes, and photocatalytic activity for the degradation of cationic dyes in presence of UV and solar radiation. Thus, ample opportunities exist in further research for the development of MOFs as substitutes for existing photocatalysts.

Another class of compounds, which are used increasingly in recent days is the polyoxometallates (POMs), which represent a group of molecular clusters based on early-transition-metal-oxygen-anions.[251,252] Some of the standard POM structures are (i) Keggin $[XM_{12}O_{40}]^{n-}$ (ii) Dawson $[X_2M_{18}O_{62}]^{n-}$ (iii) Anderson $[XM_6O_{24}]^{n-}$ (iv) Lindqvist $[M_6O_{19}]^{n-}$ structures, where X is the heteroatom (P^{5+}, Si^{4+}, B^{3+}), and M is usually Mo or W. Some of the interesting properties of POMs are that they are metal oxide-like in nature, highly stable, photoreducible, superacidic ($pK_a < 0$), soluble in water and oxygen carrying solvents, and hence exhibit catalytic activity, ionic conductivity, reversible redox behavior and cooperative electronic phenomena.[251] For photocatalytic applications, where surface area and post-catalyst separation are important, homogeneous POMs are impregnated onto various types of supports like silica, titania, mesoporous molecular sieves (eg. MCM-48), NaY zeolites, activated carbon and polymeric membranes.[253] The photocatalytic activity exhibited by the POMs is initiated by the excitation of oxygen-to-metal-charge-transfer (OMCT) band, according to the following equation:[253]

$$[W^{6+}-O^{2-}-W^{6+}] \xrightarrow{h\nu} [W^{5+}-O^{-}-W^{6+}].$$
$$(94)$$
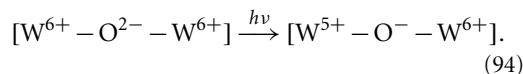
The charge transfer from O^{2-} to W^{6+} leads to the formation of a hole center (O^-), and a trapped electron center (W^{5+}). Moreover, the presence of POM on anatase TiO_2 was found to induce dopant energy level between the valence and conduction band of TiO_2, which resulted in enhanced photocatalytic activity of the composite due to the efficient separation of photogenerated charge carriers. The simultaneous, synergistic photoreduction of Cr^{6+} to Cr^{3+}, and the photooxidation of salicylic acid and isopropanol was also investigated using $PW_{12}O_{40}^{3-}$ and $SiW_{12}O_{40}^{4-}$ materials.[254]

The photocatalytic activity exhibited by vanadates, Bi molybdates and perovskite materials is due to band gap excitation, which results in the generation of charge carriers. The band gap of these non-semiconductor based materials is characterized by the energy difference between the HOMO and LUMO. Moreover, the electronic structure of these materials plays a significant role in the mobility of the charge carriers, thereby resulting in high degradation rates of the organic compounds compared to DP-25. For example, the high photoactivity of barium bismuth molybdates is due to the large overlap of the hybridized valence (Bi6s and O2p orbitals) and conduction band (Bi6p and Mo4d orbitals).[231,232] Similarly, the VO_6 octahedra in $LnVO_3$ perovskite,[239] and VO_4 and MoO_4 tetrahedra in lanthanide molybdovanadates[236] have been found to be responsible for efficient charge transfer to the surface of the material, which enhances the photoactivity.

It is worthwhile to note that many catalysts, inspite of their very low surface area (c.a. 2–5 or <1 m^2 g^{-1}), exhibit better photocatalytic degradation rates compared to DP-25 (50 m^2 g^{-1}). This observation shows that the electronic structure and band gap of the material is more influential in deciding the photocatalytic activity, with narrow band gap materials facilitating the easy mobility of charge carriers. However, higher surface area along with favorable surface charge (pH_{pzc}) complements the photocatalytic activity by facilitating the adsorption of the reactants. This is, in fact, a requirement for the self-sensitized degradation of dyes in presence of visible radiation. Ji et al.[247] have demonstrated the self-sensitized degradation of methyl orange dye on CeO_2, where the HOMO and LUMO of the dye lies within the band gap of CeO_2 ($E_{BG} = 5$ eV). The photoactivity exhibited by CeO_2 is due to the injection of electron form the LUMO of the dye to the Ce4f band, which lies in between the valence and conduction band of CeO_2.

Deshpande and Madras[235] have shown that $Fe_xCe_{1-x}VO_4$ synthesized by combustion synthesis exhibits a higher surface area, which is 10 to 20 times higher compared to the one synthesized by solid state technique.[234] The presence of Fe in the ionic 2+ state was found to accelerate the degradation of dyes by (i) enhancing the redox processes (V^{5+} to V^{4+} when Fe^{2+} oxidizes to Fe^{3+}, and Ce^{3+} to Ce^{4+} when Fe^{3+} reduces to

Figure 19: Time evolution of concentration of cyclohexanol and cyclohexanone during the selective photocatalytic oxidation of cyclohexane in presence of different catalysts. Higher selectivity of cyclohexanone obtained in presence of 1% Ag substituted TiO_2, and Ce orthovanadates are evident from the figure. (Redrawn from ref. 130,260,261.)
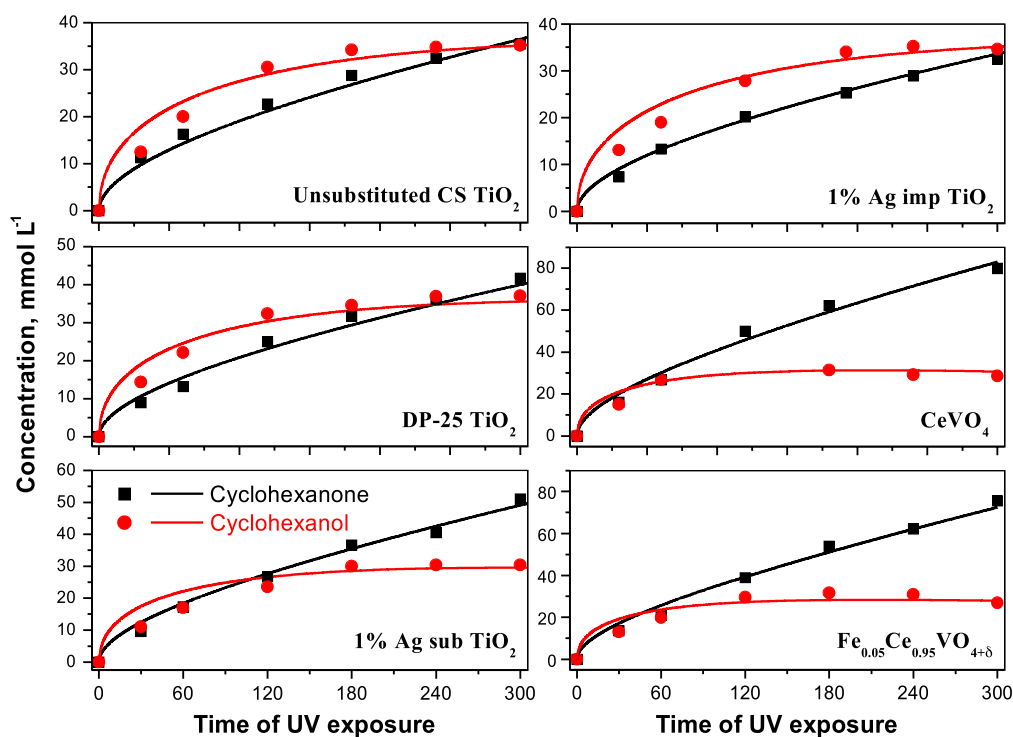
Fe^{2+}), and (ii) generating more hydroxyl radicals by photo-Fenton-like reactions. Thus, the different materials discussed in this section are potential catalysts for the photocatalytic degradation of organic compounds. However, the replacement of the current TiO_2 based catalysts with these materials demands more research concerning their long term stability, reusability and cost-effectiveness of the synthesis protocol involved with these materials.

11. Green chemistry using photocatalysis

Green chemistry refers to the synthesis of organic compounds using the following principles:[255] (i) usage of less hazardous solvents to produce fine chemicals, (ii) highly selective conversions using catalysts, (iii) design of safer processes at mild reaction conditions, (iv) usage of renewable energy and feedstocks and (v) design of degradable materials. Thus, green chemistry aims for the environmentally safe and energy efficient synthesis of chemicals. Previous discussion elucidates the application of photocatalysis to the degradation, i.e., complete oxidation (or mineralization), of the organic pollutants to innocuous products like CO_2, H_2O and other inorganic ions. However, controlled

oxidation of organic compounds opens up a new dimension to photocatalysis, whereby organic compounds can be synthesized with high selectivity in a "one-pot" process. In fact, green chemistry and photochemistry were born at the same time,[256] when the scientist Giacomo Ciamician, in the early 20th century, demonstrated a wide variety of organic reactions like oxidation, reduction, Norrish type I and type II reactions, autooxidation and condensation, using solar radiation.

Many recent reviews feature the different organic transformation reactions that have been carried out using photocatalysis using a wide variety of catalysts including TiO_2 and its modified forms, POMs, zeolites, mixed metal oxides (Al_2O_3/SiO_2), and organic species like porphyrins and phthalocyanines.[23,255−258] The reactions include (i) oxidation of alkanes to alcohols, aldehydes, ketones and carboxylic acids, alcohols to aldehydes and ketones, (ii) hydroxylation of aromatics, (iii) epoxidation of alkenes, (iv) reduction of nitro-aromatics, (iv) reduction of CO_2, (v) C–N and C–C coupling reactions, (vi) dehydrogenation of primary and secondary alcohols, (vii) carbonylation to

produce carbamate species, and (viii) oxidation of polyaromatic compounds. Zhang et al.[259] have recently studied the aerobic oxidation of aliphatic and aromatic alcohols using visible light, in presence of a novel system of anthraquinonic dye (Alizarin Red S) sensitized TiO_2, and a nitroxyl radical (2,2,6,6-tetramethylpiperidinyloxyl). The mechanism involves the formation of a dye radical cation, which oxidizes the nitroxyl radical. This oxidized species was responsible for the selective oxidation of alcohols to aldehydes. Conversions as high as 60% have been obtained for most of the alcohols with over 95% selectivity for the aldehydes.

Recently, we have evaluated the selective oxidation of cyclohexane to cyclohexanone, over different catalyst materials like Ag substituted and impregnated TiO_2,[130] lanthanide orthovanadates ($LnVO_4$),[260] lanthanide molybdovanadates ($LnMoVO_4$; Ln = Ce, Nd, Pr),[260] and metal substituted $CeVO_4$ ($M_xCe_{1-x}VO_4$; M = Li, Ca and Fe).[261] This reaction is an industrially important one, as this is an intermediate step in the manufacture of ε-caprolactum, which is used as a raw material for the production of Nylon 6. Figure 19 shows the time evolution profiles of cyclohexanol and cyclohexanone obtained with different catalysts. It is evident that undoped CS TiO_2, DP-25 TiO_2 and 1% Ag impregnated TiO_2 exhibit equal selectivities for the formation of cyclohexanol and cyclohexanone, while 1% Ag^+ substituted TiO_2, $CeVO_4$ and 5% Fe substituted $CeVO_4$ show selectivities of 63%, 74% and 74% for cyclohexanone, respectively. The conversions achieved with these systems were c.a. 12%. We have also developed a mechanistic model to describe the time evolution of the oxidation products of cyclohexane.[260,261] The concentration profiles in the figure clearly suggest that, in the initial time period, both cyclohexanol and cyclohexanone are formed at nearly equal rates, while at longer reaction time, the concentration of cyclohexanol saturates at a steady state value, indicating the oxidation of cyclohexanol to cyclohexanone. Despite the large number of studies, which show the possibility of the selective synthesis of organics using photocatalysis in presence of UV radiation, this area is still immature, which requires high conversions ($>90\%$) to be achieved using sunlight as an alternate, renewable energy source.

12. Concluding remarks and emerging trends

In this review, we have addressed the basic principles of photocatalysis for environmental remediation. Over the past two decades, nano-TiO_2 has set the standard as a benchmark photocatalyst for the degradation and mineralization of a wide range of toxic organic compounds like chlorinated organics, phenolics, dyes, pesticides, pharmaceutical compounds and drugs, VOCs, NO_x, CO, and polymers and plastics. The anti-microbial activity of TiO_2 for the purification of drinking water is also well established. Many modified forms of TiO_2 like anion substituted TiO_2, dye sensitized TiO_2, polymer/TiO_2 composites, core-shell TiO_2, and co-catalyst coupled TiO_2 have been developed to enhance the visible light activity of first generation TiO_2 or pristine TiO_2. Many non-TiO_2 based materials like the MOFs, polyoxometalates, perovskites, conjugated polymers, mesoporous materials and Bi based oxides exhibit better photocatalytic activity compared to the commercial DP-25 TiO_2, which is used as a yardstick for photoactivity assessment. Hybrid treatment techniques, involving the combination of photocatalysis with other AOPs like the Fenton's reagent, ultrasound, microwave and electrolysis show synergistic effect for the degradation of organic compounds, and are therefore promising as future processes. Future research in wastewater remediation should focus on the photocatalytic degradation of "real" effluents, which are composed of a number of organic compounds, metal ions and microorganisms. Of particular interest in this direction is to probe if the presence of one compound alters the mechanism and pathway of degradation of the other. Therefore, the discussion in the review suggests that, a cleaner and greener environment, and renewable and sustainable energy economy can be achieved through photocatalysis. The authors do believe that more exciting results in this field will be forthcoming in the next decades.

References

1. Fujishima A, Honda K (1972) Nature 238:37–38.
2. Frank SN, Bard AJ (1977) J Phys Chem 81:1484–1488.
3. Pruden AL, Ollis DF (1983) J Catal 82:404–417.
4. Hsiao C-Y, Lee C-L, Ollis DF (1983) J Catal 82:418–423.
5. Matsunaga T, Tomato R, Nakajima T, Wake H (1985) FEMS Microbiol Lett 29:211–214.
6. O'Regan B, Grätzel M (1991) Nature 353:737–740.
7. Kitano M, Matsuoka M, Ueshima M, Anpo M (2007) Appl Catal A: Gen 325:1–14.
8. Hoffmann MR, Martin ST, Choi W, Bahnemann DW (1995) Chem Rev 95:69–96.
9. Linsebigler AL, Lu G, Yates JT (1995) Chem Rev 95:735–758.
10. Mills A, Hunte SL (1997) J Photochem Photobiol A: Chem 108:1–35.
11. Fujishima A, Rao TN, Tryk DA (2000) J Photochem Photobiol C: Photochem Rev 1:1–21.
12. Carp O, Huisman CL, Reller A (2004) Prog Solid State Chem 32:33–177.
13. Fujishima A, Zhang X, Tryk DA (2008) Surf Sci Rep 63:515–582.

14. Chen X, Mao SS (2007) Chem Rev 107:2891–2959.
15. Legrini O, Oliveros E, Braun AM (1993) Chem Rev 93:671–698.
16. Herrmann J-M (1999) Catal Today 53:115–129.
17. Bhatkhande DS, Pangarkar VG, Beenackers AACM (2001) J Chem Technol Biotechnol 77:102–116.
18. Kabra K, Chaudhary R, Sawhney RL (2004) Ind Eng Chem Res 43:7683–7696.
19. Zhao J, Chen C, Ma W (2005) Top Catal 35:269–278.
20. Gaya UI, Abdullah AH (2008) J Photochem Photobiol C: Photochem Rev 9:1–12.
21. Malato S, Fernández-Ibáñez P, Maldonado MI, Blanco J, Gernjak W (2009) Catal Today 147:1–59.
22. Kudo A, Miseki Y (2009) Chem Soc Rev 38:253–278.
23. Palmisano G, Augugliaro V, Pagliaro M, Palmisano L (2007) Chem Commun 3425–3437.
24. Wada Y, Yin H, Yanagida S (2002) Catal Sur Japan 5:127–138.
25. Zhang Q, Gao L (2006) J Eur Ceram Soc 26:1535–1545.
26. Sato S, Oimatsu S, Takahashi R, Sodesawa T, Nozaki F (1997) Chem Commun 2219–2220.
27. Addamo M, Augugliaro V, Paola AD, García-López E, Loddo V, Marcí G, Molinari R, Palmisano L, Schiavello M. (2004) J Phys Chem B 108:3303–3310.
28. Nagaveni K, Hegde MS, Ravishankar N, Subbanna GN, Madras G (2004) Langmuir 20:2900–2907.
29. Mohamed MM, Bayoumy WA, Khairy M, Mousa MA (2007) Micropor Mesopor Mater 103:174–183.
30. Venkatachalam N, Palanichamy M, Murugesan V (2007) Mater Chem Phys 104:454–459.
31. Dong X, Tao J, Li Y, Zhu H (2010) Appl Surf Sci 256:2532–2538.
32. Cheng Y, Sun H, Jin W, Xu N (2007) Chem Eng J 128:127–133.
33. Khan SUM, Al-Shahry M, Ingler Jr. WB (2002) Science 297:2243–2244.
34. Zhang Z, Wang C-C, Zakaria R, Ying JY (1998) J Phys Chem B 102:10871–10878.
35. Ryu J, Choi W (2008) Environ Sci Technol 42:294–300.
36. Hidalgo MC, Colón G, Navío JA (2002) J Photochem Photobiol A: Chem 148:341–348.
37. Hathway T, Jenks WS (2008) J Photochem Photobiol A: Chem 200:216–224.
38. Kritikos DE, Xekoukoulotakis NP, Psillakis E, Mantzavinos D (2007) Water Res 41:2236–2246.
39. Sivalingam G, Nagaveni K, Hegde MS, Madras G (2003) Appl Catal B: Environ 45:23–38.
40. Aarthi T, Madras G (2007) Ind Eng Chem Res 46:7–14.
41. Vinu R, Akki SU, Madras G (2010) J Hazard Mater 176:765–773.
42. Sivalingam G, Priya MH, Madras G (2004) Appl Catal B: Environ 51:67–76.
43. Priya MH, Madras G (2006) J Photochem Photobiol A: Chem 179, 256–262.
44. Priya MH, Madras G (2006) J Photochem Photobiol A: Chem 178:1–7.
45. Vijayalakshmi SP, Madras G (2006) J Appl Polym Sci 100:3997–4003.
46. Sivalingam G, Madras G (2004) Appl Catal A: Gen 269:81–90.
47. Aarthi P, Madras G (2008) Catal Commun 9:630–634.
48. Lasa H, Serrano B, Salaices M (2005) Photocatalytic reaction engineering. Springer, New York.
49. Chiou C-S, Shie J-L, Chang C-Y, Liu C-C, Chang C-T (2006) J Hazard Mater B 137:1123–1129.
50. Lim LLP, Lynch RJ, In S-I (2009) Appl Catal A: Gen 365:214–221.
51. Lee J-M, Kim M-S, Kim B-W (2004) Water Res 38:3605–3613.
52. Tryba B (2008) J Hazard Mater 151:623–627.
53. Nakashima T, Ohko Y, Tryk DA, Fujishima A (2002) J Photochem Photobiol A: Chem 151:207–212.
54. Magalhães F, Lago RM (2009) Sol Energy 83:1521–1526.
55. Faramarzpour M, Vossoughi M, Borghei M (2009) Chem Eng J 146:79–85.
56. Rachel A, Lavedrine B, Subrahmanyam M, Boule P (2002) Catal Commun 3:165–171.
57. Ollis DF (1985) Environ Sci Technol 19:480–484.
58. Turchi CS, Ollis DF (1990) J Catal 122:178–192.
59. Ollis DF, Pelizzetti E, Serpone N (1991) Environ Sci Technol 25:1522–1529.
60. Blake DM (2001) NREL/TP-510–31319, National Renewable Energy Laboratory, Golden.
61. Rajeshwar K, Osugi ME, Chanmanee W, Chenthamarakshan CR, Zanoni MVB, Kajitvichyanukul P, Krishnan-Ayer R (2008) J Photochem Photobiol C: Photochem Rev 9:171–192.
62. Rauf MA, Ashraf SS (2009) Chem Eng J 151:10–18.
63. Konstantinou IK, Albanis TA (2004) Appl Catal B: Environ 49:1–14.
64. Akpan UG, Hameed BH (2009) J Hazard Mater 170:520–529.
65. Han F, Kambala VSR, Srinivasan M, Rajarathnam D, Naidu R (2009) Appl Catal A: Gen 359:25–40.
66. Houas A, Lachheb H, Ksibi M, Elaloui E, Guillard C, Herrmann J-M (2001) Appl Catal B: Environ 31:145–157.
67. Epling GA, Lin C (2002) Chemosphere 46:561–570.
68. Silva CG, Wang W, Faria JL (2006) J Photochem Photobiol A: Chem 181:314–324.
69. Stylidi M, Kondarides DI, Verykios XE (2003) Appl Catal B: Environ 40:271–286.
70. Sleiman M, Vildozo D, Ferronato C, Chovelon J-M (2007) Appl Catal B: Environ 77:1–11.
71. Saquib M, Muneer M (2002) Dyes Pigments 53:237–249.
72. Vautier M, Guillard C, Herrmann J-M (2001) J Catal 201:46–59.
73. Hu C, Yu JC, Hao Z, Wong PK (2003) Appl Catal B: Environ 42:47–55.
74. Chen C-C, Lu C-S (2007) Environ Sci Technol 41:4389–4396.
75. Wu T, Liu G, Zhao J, Hidaka H, Serpone N (1998) J Phys Chem B 102:5845–5851.
76. Park H, Choi W (2005) J Phys Chem B 109:11887–11674.
77. Wu C-H, Chern J-M (2006) Ind Eng Chem Res 45:6450–6457.
78. Li X, Cubbage JW, Jenks WS (1999) J Org Chem 64:8525–8536.
79. Priya MH, Madras G (2006) Ind Eng Chem Res 45:482–486.
80. Levenspiel O (1999) Chemical reaction engineering. John Wiley, Singapore.
81. Konstantinou IK, Zarkadis AK, Albanis TA (2001) J Environ Qual 30:121–130.
82. Zhu X, Yuan C, Bao Y, Yang J, Wu Y (2005) J Mol Catal A: Chem 229:95–105.
83. Moctezuma E, Leyva E, Palestino G, de Lasa H (2007) J Photochem Photobiol A: Chem 186:71–84.
84. Wei L, Shifu C, Wei Z, Sujuan Z (2009) J Hazard Mater 164:154–160.
85. Aungpradit T, Sutthivaiyakit P, Martens D, Sutthivaiyakit S, Kettrup AAF (2007) J Hazard Mater 146:204–213.
86. Yu B, Zeng J, Gong L, Zhang M, Zhang L, Chen X (2007) Talanta 72:1667–1674.
87. Molinari R, Pirillo F, Loddo V, Palmisano L (2006) Catal Today 118:205–213.
88. Chatzitakis A, Berberidou C, Paspaltsis I, Kyriakou G, Sklaviadis T, Poulios I (2008) Water Res 42:386–394.
89. An T, Yang H, Li G, Song W, Cooper WJ, Nie X (2010) Appl Catal B: Environ 94:288–294.
90. Abellán MN, Bayarri B, Giménez J, Costa J (2007) Appl Catal B: Environ 74:233–241.

91. Yang L, Yu LE, Ray MB (2008) Water Res 42:3480–3488.

92. Méndez-Arriaga F, Esplugas S, Giménez J (2008) Water Res 42:585–594.

93. Radjenovič J, Sirtori C, Petrovič M, Barceló D, Malato S (2009) Appl Catal B: Environ 89:255–264.

94. Calza P, Massolino C, Monaco G, Medana C, Baiocchi C (2008) J Pharm Biomed Anal 48:315–320.

95. Cheng YW, Chan RCY, Wong (2007) Water Res 41:842–852.

96. Prasad GK, Agarwal GS, Singh B, Rai GP, Vijayaraghavan R (2009) J Hazard Mater 165:506–510.

97. Liu H-L, Yang TC-K (2003) Process Biochem 39:475–481.

98. Fu G, Vary PS, Lin C-T (2005) J Phys Chem B 109:8889–8898.

99. Kubacka A, Ferrer M, Martínez-Arias A, Fernández-García M (2008) Appl Catal B: Environ 84:87–93.

100. Hu C, Guo J, Qu J, Hu X (2007) Langmuir 23:4982–4987.

101. Wu T-S, Wang K-X, Li G-D, Sun S-Y, Sun J, Chen J-S (2010) ACS Appl Mater Interf 2:544–550.

102. Wu P, Xie R, Imlay JA, Shang JK (2009) Appl Catal B: Environ 88:576–581.

103. Akhavan O, Ghaderi E (2009) J Phys Chem C 113:20214–20220.

104. Pelaez M, de la Cruz AA, Stathatos E, Falaras P, Dionysiou DD (2009) Catal Today 144:19–25.

105. Cho M, Chung H, Choi W, Yoon J (2004) Water Res 1069–1077.

106. Matsunaga T, Tomoda R, Nakajima T, Nakamura N, Komine T (1988) Appl Environ Microbiol 54:1330–1333.

107. Saito T, Iwase T, Horie J, Morioka T (1992) J Photochem Photobiol B: Biol 14:369–379.

108. Maness P-C, Smolinski S, Blake DM, Hyang Z, Wolfrum EJ, Jacoby WA (1999) Appl Environ Microbiol 65:4094–4098.

109. Rincón A-G, Pulgarin C (2004) Appl Catal B: Environ 51:283–302.

110. Sharma VK, Yngard RA, Lin Y (2009) Adv Coll Interf Sci 145:83–96.

111. Benabbou AK, Derriche Z, Felix C, Lejeune P, Guillard C (2007) Appl Catal B: Environ 76:257–263.

112. Marugán J, van Grieken R, Sordo C, Cruz C (2008) Appl Catal B: Environ 82:27–36.

113. Marugán J, van Griekan R, Pablos C, Sordo C (2010) Water Res 44:789–796.

114. Azevedo EB, Neto FRA, Dezotti M (2004) Appl Catal B: Environ 54:165–173.

115. Devi LG, Murthy BN, Kumar SG (2009) Chemosphere 76:1163–1166.

116. Chen D, Ray AK (2001) Chem Eng Sci 56:1561–1570.

117. Prairie MR, Evans LR, Stange BM, Martinez SL (1993) Environ Sci Technol 27:1776–1782.

118. Chen C, Li X, Ma W, Zhao J, Hidaka H, Serpone N (2002) J Phys Chem B 106:318–324.

119. Kyung H, Lee J, Choi W (2005) Environ Sci Technol 39:2376–2382.

120. Sun B, Reddy EP, Smirniotis PG (2005) Environ Sci Technol 39:6251–6259.

121. Wang N, Chen Z, Zhu L, Jiang X, Lv B, Tang H (2007) J Photochem Photobiol A: Chem 191:193–200.

122. Vinu R, Madras G (2008) Environ Sci Technol 42:913–919.

123. Aarthi P, Narahari P, Madras G (2007) J Hazard Mater 149:725–734.

124. Choi W, Termin A, Hoffmann MR (1994) J Phys Chem 98:13669–13679.

125. Serpone N, Lawless D, Disdier J, Herrmann J-M (1994) Langmuir 10:643–652.

126. Shah SI, Li W, Huang C-P, Jung O, Ni C (2002) Proc Nat Acad Sci 99:6482–6486.

127. Dvoranová D, Brezová V, Mazúr M, Malati MA (2002) Appl Catal B: Environ 37:91–105.

128. Nagaveni K, Hegde MS, Madras G (2004) J Phys Chem B 108:20204–20212.

129. Vinu R, Madras G (2008) J Mol Catal A: Chem 291:5–11.

130. Vinu R, Madras G (2009) Appl Catal A: Gen 366:130–140.

131. Štengl V, Bakardjieva S, Murafa N (2009) Mater Chem Phys 114:217–226.

132. Roy S, Hegde MS, Ravishankar N, Madras G (2007) J Phys Chem C 111:8153–8160.

133. Paola AD, García-López E, Ikeda S, Marcí G, Ohtani B, Palmisano L (2002) Catal Today 75:87–93.

134. Asahi R, Morikawa T, Ohwaki T, Aoki K, Taga Y (2002) Science 293:269–271.

135. Khan SUM, Al-Shahry M, Ingler Jr. WB (2003) Science 301:1673d.

136. Liu G, Wang L, Yang HG, Cheng H-M, Lu GQM (2010) J Mater Chem 20:831–843.

137. Serpone N (2006) J Phys Chem B 110:24287–24293.

138. Nagaveni K, Sivalingam G, Hegde MS, Madras G (2004) Appl Catal B: Environ 48:83–93.

139. Xiao Q, Zhang J, Xiao C, Si Z, Tan X (2008) Sol Energy 82:706–713.

140. Yu T, Tan X, Zhao L, Yin Y, Chen P, Wei J (2009) Chem Eng J. doi: 10.1016/j.cej.2009.10.051.

141. Liu S, Chen X (2008) J Hazard Mater 152, 48–55.

142. Cheng Y, Sun H, Jin W, Xu N (2007) Chem Eng J 128:127–133.

143. Zhong J, Chen F, Zhang J (2010) J Phys Chem C 114:933–939.

144. Ao Y, Xu J, Fu D, Yuan C (2009) Micropor Mesopor Mater 122:1–6.

145. Zhang H, Zong R, Zhao J, Zhu Y (2008) Environ Sci Technol 42:3803–3807.

146. Wang Q, Chen C, Zhao D, Ma W, Zhao J (2008) Langmuir 24:7338–7345.

147. Kim TW, Ha HW, Paek M-J, Hyun S-H, Baek I-H, Choy J-H, Hwang S-J (2008) J Phys Chem C 112:14853–14862.

148. Zhang H, Lv X, Li Y, Wang Y, Li J (2009) ACS Nano. doi: 10.1021/nn901221k.

149. Li G-S, Zhang D-Q, Yu JC (2009) Environ Sci Technol 43:7079–7085.

150. Ho W, Yu JC, Lin J, Yu J, Li P (2004) Langmuir 20:5865–5869.

151. Wang D, Zhang J, Luo Q, Li X, Duan Y, An J (2009) J Hazard Mater 169:546–550.

152. Ge L, Xu M, Fang H (2006) J Mol Catal A: Chem 258:68–76.

153. Li Y, Zhang H, Hu X, Zhao X, Han M (2008) J Phys Chem C 112:14973–14979.

154. He Z, Xie L, Tu J, Song S, Liu W, Liu Z, Fan J, Liu Q, Chen J (2009) J Phys Chem C. doi: 10.1021/jp908946c.

155. Gilma GO, Carlos APM, Fernando MO, Edgar AP-M (2005) Catal Today 107–108:589–594.

156. An G, Ma W, Sun Z, Liu Z, Han B, Miao S, Miao Z, Ding K (2007) Carbon 45:1795–1801.

157. Zhao W, Sun Y, Castellano FN (2008) J Am Chem Soc 130:12566–12567.

158. Sun Q, Xu Y (2009) J Phys Chem C 113:12387–12394.

159. Xiangzhong L, Wei Z, Jincai Z (2002) Sci China Ser B 45:421–425.

160. Davydov L, Reddy EP, France P, Smirniotis PG (2001) J Catal 203:157–167.

161. Ishibai Y, Sato J, Nishikawa T, Miyagishi S (2008) Appl Catal B: Environ 79:117–121.

162. Granados-Oliveros G, Páez-Mozo EA, Ortega FM, Ferronato C, Chovelon J-M (2009) Appl Catal B: Environ 89:448–454.

163. Ross H, Bendig J, Hecht S (1994) Solar Energy Mater Solar Cells 33:475–481.

164. Bae E, Choi W (2003) Environ Sci Technol 37:147–152.

165. Bessekhouad Y, Robert D, Weber JV (2004) J Photochem

Photobiol A: Chem 163:569–580.

166. Bessekhouad Y, Robert S, Weber J-V (2005) Catal Today 101:315–321.

167. Brahimi R, Bessekhouad Y, Bouguelia A, Trari M (2008) J Photochem Photobiol A: Chem 194:173–180.

168. Duncan WR, Prezhdo OV (2007) Annu Rev Phys Chem 58:143–184.

169. Rabek JF (1996) Photodegradation of polymers. Springer-Varlag, Berlin.

170. Kim W, Park J, Jo HJ, Kim H-J, Choi W (2008) J Phys Chem C 112:491–499.

171. Georgekutty R, Seery MK, Pillai SC (2008) J Phys Chem C 112:13563–13570.

172. Qiu R, Zhang D, Mo Y, Song L, Brewer E, Huang X, Xiong Y (2008) J Hazard Mater 156:80–85.

173. Ru J, Huayue Z, Xiaodong L, Ling X (2009) Chem Eng J 152:537–542.

174. Muruganandham M, Kusumoto Y (2009) J Phys Chem C 113:16144–16150.

175. Central pollution control board. Plastic waste management. Parivesh. www.cpcb.nic.in/139–144.pdf. Accessed 20 Feb 2010.

176. Kaczmarek H, Kamińska A, Świątek M, Rabek JF (1998) Die Angew Makromol Chem 261/262:109–121.

177. Vinu R, Madras G (2008) J Phys Chem B 112:8928–8935.

178. Marimuthu A, Madras G (2008) Ind Eng Chem Res 47:2182–2190.

179. Konaganti VK, Madras G (2009) Polym Degrad Stab 94:1325–1335.

180. Zan L, Wang S, Fa W, Hu Y, Tian L, Deng K (2006) Polymer 47:8155–8162.

181. Zan L, Fa W, Wang S (2006) Environ Sci Technol 40:1681–1685.

182. Penot G, Arnaud R, Lemaire J (1983) Die Ang Makromol Chem 117:71–84.

183. Zhang L, Liu P, Su Z (2006) Polym Degrad Stab 91:2213–2219.

184. Miyauchi M, Li Y, Shimizu H (2008) Environ Sci Technol 42:4551–4554.

185. Liau LC-K, Tung M-T (2006) Ind Eng Chem Res 45:2199–2205.

186. Chiantore O, Trossarelli L, Lazzari M (2000) Polymer 41:1657–1668.

187. Kaczmarek H, Kamińska A, van Herk A (2000) Eur Polym J 36:767–777.

188. Xu W, Raftery D, Francisco JS (2003) J Phys Chem B 107:4537–4544.

189. Stokke JM, Mazyck DW (2008) Environ Sci Technol 42:3808–3813.

190. Demeestere K, Visscher AD, Dewulf J, Leeuwen MV, Langenhove HV (2004) Appl Catal B: Environ 54:261–274.

191. Yamazaki-Nishida S, Cervera-March S, Nagano KJ, Anderson MA, Hori K (1995) J Phys Chem 99:15814–15821.

192. Hou Y, Wang X, Wu L, Ding Z, Fu X (2006) Environ Sci Technol 40:5799–5803.

193. Bouzaza A, Vallet C, Laplanche A (2006) J Photochem Photobiol A: Chem 177:212–217.

194. Sleiman M, Ferronato C, Chovelton J-M (2008) Environ Sci Technol 42:3018–3024.

195. Li XZ, Hou MF, Li FB, Chua H (2006) Ind Eng Chem Res 45:487–494.

196. Irokawa Y, Morikawa T, Aoki K, Kosaka S, Ohwaki T, Taga Y (2006) Phys Chem Chem Phys 8:1116–1121.

197. Li D, Ohashi N, Hishita S, Kolodiazhnyi T, Haneda H (2005) J Solid State Chem 178:3293–3302.

198. Wang X, Yu JC, Chen Y, Wu L, Fu X (2006) Environ Sci Technol 40:2369–2374.

199. Amano F, Nogami K, Tanaka M, Ohtani B (2010) Langmuir. doi: 10.1021/la904274c.

200. Li D, Chen Z, Chen Y, Li W, Huang H, He Y, Fu X (2008) Environ Sci Technol 42:2130–2135.

201. Roy S, Hegde MS, Madras G (2009) Appl Energy 86:2283–2297.

202. Roy S, Baiker A (2009) Chem Rev 109:4054–4091.

203. Brodén G, Rhodin TN, Brucker C, Benbow R, Hurych Z (1976) Surf Sci 59:593–611.

204. Brown WA, King DA (2000) J Phys Chem B 104:2578–2595.

205. Lim TH, Jeong SM, Kim SD, Gyenis J (2000) J Photochem Photobiol A: Chem 134:209–217.

206. Zhang J, Ayusawa T, Minagawa M, Kinugawa, Yamashita H, Matsuoka M, Anpo M (2001) J Catal 198:1–8.

207. Bowering N, Walker GS, Harrison PG (2006) Appl Catal B: Environ 62:208–216.

208. Anpo M, Matsuoka M, Yamashita H (1997) Catal Today 35:177–181.

209. Zhang J, Hu Y, Matsuoka M, Yamashita H, Minagawa M, Hidaka H, Anpo M (2001) 105:8395–8398.

210. Cho BK (1992) J Catal 138:255–266.

211. Roy S, Aarthi T, Hegde MS, Madras G (2007) Ind Eng Chem Res 46:5798–5802.

212. Teramura K, Tanaka T, Funabiki T (2003) Langmuir 19:1209–1214.

213. Dalton JS, Janes PA, Jones NG, Nicholson JA, Hallam KR, Allen GC (2002) Environ Poll 120:415–422.

214. Wu JCS, Cheng Y-T (2006) J Catal 237:393–404.

215. Wu Z, Sheng Z, Wang H, Liu Y (2009) Chemosphere 77:264–268.

216. Wu Z, Sheng Z, Liu Y, Wang H, Tang N, Wang J (2009) J Hazard Mater 164:542–548.

217. Li FB, Li XZ, Ao CH, Hou MF, Lee SC (2004) Appl Catal B: Environ. 54:275–283.

218. Signoretto M, Ghedini E, Trevisan V, Bianchi CL, Ongaro M, Cruciani G (2010) Appl Catal B: Environ 95:130–136.

219. Ohko Y, Nakamura Y, Fukuda A, Matsuzawa S, Takeuchi (2008) J Phys Chem C 112:10502–10508.

220. Ballari MM, Hunger M, Hüsken G, Brouwers HJH (2010) Appl Catal B: Environ 95:245–254.

221. Yu QL, Brouwers HJH (2009) Appl Catal B: Environ 92:454–461.

222. Li G-S, Zhang D-Q, Yu JC (2009) Environ Sci Technol 43:7079–7085.

223. Kim J-Y, Kim C-S, Chang H-K, Kim T-O (2010) Adv Powder Technol. doi: 10.1016/j.apt.2009.12.008.

224. Huang C-H, Wang I-K, Lin Y-M, Tseng Y-H, Lu C-M (2010) J Mol Catal A: Chem 316:163–170.

225. Hernández-Alonso MD, Fresno F, Suárez S, Coronado JM (2009) Energy Environ Sci 2:1231–1257.

226. Mahata P, Madras G, Natarajan S (2006) J Phys Chem B 110:13759–13768.

227. Mahata P, Madras G, Natarajan S (2007) Catal Lett 115:27–32.

228. Paul AK, Madras G, Natarajan S (2009) Phys Chem Chem Phys 11:11285–11296.

229. Yue B, Zhou Y, Xu J, Wu Z, Zhang X, Zou Y, Jin S (2002) Environ Sci Technol 36:1325–1329.

230. Carriazo D, Addamo M, Marcì G, Martín C (2009) Appl Catal A: Gen 356:172–179.

231. Muktha B, Madras G, Guru Row TN (2007) J Photochem Photobiol A: Chem 187:177–185.

232. Muktha B, Aarthi T, Madras G, Guru Row TN (2006) J Phys Chem B 110:10280–10286.

233. Mahapatra S, Madras G, Guru Row TN (2007) Ind Eng Chem Res 46:1013–1017.

234. Mahapatra S, Vinu R, Saha D, Guru Row TN, Madras G

(2009) Appl Catal A: Gen 361:32–41.

235. Deshpande PA, Madras G (2010) Chem Eng J. doi: 10.1016/j.cej.2010.01.056.

236. Mahapatra S, Madras G, Guru Row TN (2007) J Phys Chem C 111:6505–6511.

237. Mahata P, Aarthi T, Madras G, Natarajan S (2007) J Phys Chem C 111:1665–1674.

238. Tang J, Zou Z, Ye J (2007) J Phys Chem C 111:12779–12785.

239. Saha D, Mahapatra S, Guru Row TN, Madras G (2009) Ind Eng Chem Res 48:7489–7497.

240. Muktha B, Madras G, Guru Row TN, Scherf U, Patil S (2007) J Phys Chem B 111:7994–7998.

241. Xia F, Ou E, Wang L, Wang J (2008) Dyes Pigments 76:76–81.

242. Muktha B, Priya MH, Madras G, Guru Row TN (2005) J Phys Chem B 109:11442–11449.

243. Long M, Cai W, Cai J, Zhou B, Zhai X, Wu Y (2006) J Phys Chem B 110:20211–20216.

244. Shang M, Wang W, Sun S, Zhou L, Zhang L (2008) J Phys Chem C 112:10407–10411.

245. Ren J, Wang W, Zhang L, Chang J, Hu S (2009) Catal Commun 10:1940–1943.

246. Zhang J, Shi F, Lin J, Chen D, Gao J, Huang Z, Ding X, Tang C (2008) Chem Mater 20:2937–2941.

247. Ji P, Zhang J, Chen F, Anpo M (2009) Appl Catal B: Environ 85:148–154.

248. Natarajan S, Mahata P (2009) Chem Soc Rev 38:2304–2318.

249. Lee JY, Farha OK, Roberts J, Scheidt KA, Nguyen SBT, Hupp JT (2009) Chem Soc Rev 38:1450–1459.

250. Alvaro M, Carbonell E, Ferrer B, Xamena FXL, Garcia H (2007) Chem Eur J 13:5106–5112.

251. Long D-L, Cronin L (2006) Chem Eur J 12:3698–3706.

252. Katsoulis DE (1998) Chem Rev 98:359–387.

253. Guo Y, Hu C (2007) J Mol Catal A: Chem 262:136–148.

254. Gkika E, Troupis A, Hiskia A, Papaconstantinou E (2006) Appl Catal B: Environ 62:28–34

255. Herrmann J-M, Duchamp C, Karkmaz M, Hoai BT, Lachheb H, Puzenat E, Guillard C (2007) J Hazard Mater 146:624–629.

256. Albini A, Fagnoni M (2004) Green Chem 6:1–6.

257. Shiraishi Y, Hirai T (2008) J Photochem Photobiol C: Photochem Rev 9:157–170.

258. Ravelli D, Dondi D, Fagnoni M, Albini A (2009) Chem Soc Rev 38:1999–2011.

259. Zhang M, Chen C, Ma W, Zhao J (2008) Angew Chem Int Ed 47:9730–9733.

260. Mahapatra S, Vinu R, Guru Row TN, Madras G (2008) Appl Catal A: Gen 351:45–53.

261. Mahapatra S, Vinu R, Saha D, Guru Row TN, Madras G (2009) Appl Catal A: Gen 361:32–41.

Giridhar Madras received his chemical engineering degree from Indian Institute of Technology at Madras in 1990. He subsequently obtained his Ph.D. degree in chemical engineering from Texas A&M University, USA, in 1994. Subsequently, he worked in the University of California at Davis, USA. He returned to India as an Assistant Professor of chemical engineering at the Indian Institute of Science, Bangalore in 1998. Since 2007, he has been a Full Professor at the Chemical Engineering Department, and is currently the Chairman of the National Center of Scientific Information. He is also an associate faculty in Solid State and Structural Chemistry, Nanoscience and the center for nanotechnology.

He received the Scopus Young Scientist Award from Elsevier for being the most cited young author in engineering. He was awarded the presidential Swarnajayanthi fellowship by the Department of Science and Technology, India,in 2006 and the S.S. Bhatnagar prize from CSIR, India in 2009 for his contributions to the field of engineering. He has published more than 225 international journal articles, which have more than 3000 citations with a h-index of 27. He is listed by Web of Science as among the top 1% of all scientists in the world. He is currently a member of the Editorial Board of several journals including Current Science and International journal of polymer science. His research interests are in the areas of polymers, supercritical fluids, catalysis, and reaction engineering.

R. Vinu has recently submitted his Ph.D. thesis in Chemical Engineering, Indian Institute of Science. He obtained his Bachelors degree in Chemical Engineering from A.C. College of Technology, Anna University, Chennai in 2006. His research is currently focused on the kinetics of photo-initiated organic and polymer reactions for environmental applications.